Exploring Experimental Autoimmune Encephalomyelitis as an Animal Model to Study Trigeminal Dysfunction in Multiple Sclerosis

by

Kevin C. Thorburn

A thesis submitted in partial fulfillment of the requirements for the degree of

Doctor of Philosophy

Department of Pharmacology
University of Alberta

Abstract

Altered sensation along the distribution of the trigeminal nerve is a well-recognized complication of Multiple Sclerosis (MS). However, the mechanisms underlying trigeminal sensory disturbances in MS are poorly understood. This can be attributed, at least in part, to the lack of animal models that exhibit MS-like trigeminal dysfunction and pathology. The data presented in this thesis contributes to the literature by demonstrating that a particular animal model, experimental autoimmune encephalomyelitis (EAE), could be an invaluable tool for studying MS-related trigeminal sensory disturbances.

The goal of Chapter 1 was to assess whether or not EAE could be used to study MS-related trigeminal dysfunction and pathology. I started by establishing a novel behavioral test in the lab which gave me the ability to assess facial sensitivity in freely moving mice. This test was based on a previously published protocol and involved applying puffs of air to the whisker pads of mice. Behaviors evoked by the air puffs were captured on a camera and graded according to a scoring system used in the aforementioned protocol. I found that prior to the induction of EAE, the puffs of air would typically evoke reflexive withdrawal behaviors. By contrast, following the induction of EAE the air puffs triggered pronounced nocifensive behaviors (e.g. facial swipes down the snout). Given the pronounced change in facial sensitivity, I next wanted to investigate trigeminal pathology that may be associated with this change in facial sensitivity. I used immunohistochemistry to assess inflammation and demyelination at several points along the trigeminal primary afferent pathway. I found that in tissue obtained from mice with EAE, inflammation and demyelination could be detected at the level of the trigeminal ganglion (TG), trigeminal nerve root, and trigeminal brainstem complex.

Following up on the data obtained in Chapter 1, the goal for Chapters 2 and 3 was to further investigate mechanisms underlying the facial hypersensitivity observed in mice with EAE. In Chapter 2, I assessed the excitability of TG neurons *in vitro* using calcium imaging. I found that the sensitivity of TG neurons to pro-nociceptive agonists (e.g. capsaicin and adenosine triphosphate (ATP)) was unaltered by EAE. Additionally, the magnitude of the calcium responses evoked by these agonists was unaltered by EAE. By contrast, the magnitude of the calcium responses evoked by potassium chloride (KCl) was significantly greater in neurons obtained from animals with EAE relative to controls. Collectively, the data

presented in Chapter 2 demonstrates that the excitability of trigeminal primary afferent neurons is increased in EAE. This change in excitability could be a major contributing factor to the altered facial sensitivity observed in mice with EAE.

Finally, during my analysis of the trigeminal pathway in EAE, I noticed that expression of the astrocyte marker glial fibrillary acidic protein (GFAP) decreases at the trigeminal root entry zone. Given that astrocyte disruption is a rarely touched upon topic in neuroscience, I decided to follow-up on this finding and made it the focus of Chapter 3. There I demonstrate that in EAE, the loss of GFAP at the trigeminal root is highly heterogenous both within and between animals. I also show that the loss of GFAP is associated with an accumulation of amyloid precursor protein (APP), a marker of axonal injury. Upon further investigation, I found that tissue sections with GFAP loss had exacerbated inflammation and demyelination. Additionally, I provide evidence that astrocyte loss is not limited to the trigeminal root and can also be detected in the spinal cord. In order to identify a mechanism that may underlie trigeminal injury in EAE, I introduced a novel cell culture technique, immunopanning, to the lab. Using immunopan-purified astrocytes and cortical neurons, I demonstrate that injured astrocytes lose the capacity to support neurons in vitro. Collectively, the data presented in Chapter 3 suggests that EAE is associated with trigeminal nerve injury, which in turn may be mediated by a loss of astrocytes that protect the trigeminal nerve from inflammatory disease processes.

In summary, the work presented in this thesis is the first to demonstrate that EAE is associated with trigeminal pathology and facial pain behaviors. In addition, this work reveals mechanisms that may contribute to trigeminal sensory disturbances in EAE and, potentially, MS.

Preface

This thesis is an original work by Kevin C. Thorburn. The research project, of which this thesis is a part, received research ethics approval from the University of Alberta Research Ethics Board, Project Name “Assessing sensory function in EAE”, AUP00000274, Approved Fall 2007.

Chapter 1 of this thesis has been published as K. C. Thorburn, J. W. Paylor, C. A. Webber, I. R. Winship, and B. J. Kerr. “Facial hypersensitivity and trigeminal pathology in mice with experimental autoimmune encephalomyelitis.” Pain, vol. 17 issue 4, 483-498. I was responsible for the concept formation, data collection and analysis, as well as the manuscript composition. J. Paylor assisted with image acquisition. C. Webber assisted with image analysis. I. Winship assisted with manuscript edits. B.J. Kerr was the supervisory author and assisted with manuscript edits.

For the data presented in Chapters 2 and 3, I was responsible for the concept formation, data collection and analysis.

Acknowledgements

None of the work presented in this thesis would have been possible without contributions from many individuals. First and foremost, I want to thank my parents for their constant and unconditional support throughout the years. I extend thanks to the various students I worked with – Saad, Katherine, Timo, Wes, and Ana – who provided feedback and technical assistance with many of the experiments described below. I also acknowledge my supervisor, Dr. Bradley Kerr, and supervisory committee members, Dr. Christine Webber and Dr. Peter Smith. Finally, I want to extend a huge thanks to the MS Society of Canada for not only providing me with funding for the entirety of my studies, but for also giving me the opportunity to engage with the MS community and develop my public speaking skills.

Table of Contents

List of Figures

List of Abbreviations and Symbols

AB: Antibody buffer

ACM: Astrocyte conditioned media

ACSF: Artificial cerebrospinal fluid

ANOVA: Analysis of variance

ATP: Adenosine triphosphate

AQP4: Aquaporin-4

BBB: Blood-brain barrier

BS: Brainstem

BSA: Bovine serum albumin

CCI-ION: Chronic constriction injury to the infraorbital nerve

CFA: Complete Freund's Adjuvant

CNS: Central nervous system

DAPI: 4′,6-diamidino-2-phenylindole

DRG: Dorsal root ganglion/ganglia

D-PBS: Dulbecco's phosphate buffered saline

EAE: Experimental autoimmune encephalomyelitis

GABA: γ-aminobutyric acid

GFAP: Glial fibrillary acidic protein

HBSS: Hank's balanced salt solution

Iba1: Ionized calcium-binding adapter molecule 1

IHC: Immunohistochemistry

IL-1β: Interleukin-1β

IP: Immunopanning

IR: Immunoreactivity

KCl: Potassium chloride

MOG: Myelin oligodendrocyte glycoprotein

MRI: Magnetic resonance imaging

MVD: Microvascular decompression

MS: Multiple Sclerosis

PB: Phosphate buffer

PBS: Phosphate buffered saline

PBStw Phosphate buffered saline (with tween)

PI: Post induction

PNS: Peripheral nervous system

PDL: Poly-D lysine

Pr5: Principle sensory trigeminal nucleus

RIPA: Radioimmunoprecipitation

SGC: Satellite glial cell

Sp5C: Spinal trigeminal nucleus caudalis

Sp5I: Spinal trigeminal nucleus interpolaris

Sp5O: Spinal trigeminal nucleus oralis

TZ: Transition zone

TG: Trigeminal ganglion/ganglia

TN: Trigeminal neuralgia

TNFα: Tumor necrosis factor α

TREZ: Trigeminal root entry zone

Introduction

Multiple Sclerosis (MS) is a disease that is characterized by immune-mediated destruction of central nervous system (CNS) myelin[1]. A well-recognized complication of MS is altered sensation and/or motor function in the structures innervated by the trigeminal nerve (e.g. face, mouth, and jaws)[2]. Trigeminal symptoms in MS are heterogeneous and can range from a loss of sensation (hyposthesia) to excruciating facial pain (e.g. trigeminal neuralgia)[2]. Trigeminal dysfunction in MS is poorly understood and can have a significant impact on a patient's physical and mental health[3]. Additionally, treatment options for trigeminal sensory disturbances are limited and there is a lack of studies that have attempted to investigate the mechanisms underlying MS-related trigeminal dysfunction. Thus, the field could benefit greatly from the study of animal models that: (1) have trigeminal pathology similar to MS and (2) exhibit behaviors indicative of trigeminal dysfunction.

Prevalence and clinical characteristics of trigeminal dysfunction in MS

Trigeminal symptoms in MS are diverse and can range from numbness to agonizing pain[2,4]. The prevalence of trigeminal sensory disturbances in MS is difficult to gauge, as this particular group of symptoms has never been the subject of a large, prospective, epidemiological study. Nevertheless, based on individual clinical studies, trigeminal symptoms appear to occur in up to 78% of people with MS[4,5].

The link between MS and trigeminal dysfunction was noted as early as 1887 by the neurologist Hermann Oppenheim[6]. In one particular publication, Oppenheim wrote of a "sensory disturbance in the [trigeminal] nerve" and it is now believed that he was describing one of the earliest, if not first, documented cases of MS-related trigeminal neuralgia (TN)[6]. Of the various trigeminal symptoms associated with MS, none have captivated the attention of neurologists and neurosurgeons to the same extent as TN. Indeed, despite being relatively rare amongst people with MS, TN receives a disproportionate amount of attention in the MS-trigeminal literature (fig. i). People with TN experience recurrent attacks (paroxysms) of excruciating facial pain that can be triggered by everyday activities such as talking and eating. To illustrate the intensity and debilitating nature of TN, one patient's description of a pain paroxysm has been provided below:

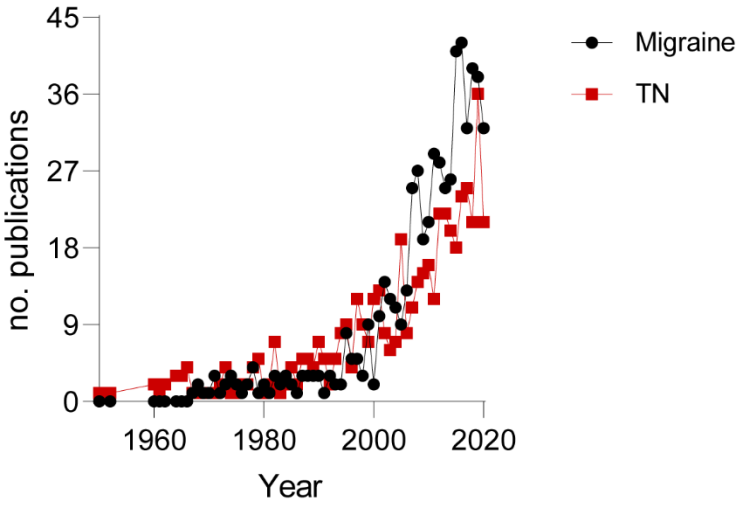

Figure i. Number of publications pertaining to the search phrases "migraine and MS" (black) or "trigeminal neuralgia and MS" (red) between the period of 1950-2020. Despite migraine being more prevalent in MS, the number of papers related to MS-related TN is on par with that of MS-related migraine. Data extracted from Pubmed search feature on 08/27/2020.

"Supper with friends. Candles and wonderful food. Suddenly my face is split apart—the bones feel as though they are shattering and the flesh raked aside by red-hot claws. I lean forward, the food falls from my mouth. The guests stare, concerned and appalled. I cannot speak to explain why the tears stream down my face. I cannot even swallow, my own saliva dribbling onto my plate. All I can do is try not to scream. If I look into a mirror I cannot believe that there is no sign of injury, no blood pouring out of my eye"[7].

As mentioned above, TN is relatively rare amongst people with MS and has a prevalence rate between 1.9-6.3%[8–10]. However, a recent study suggests that TN is 15-times more common in people with MS compared to the general neurological population[8]. Additionally, a study comparing MS- and non-MS-related TN found that a significantly greater proportion of patients with MS-related TN rated their pain as having a high impact on their quality of life[3]. A unique feature of TN is that it can be effectively managed with pharmacological and surgical interventions[9]. First-line pharmacological options for TN are anticonvulsants such as carbamazepine and phenytoin. However, anticonvulsants are limited by

intolerable side effects and their efficacy for managing TN pain can wane over time[9]. In medically refractory TN, surgical options can be carried out which either involve: (1) microvascular decompression (MVD) or (2) deliberate destruction of a particular part of the trigeminal nerve[9]. MVD is carried out based on the premise that TN is most commonly caused by a blood vessel that compresses the trigeminal nerve[11]. MVD can produce instant and prolonged pain relief. However, it is well-recognized that MVD is substantially less effective in patients with MS[9]. Indeed, less than 50% of patients with MS-related TN remain pain free 5 years after receiving MVD[12,13]. By contrast, approximately 80% of patients with non-MS-related TN remain pain free by the 5 year post-surgery timepoint[9,14]. Destructive surgical procedures can also be extremely limited in efficacy. Up to 83% of MS patients undergoing a destructive surgery for TN do not attain prolonged pain relief[15]. Krishan et al, observed that of 26 trigeminal nerves that were subjected to a destructive procedure, 23 required subsequent procedures because patients either did not attain immediate pain relief or the pain recurred[16]. Astonishingly, symptomatic nerves in this study required, on average, 4.7 destructive procedures before patients attained adequate pain relief[16]. Given that these procedures involve destruction of the trigeminal nerve, up to 25% of patients may experience additional trigeminal dysfunction such as facial numbness and jaw weakness[16,17]. Thus, despite the amount of attention that TN receives, it remains a significant complication of MS that is poorly understood.

Additional trigeminal sensory disturbances that can occur in MS include hyposthesia, paraethesia (an abnormal sensation), dysesthesia (a painful abnormal sensation) and ongoing pain[2,4]. These symptoms appear to be more common than TN, with a prevalence of at least 4.3-18.5%[4]. However, the impact that these symptoms have on patients is poorly defined. Additionally, it is not clear how these symptoms are managed.

In recent years there has been a growing recognition of an association between MS and the various types of headaches (e.g. migraine and tension-type headache; see fig i)[5,18,19]. Headache is a significant complication in MS and is associated with increased relapse rates[18,19], greater disease burden[19], and poorer quality of life ratings[5]. Up to 78% of people with MS experience headache[5], and it is now recognized that headache is more common in people with MS relative to the general population[20]. The

pathogenesis and pathophysiology of headache is not entirely understood. However, inflammation and dysfunction of the trigeminal nerve is believed to be a feature shared by the various types of headache pain[21]. At present, the relationship between MS, headache, and trigeminal dysfunction is not known. Brainstem lesions or inflammation-mediated irritation of the trigeminal nerve have been proposed as potential mechanisms underlying MS-related headache[22]. However, neither mechanism has yet to be definitively proven.

Trigeminal dysfunction in MS can also be detected by assessing trigeminal somatosensory evoked potentials[4,23,24]. The assessment of sensory evoked potentials is based on the premise that a stimulus applied to the periphery will result in primary afferent electrical activity that can be detected with electrodes applied to the skin[24]. Any interruption in the primary afferent pathway, such as that caused by demyelination or axonal injury, will delay or diminish the detected activity, giving an indication to the integrity of the sensory pathway[24]. In patients with MS, assessment of trigeminal sensory evoked potentials reveals waveforms with components that are either diminished or delayed relative to controls. For example, Cruccu et al. observed that up to 89% of MS patients with trigeminal symptoms show delayed trigeminal evoked potentials[2]. Additionally, Bergamaschi et al., observed signal abnormalities in 65% of the patients included in their study[4]. Interestingly, Bergamaschi et al. observed that 47% of patients with abnormal trigeminal potentials did not exhibit any sensory disturbances in the face[4]. Thus, the trigeminal nerve can be dysfunctional in MS without manifesting in sensory disturbances. What has yet to be established is if sub-clinical trigeminal dysfunction eventually leads to altered sensation.

Trigeminal dysfunction in MS can have a substantial impact on a patient's physical and mental wellbeing[3,5]. Indeed, pain and motor impairment in the orofacial region can dissuade patients from engaging in proper oral healthcare and can limit the desire to eat[25]. Despite the high prevalence of trigeminal dysfunction in MS, the mechanisms underlying these various conditions are poorly understood. However, there is a long-standing body of literature that has documented trigeminal lesions in MS[2,26–28]. An understanding of this pathology could shed light on the mechanisms that underly orofacial manifestations of MS.

The trigeminal somatosensory system

All sensation begins with the activation of specialized receptor structures that convert (transduce) various stimuli (e.g. mechanical or thermal) into electrical potentials. The receptor structures that transduce orofacial stimuli are primary afferent neurons that belong to the ophthalmic (V1), maxillary (V2), or mandibular (V3) branches of the trigeminal nerve (figure ii)[29]. Generated electrical potentials are conveyed along V1, V2 and V3 towards the trigeminal ganglion (TG), which houses the cell bodies of the primary afferents. From the TG, the potentials are relayed to the CNS via the trigeminal nerve root, which connects to the lateral aspect of the pons (see Fig 1.5). Upon entering the CNS, trigeminal afferents project to specific nuclei located through the brainstem. Collectively, these nuclei make up the spinal trigeminal brainstem complex (see Fig 1.5) and each nucleus receives preferential input from specific afferent subtypes[30]. For example, the caudal nucleus (Sp5C) primarily receives innervation from small diameter A-delta and C fibers that typically relay signals generated by noxious or painful stimuli[30]. By contrast, the principle sensory nucleus (Pr5) primarily receives input from large diameter afferents that convey information about light touch and proprioception[30]. Within each brainstem nucleus are the cell bodies of the secondary sensory neurons which project to various cortical and subcortical structures that ultimately give rise to what we perceive as a specific orofacial sensation.

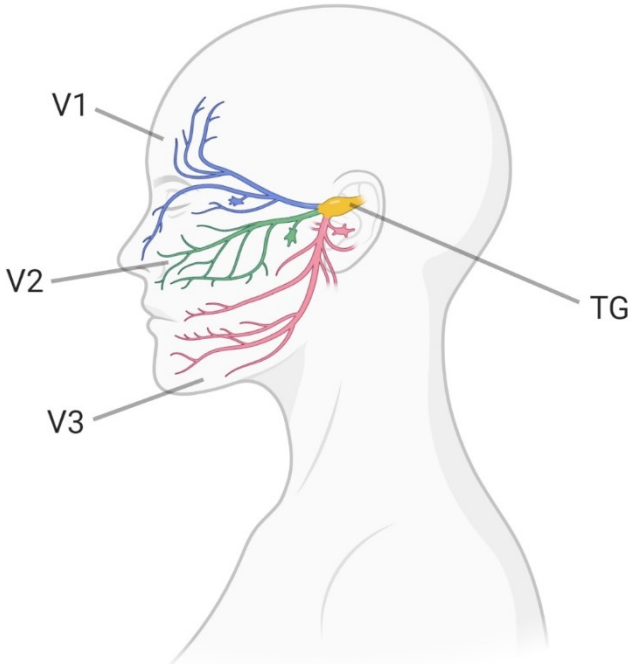

Figure ii. Innervation of the orofacial structures by the ophthalmic (V1), maxillary (V2) and mandibular (V3) branches of the trigeminal nerve. The cell bodies of trigeminal primary afferent neurons reside within the trigeminal ganglion (TG). Figure created in BioRender.

One particular aspect of the trigeminal pathway that is worth introducing at this point is the trigeminal nerve root. As mentioned above, the trigeminal root acts as a conduit for electrical potentials that are conveyed to the CNS. At a particular point along the course of the trigeminal root, the peripheral nervous system (PNS) interfaces with the CNS. The point at which the two nervous systems meet is known as the central-peripheral myelin transition zone, or the trigeminal root entry zone (TREZ). As the former name implies, there is a transition in the type of myelin that ensheathes the axons traversing the interface. On the PNS side of the interface, myelination is provided by Schwann cells. By contrast, myelination on the CNS side is provided by oligodendrocytes[31]. At the interface, the two nervous systems are physically separated by a barrier structure called the glia limitans which is formed by astrocytes (discussed below)[31]. The TREZ is a structure of particular significance in MS, as it is a well-recognized region in which MS lesions occur[2].

Trigeminal lesions in multiple sclerosis

Hermann Oppenheim was previously mentioned as being one of the first to document an association between MS and trigeminal dysfunction[6]. Oppenheim also provided some of the earliest descriptions of trigeminal pathology in MS tissue[6]. Specifically, Oppenheim observed “a sclerotic focus at the seat where the trigeminus leaves”[6]. It is now recognized that Oppenheim was describing a lesion affecting the trigeminal root[6]. Subsequent to Oppenheim’s initial report, pathologists throughout the 20th century continued to observe lesions affecting not only the trigeminal root, but also the trigeminal tracts that course through the brainstem[6]. These early studies focused on describing gross features of the lesion and were limited to myelin stains of the brainstem and trigeminal root[6,32]. Thus, the cellular and molecular characteristics of trigeminal lesions in MS went, and still are, largely unexplored.

With the popularization of magnetic resonance imaging (MRI) towards the end of the 20th century[6], it became possible to visualize trigeminal abnormalities in living patients. Imaging studies have largely confirmed what early pathologists described (i.e. that MS lesions can affect the trigeminal root and brainstem trigeminal tracts)[2,26–28]. However, imaging studies have revealed that the relationship between radiological abnormalities and facial sensory disturbances is not straightforward. For example, da Silva et al. observed that out of 8 MS patients with trigeminal MRI abnormalities, only 3 presented with altered facial sensation (paresthesia)[26]. Similarly, Cruccu et al. found that out of 50 MS patients without any sign of facial sensory disturbance, 16 showed evidence of a trigeminal lesion[2]. It is not yet clear if asymptomatic radiological lesions eventually turn symptomatic, or if lesions have to be undergoing active pathological processes to be associated with facial sensory disturbances[27]. The discrepancy between radiological and clinical findings can be explained, at least partially, by the relatively low visual fidelity of conventional MRI. Other than being able to visualize the location of a lesion, conventional MRI does not give any indication about pathological processes (e.g. axonal degeneration) that may be occurring within a lesion. MRI technology is constantly evolving, and new imaging protocols have emerged which allow for increasingly detailed examinations of the trigeminal nerve[33]. For example, diffusion tensor imaging, which measures water diffusion within a nerve, is revealing how microstructural changes to the trigeminal nerve is a better predictor of facial sensory disturbance compared to the mere presence of a lesion. In TN for example, diffusion imaging has revealed that vascular compression alone is not sufficient to elicit TN. Rather, severe compression that causes atrophy of nerve fibers appears to be a significantly greater predictor of TN pain[34]. Thus, it may be that in MS, trigeminal lesions require an element of neurodegeneration before becoming symptomatic. Ultimately, there needs to be a better understanding of how MS lesions impact the trigeminal nerve. MS lesions are a manifestation of highly dynamic interactions that occur between numerous different cell types[1,35] - many of which have the capacity to alter the structure and/or function of the trigeminal nerve.

The multiple sclerosis lesion

The pathological hallmark of MS is focal demyelination that is disseminated throughout the CNS[35]. It is generally accepted that demyelination in MS is caused by aberrantly activated immune cells which

infiltrate the CNS parenchyma[1]. At present, the target(s) of these immunes cells is still not entirely clear – though myelin, or myelin-like, molecules have long been suspected[1]. Under normal circumstances, the CNS exhibits a degree of 'immune privilege' and is not as readily accessible to immune cells compared to most other tissues[36]. This relative immune privilege is provided by several barrier structures, such as the blood-brain barrier (BBB), which restrict immune cell migration into the brain and spinal cord parenchyma[37]. In MS, it is believed that there is an initial inflammatory event that compromises the integrity of the blood-brain barrier (BBB)[1,38]. Following a breach in BBB integrity, aberrantly activated immune cells migrate into the CNS parenchyma and trigger additional inflammation, demyelination, and axonal injury/loss. As mentioned above, MS lesions are created by a dynamic interplay between numerous different cell types - chief amongst which are peripherally derived T cells and macrophages, as well as CNS resident microglia and astrocytes.

T cells

T cells are a critical component of the adaptive immune responses which provide the body with targeted and long-term protection from pathogens[39]. T cells circulate through virtually every organ and tissue, including the CNS, and reconnoiter their environment for antigens (any molecule capable of evoking an immune response)[40]. In order to activate T cells, an antigen must first be presented to a T cell, which is usually carried out by an innate immune cell (discussed below)[41]. Additionally, there must be binding of complementary co-stimulatory molecules that are expressed by the T cell (e.g. CD4 and CD8) as well as the antigen presenting cell[41]. Once all requisite binding is achieved, T cells proliferate and differentiate into effector cells which act to clear the source of the antigen from the body. T cells have the capacity to recognize a wide variety of antigens, including those expressed by cells endogenous to the body. In order to prevent T cells from directing an attack against endogenous antigens, there are several mechanisms in place which regulate and 'teach' T cells to be tolerant of endogenously expressed antigens[40].

It is generally believed that MS is caused by aberrantly activated (or insufficiently regulated) effector T cells which infiltrate the CNS parenchyma and incite inflammation, demyelination, and axonal injury[1]. At present it is not entirely clear what initiates the aberrant activation/insufficient regulation of T cells in MS. However, it is recognized that T cell tolerance of CNS myelin (or myelin-like) antigens is impaired[1,38],

which enables T cells to mount an immune response against the CNS. Under normal circumstances, autoreactive T cell entry into the CNS would be restricted by barrier structures such as the BBB and astrocyte glia limitans[36]. However, and for reasons that are still unclear, the integrity of these barriers is compromised in MS which allows the CNS-directed T cells to infiltrate the brain and spinal cord parenchyma[35].

Effector T cells, identified by their expression of markers such as CD4 and CD8, are well-recognized constituents of the cellular infiltrates that associate with MS lesions[1,35]. Several lines of evidence indicate that effector T cells are key contributors to MS pathophysiology. For example, disease exacerbation is associated with increased levels of circulating myelin-reactive T cells[42]. Additionally, administration of exogenous interferon γ, a cytokine produced by CD4+ T cells, exacerbates disease in MS patients[43]. Similarly, blockade of interleukin-17, another cytokine produced by CD4+ T cells, reduces lesion formation in MS[42]. Finally, mutations in genes that encode T cell receptors are the strongest genetic risk factor for developing MS[1,42].

T cell infiltration of the trigeminal pathway has yet to be described in MS. In animal models of neuropathic pain, peripheral nerve injury results in T cells infiltrating into the dorsal horn of the spinal cord[44]. These T cells are believed to be critical contributors to the mechanisms that underlie persistent pathological pain. Indeed, neuropathic pain behaviors after peripheral nerve injury are attenuated in animals lacking CD4+ T cells[45]. Additionally, adoptive transfer of CD4+ T cells into T cell deficient animals is sufficient to induce pain behaviors[45]. Thus, in MS it may be that infiltrating T cells not only drive disease processes, but also influence trigeminal neurons to alter facial sensitivity.

Macrophages and microglia

In contrast to the highly specific nature of the adaptive immune system, the innate immune system acts as a broad, first line of defense against pathogens[41]. Innate immune cells act directly against pathogens but also initiate adaptive immune responses by presenting antigens to T cells[41]. Despite its immune privilege, the CNS is surveilled by innate immune cells that circulate through cerebral blood vessels (e.g. monocytes) or reside in the meninges, choroid plexus, and perivascular spaces (e.g. macrophages)[37].

Under normal circumstances, innate immune cells have restricted access to the brain and spinal cord parencyma[36]. However, this does not mean that the CNS parenchyma lacks a resident innate immune population. Instead, the CNS parenchyma contains microglia, the principle immune cell of the CNS, which can carry out innate immune functions[37]. In response to CNS injury or disease, microglia rapidly activate and monocytes are recruited into the parenchyma where they can differentiate into macrophages[46]. In certain contexts, monocyte-derived macrophages and activated microglia can be neuroprotective and facilitate repair and regeneration[37]. However, both cell types can also fuel neurotoxic inflammation and directly contribute to CNS injury and disease[37,47].

It is well-established that MS lesions contain monocyte-derived macrophages and activated microglia[35]. However, it is not entirely clear how these cells contribute to MS pathophysiology[47]. Relative to healthy individuals, monocytes isolated from the blood of MS patients secrete more inflammatory cytokines and have greater expression of co-stimulatory molecules that are involved in T cell activation[48]. In line with these findings, in an animal model of autoimmune demyelination (discussed below), depleting monocytes attenuates or prevents clinical symptoms and reduces T cell infiltration into the CNS[47]. Despite the seemingly detrimental role that monocytes play in MS, they have also been found to have protective and reparative functions[37]. For example, monocyte-derived macrophages clear growth-inhibitory myelin debris and in an animal model of toxin-induced demyelination, entry of monocytes into the spinal cord coincides with the appearance of remyelinated axons[47].

Like monocyte-derived macrophages, microglia have an incompletely defined role in MS pathophysiology. In both MS and related animal models, microglial activation can be detected prior to the onset of demyelination[46,47]. Activated microglia produce proinflammatory cytokines and toxic mediators that can directly injure oligodendrocytes and neurons[47]. Thus, microglia have been postulated to be instigators of MS. In line with this theory, inhibiting microglia attenuates disease severity in animal models[47]. Additionally, a recent clinical trial demonstrated that minocycline reduced the risk of developing MS after an initial demyelinating event[49]. Minocycline is an antibiotic that acts, in part, by inhibiting microglia. Collectively, these data suggest that microglia promote disease progression in MS. However, microglia

have well-recognized neuroprotective and reparative functions[47]. For example, microglia contribute to clearance of myelin debris and can stimulate oligodendrocyte differentiation to facilitate remyelination[50].

Advancements in genetic models and gene sequencing are dramatically increasing the fields knowledge of the roles that macrophages and microglia play in MS pathophysiology[47,51]. However, it is not known how macrophages and microglia influence the trigeminal system in MS. In animal models of trigeminal neuropathic pain, depletion of macrophages attenuates pain behaviors[52]. Additionally, microglia can directly influence neuronal activity[53] and it is now recognized that microglial activation is sufficient to evoke neuropathic pain behaviors in animals[53]. Therefore, it is possible that macrophages and microglia influence neuronal activity and facial sensitivity in MS.

Astrocytes

Astrocytes are a type of glial cell which are found throughout the CNS[36,54–56]. Astrocytes perform a wide range of functions that are essential for CNS homeostasis. For example, astrocytes maintain extracellular ion concentrations, scavenge toxic reactive oxygen species, and release molecules such as cholesterol and lactate which are used by neurons to form new synapses and create ATP[54]. Astrocytes also create one of the barrier structures, the glia limitans, which contributes to CNS immune privilege[36]. Historically, astrocytes were believed to be passive bystanders in CNS pathologies and the idea that they may actively contribute to disease went unappreciated[56]. It is now known however that astrocytes not only contribute to CNS pathologies[56], but can actively drive neuronal injury and degeneration[55,57].

Astrocytes are exquisitely sensitive to perturbations in the CNS. In response to CNS damage or disease, astrocytes become reactive and undergo a process called astrogliosis[58]. This process is characterized by changes in astrocyte gene expression, morphology, and function[58,59]. Up until relatively recently, reactive astrocytes were only recognized for their role in creating a scar after CNS trauma and disease[58]. This scar was originally demonstrated to be prohibitive to axonal growth[60] and thus astrocytes were shone in a negative light in the context of CNS regeneration[60,61]. However, as various technologies (e.g. transgenic animals and gene sequencing)[62,63] and techniques (astrocyte purification)[64] emerged it became evident that astrocyte functions extend far beyond just making a scar. It is now recognized that reactive

astrocytes can adopt a multitude of phenotypes associated with functions that can range from neuroprotective to neurotoxic[55,57,62,63]. A key concept that has become increasingly apparent is that a reactive astrocytes phenotype is dictated by the context in which it is stimulated[55,63]. For example, astrocytes isolated from the cortices of mice that received a stroke express genes that facilitate synaptogenesis and neuronal survival. By contrast, cortical astrocytes, isolated from animals that received a systemic injection of bacterial endotoxin, express genes associated with synaptic pruning and neurotoxic inflammation[57,63]. Importantly, this study revealed that astrocytes isolated from each condition shared a core set genes associated with activation[63] – giving rise to the concept of pan-reactive astrocyte markers[57,63].

Within the context of MS, there are only few key features of astrocytes that are well-established: (1) astrocytes are found in close association to MS lesions and (2) the cells have a hypertrophic appearance[35] – indicating that the cells are in a reactive state[58]. In the vast majority of histopathological studies, astrocytes in MS lesions are visualized using antibodies directed against glial fibrillary acidic protein (GFAP)[35] – the prototypical marker for astrocytes. However, it is now recognized that GFAP is a pan-reactive marker that is expressed in a variety of activation states[57,63]. Thus, an increase in GFAP gives no indication about specific effector functions. Given the fields reliance on a single pan-reactive marker, it is no surprise that the role of astrocytes in MS lesion dynamics is still not known[65]. Indeed, both beneficial and detrimental functions have been ascribed to astrocytes in MS. For example, it is well-recognized that astrocytes release cytokines and chemokines that disrupt the BBB and recruit peripheral immune cells into the CNS parenchyma[65]. Additionally, astrocytes may act as antigen-presenting cells that activate infiltrating T cells, furthering lesion activity[65]. In contrast to these seemingly detrimental roles, astrocytes phagocytose and clear growth-inhibitory myelin debris[57,65] and act to restrict immune cell infiltration into the CNS parenchyma[62]. Recent studies utilizing single cell gene sequencing have revealed that MS may be influenced by numerous subtypes of astrocytes with unique gene expression profiles[57,66,67]. For example, in an animal model of MS, Wheeler et al. recently identified 7 unique astrocyte populations that expanded or contracted during the course of disease. One of these populations expanded 3-fold during peak disease and was characterized by the expression of proinflammatory genes, suggesting that these astrocytes contribute to disease progression. In line with this idea, inhibiting specific

signaling pathways within this astrocyte population resulted in attenuated disease severity. Unfortunately, data from the remaining 6 populations was not commented on. Nevertheless, the data obtained by Wheeler et al. highlights that the astrocyte response in MS likely involves dynamic subsets of astrocytes. Given that each subset has a unique gene expression profile, the cells within each population may also have unique, and possibly antagonistic, functions which could reconcile the conflicting data that previous studies have generated[65].

Aside from becoming reactive, astrocytes may also be damaged during the course of MS[65,68]. Compared to reactive astrocytes, substantially less is known about the biology of injured astrocytes in MS. In fact, astrocyte injury is a concept that is recognized, but poorly understood, across a variety of CNS pathologies including stroke, Alzheimer's Disease, and Amyotrophic Lateral Sclerosis[59]. In tissue samples obtained from MS patients, Brosnan and Raine observed that astrocyte endfeet appeared swollen and detached from the endothelial basement membrane[68]. Additionally, Magliozzi et al. observed a breakdown of the glia limitans in the cortices of MS patients[69]. Ultimately, the mechanisms and consequences of astrocyte injury are unknown. However, as will be discussed in chapter 3, astrocyte injury in MS may be associated with exacerbated inflammation and axonal injury.

Astrocyte reactivity in MS trigeminal tissue has so far been unexplored. Reactive astrocytes are observed in the trigeminal nucleus caudalis following an injury to a peripheral branch of the trigeminal nerve[70]. These cells are believed to play a key role in the maintenance of trigeminal neuropathic pain, as inhibiting their function suppresses facial pain behaviors in animals[70]. Thus, in addition to potential contributions from T cells and microglia/macrophages, astrocytes are also likely contributors to altered facial sensation in MS.

Animal models of trigeminal dysfunction

Animal models of trigeminal dysfunction predominately focus on elucidating mechanisms of inflammatory and neuropathic pain as well as headache. Vos et al. were the first to adapt the chronic constriction injury model for the trigeminal system. They found that chronic constriction of the infraorbital nerve (CCI-ION) resulted in rats becoming hypersensitive to mechanical stimulation of the face. Additionally, rats with

nerve injury engaged in more face-directed grooming and exhibited spontaneous freezing behaviors, indicating that they may be experiencing facial paresthesia and/or dysesthesia[3]. The work done by Vos et al. was particularly promising because it was the first demonstration of a model that was associated with behavioral changes reminiscent of what is observed in humans with pathological facial pain[2]. Subsequent to the initial report by Vos et al., numerous groups began studying the CCI-ION model and identified cellular and molecular changes underlying the changes in facial sensitivity[71,72]. Unfortunately, despite the popularization of the CCI-ION model, it may be of limited use for the study of MS-related trigeminal sensory disturbances. The peripheral location of the lesion in the CCI-ION model is in stark contrast to the pathology in MS which seems to be centered on the trigeminal root and brainstem tracts[27,28]. This is an important distinction because an injury to a peripheral branch of a nerve elicits behavioral and cellular responses that differ from those evoked by an injury to a sensory nerve root[73]. Additionally, within primary sensory neurons, peripheral nerve injury induces the expression of transcription factors which are not upregulated by sensory root injury[74]. This suggests that there may be unique mechanisms underlying the pain behaviors associated with each injury. Thus, to better understand trigeminal dysfunction in MS, studies should focus on animal models that have damage to the central aspects of the trigeminal nerve.

Experimental autoimmune encephalomyelitis

Experimental autoimmune encephalomyelitis (EAE) is an animal model that is commonly used to study MS[75]. EAE is typically studied in rodents and is induced by immunizing animals against a myelin antigen (e.g. myelin oligodendrocyte glycoprotein (MOG))[75]. Like MS, animals with EAE have CNS inflammation and demyelination that is associated with glial activation and peripheral immune infiltration into the CNS[1,65]. Historically, studies using EAE to study MS have relied solely on monitoring changes in motor function. However, MS is associated with a multitude of non-motor complications including pain, fatigue, and cognitive impairment[1]. It is now recognized that rodents with EAE also exhibit symptoms that extend beyond motor impairment[76]. Aicher et al. were the first to report that mice with EAE show behaviors indicative of altered sensory function. Specifically, they observed that mice with EAE were hypersensitive to a heat stimulus applied to the tail[77]. Subsequently, Olechowski et al. demonstrated that mice with EAE also exhibit tacticle alloynia (a reduced threshold for pain) in the hindpaws[78]. Associated with these

behavioral changes was T cell infiltration in the spinal cord dorsal horn, as well as activation of spinal microglia and astrocytes[78].

Up until relatively recently, trigeminal involvement in EAE was largely unknown. One study observed evidence of trigeminal lesions in mice using MRI. However, behavioral and histological assessment of trigeminal nerve function and pathology was never explored[79]. Given that EAE is associated with sensory changes and exhibits evidence of trigeminal lesions, it was proposed that this model could be an invaluable tool for studying MS-related trigeminal pathology and dysfunction[80].

Summary and purpose

Dysfunction of the trigeminal system can produce a myriad of symptoms which can negatively impact a person's quality of life. Trigeminal dysfunction occurs in a substantial proportion of MS patients but the mechanisms underlying this phenomenon are poorly defined. As a result, treatment options for trigeminal symptoms in MS are limited and there is a surprising lack of clinically relevant animal models in which novel therapeutics can be screened. Therefore, the purpose of this thesis was to identify an animal model that could be used to study the pathophysiology and pathogenesis of trigeminal dysfunction in MS.

In Chapter 1, I assessed the potential of EAE to be used as a model for studying MS-related trigeminal pathology and dysfunction. To do this, I introduced a novel behavioral assay to the lab which enabled me to assess facial sensitivity in freely moving mice.
Hypothesis 1: Mice with EAE show behaviors indicative of altered trigeminal sensation.

In Chapter 2, I investigated how EAE influences trigeminal primary afferent function. This was accomplished by measuring intracellular calcium levels in dissociated TG neurons that were stimulated by agonists or potassium chloride.
Hypothesis 2: Trigeminal ganglion excitability is altered by EAE which will be reflected by changes in intracellular calcium levels.

In Chapter 3, I investigated how astrocyte pathology in EAE may result in axonal injury at the trigeminal root. This was done using a combination of histological, biochemical, and cell culture techniques.

Hypothesis 3: Astrocyte injury results in an exacerbation of trigeminal nerve inflammation, demyelination, and axonal injury.

Chapter 1: Facial hypersensitivity and trigeminal pathology in mice with experimental autoimmune encephalomyelitis

1.0 Introduction

Multiple Sclerosis (MS) is a disease of the central nervous system (CNS) characterized by inflammation and demyelination. Approximately 2-18.5% of MS patients experience trigeminal sensory disturbances (e.g. dysesthesia, hypoesthesia) or trigeminal neuropathic pain (e.g. trigeminal neuralgia)[4,10,81,82]. Magnetic resonance imaging (MRI) studies suggest that trigeminal lesions, presumably plaques of demyelination[32,83,84], occur in 3-23% of MS patients[26,27,85]. Additionally, neurophysiological studies show that trigeminal dysfunction can occur in up to 69% of MS patients[4,82]. The relationship between trigeminal lesions, dysfunction and neuropathic pain in MS is poorly understood. Demyelinated trigeminal fibers can be a source of ectopic nerve impulses[86] that sensitize pain pathways[87]. Ephaptic cross-talk between nociceptive and demyelinated non-nociceptive fibers has also been proposed as a pain mechanism[88]. Demyelination alone however cannot entirely explain trigeminal neuropathic pain in MS[89]. Indeed, many MS patients that show evidence of trigeminal lesions or dysfunction do not experience trigeminal neuropathic pain[4,26,27,82]. Therefore, there must be additional mechanisms underlying MS-related trigeminal neuropathic pain. What is needed is an animal model that exhibits trigeminal pathology similar to that described in MS. In most trigeminal neuropathic pain models, lesions are produced by transecting, ligating or tying loose ligatures around a peripheral branch of the trigeminal nerve[90]. A limitation of these models is that the peripheral location of the lesion contrasts the MRI studies showing abnormalities at the trigeminal root entry zone (TREZ) and brainstem trigeminal nuclei in MS[2,26,27,85].

Experimental autoimmune encephalomyelitis (EAE) is an animal model that is commonly used to study the pathophysiology of MS[91]. Neuropathic-like pain behaviors such as tactile allodynia and thermal hyperalgesia are now well-recognized symptoms of EAE[92]. These behaviors are associated with demyelination, inflammation, glial activation and disrupted excitatory-inhibitory balance in the spinal cord[78,92,93]. To date, all of the studies using EAE to understand pain in MS have assessed sensory changes in the hind paws and/or tails of rodents[92]. Trigeminal lesions, detected with MRI and

immunohistochemistry, have previously been described in mice with EAE[79]. However, an assessment of facial sensitivity in these mice was not carried out. Therefore, we set out to investigate whether mice with EAE show behaviors indicative of altered facial sensitivity. We also looked for immune cell infiltration, glial activation and demyelination at the level of the trigeminal ganglion, TREZ, and trigeminal brainstem complex.

1.1 Methods

1.1.1 Animals

All animal procedures were carried out according to protocols approved by the University of Alberta Health Sciences Animal Care and Use Committee. A total of 62 C57Bl/6 female mice (Charles River, Montreal, QC, Canada) aged 8-10 weeks old were used for this study. Mice were housed in conventional caging (4-5 animals per cage), maintained on a 12 hour light-dark cycle and were given access to food and water *ad libitum*.

The animals used in this study were from two different experiments. 19 animals (11 EAE, 8 control) were used in the first experiment for behavioral assessment and immunohistochemical analysis of trigeminal tissue (ganglia and brainstems). Animals from the first experiment were sacrificed at day 35 post-EAE induction which was designated as the “chronic” stage of the disease. 43 animals were used in the second experiment for immunohistochemical analysis alone. Of the 43 animals, 33 (24 EAE, 9 control) were sacrificed at “disease onset” (see section 2.2) for analysis of trigeminal tissue at that time. The remaining 10 animals (5 EAE, 5 control) were sacrificed at the chronic time point to match the endpoint of the animals in the first experiment. Overall, group numbers are as follows: controls, n=22; onset, n=24; chronic, n=16.

1.1.2 Experimental autoimmune encephalomyelitis induction and assessment

EAE was induced by subcutaneous immunization with 50µg of myelin oligodendrocyte glycoprotein 35-55 (MOG35-55) emulsified in Complete Freund’s Adjuvant (CFA; Sigma-Aldrich, Oakville, ON) at a concentration of 1.5mg/ml. An intraperitoneal injection of 300ng Pertussis toxin (List Biological Laboratories, Cedarlane, Canada) was administered at the time of induction and 48h later. Control

animals were treated with CFA (1.5mg/ml) and Pertussis toxin alone. Post induction, mice were monitored daily and assigned a clinical score according to the following grading scale: Grade 0, mouse appears normal with no overt signs of disease; Grade 1, flaccid or paralyzed tail; Grade 2, mild hind limb weakness with an intact righting reflex; Grade 3, severe hind limb weakness with an impaired righting reflex; Grade 4, unilateral or bilateral hind limb paralysis. Disease "onset" was designated as the day at which a mouse showed the first signs of motor impairment (clinical grade 1 in the majority of cases). On average, disease onset occurred on day 14 post-induction for both experiments.

1.1.3 Air puff testing and behavioral assessment

Behaviors evoked by air puffs applied to the whisker pad have previously been used to assess facial sensitivity in mice after trigeminal injury and inflammation[94]. We implemented a protocol similar to that described by Krzyzanowska et al.[94] but allowed mice to move freely in a box made of wire mesh and transparent acrylic (3.5 x 1.75 x 1.5 in.) to reduce any effects of restraint (see Fig. 1). Prior to the induction of EAE, all mice were tested 3 times on separate days in order to establish a baseline level of sensitivity to air puff stimulation. Post EAE induction, facial sensitivity was assessed weekly starting at day 7 and ending at day 35. Facial sensitivity was also assessed at disease onset when mice showed the first signs of motor impairment. Prior to stimulation, animals were habituated to the test box for 10 min while the experimenter sat quietly in the room. Air puff stimulation consisted of air currents applied 90° to the whisker pad at 10 psi (controlled by a PicoSpritzer II). The air currents were delivered through a blunted 18 gauge needle tip that was manually placed approximately 1 in. from the snout. The temperature of the expelled air puffs did not differ from room temperature (21°C) by more than 0.3°C (measured with a Digi-Sense Thermocouple Thermometer, Cole Parmer, Canada). Three series of 4 air puffs were applied to each side of the face. After a series of air puffs had been applied to each side of the face the next series began on a randomly chosen side after the mouse resumed normal positioning. Overall, a total of 12 air puffs were applied to each side of the face over a period of approximately 6 minutes. On each side of the testing box sat two video cameras (Canon Vixia HF R500) that recorded the behavioral responses evoked by air puff stimulation. Videos were captured at 60 frames per second and were assessed in real-time. Quantification of the behaviors evoked by the air puffs was carried out by

assigning points to particular responses as described by Krzyzanowska et al.[94] Responses were scored as follows: a brisk withdrawal of the head from the stimulus probe or an attempt to attack the probe were each assigned 0.25 points. Unilateral or bilateral forepaw swipes down the snout were assigned 1 point for each swipe (up to a maximum of 2 points). Continuous unilateral or bilateral forepaw swipes down the snout (3 or more) was assigned 1.5 points. Finally, cases in which the mouse did not respond were assigned 0 points. A score for the left and right side of the face was determined by summing the points assigned to each of the behaviors evoked by air puff stimulation. Because we did not manipulate a particular side of the trigeminal system, a total air puff response score was determined by averaging the scores for the left and right sides of the face.

1.1.4 Immunohistochemistry

Mice were euthanized with an overdose of Euthansol (340 mg/ml) and intracardially perfused with saline followed by 4% paraformaldehyde in 0.1M phosphate buffer (PB). The brainstem and trigeminal ganglia were dissected, post-fixed overnight at 4°C and then transferred to a 30% sucrose solution in 0.1M PB until saturated. The tissue was then cut at 20µm (brainstem) or 10µm (trigeminal ganglia) on a cryostat and mounted on glass slides. Sections were washed 3 times in 1X phosphate-buffered saline (PBS), blocked for 1 hr in PBS containing 0.2% triton and 10% normal goat and/or donkey serum (both used for double label immunohistochemistry) and then incubated overnight at room temperature with the primary antibodies. Primary antibody concentrations were as follows: rat anti-CD4 (1:200, Serotec), rabbit anti-glial fibrillary acidic protein (GFAP) (1:1000, Dako), rat-anti GFAP (used for representative dual label immunohistochemistry only, 1:1000, Invitrogen) and Rabbit anti-ionized calcium-binding adapter molecule (Iba1) (1:500, Wako). The primary antibodies were detected with the relevant secondary antibodies conjugated to Alexa 488 or 594 (1:200, Life Technologies). For myelin staining, sections washed three times in 1X PBS and incubated with Alexa 488-conjugated fluoromyelin (1:300, Life Technologies) in 0.2% triton and 10% normal goat serum for 45 mins at room temperature. For visualization of cellular nuclei, all slides were mounted with Vectashield mounting medium containing DAPI (Vector Laboratories) prior to coverslipping.

1.1.5 Image analysis and cell counting

All image analyses and cell counts were performed by an observer blinded to the experimental group that the examined tissue was derived from. Because we did not manipulate a particular side of the trigeminal system, the data presented is the average of the values obtained for the left and right trigeminal structures. It is important to note that the number of animals used for analysis of particular brainstem nuclei does not always match the total number of animals used in the study. The reason for this is two-fold: first, 15 brainstems (from EAE animals only) were collected from the 33 animals scarified at disease onset (the remaining 18 were required for other experiments). However, both ganglia from all 33 of these animals were collected and included in the present study. Second, in a few animals, certain trigeminal nuclei could not be easily identified due to improper positioning of the brainstem during sectioning; only nuclei that could be positively identified were included in the analysis.

1.1.5.1 Trigeminal ganglion

T cell and macrophage levels in the ganglion were qualitatively assessed by manually counting the number of CD4- and Iba1-positive cells, respectively, with DAPI-labeled nuclei. Satellite glial cell activation was also qualitatively assessed by determining the fraction of neurons, identified with DAPI, surrounded by GFAP-positive satellite cells (number of neurons surrounded by GFAP-positive SGCs/total number of neurons). A neuron was considered to be surrounded by immunoreactive satellite glial cells if ≥50% of its circumference was encircled by the satellite cells[95]. Cell counts were performed on 20 times magnification images of the ophthalmic (V1), maxillary (V2) and mandibular (V3) distributions in the left and right ganglia[96]. Values for the left and right ganglia were determined by summing the amount of immunoreactive cells in V1, V2, and V3. An overall ganglion count was then determined by averaging the values for the left and right ganglia.

1.1.5.2 Myelin transition zone

Similar to the ganglion, T cell and macrophage levels were qualitatively assessed by manually counting cells with DAPI-labeled nuclei. GFAP and fluoromyelin immunoreactivity were assessed with NIH Image J by determining the mean optical density after subtracting background grey levels.

1.1.5.3 Brainstem trigeminal nuclei and tracts

Brainstem analyses were performed on 10-times magnification images of the left and right trigeminal nuclei. CD4-positive cells with DAPI-labeled nuclei were manually counted. Using NIH Image J, Iba1, GFAP and fluoromyelin immunoreactivity were qualitatively assessed by determining the percentage area of each nucleus and/or tract occupied by staining[70,72].

1.1.5.4 Image acquisition

All images used for analysis were captured on a Zeiss Axiocam MRm camera (Carl Zeiss, Oberkochen, Germany) using a Zeiss Observer Z1 inverted fluorescence microscope (Carl Zeiss, Oberkochen, Germany). Representative confocal images were captured at 126 and 157.5 (for brainstems) or 252 (for ganglia)-times magnification on a Leica DMI400B microscope (Leica Microsystems, Wetzlar, Germany). Importantly, all images for a particular stain were captured using identical microscope settings.

1.1.6 Statistical analysis

Statistical analyses were conducted using SigmaPlot software version 13.0. Air puff response scores were analyzed using a two way repeated measures ANOVA followed by a Tukey *post hoc* test. Analysis of immunohistochemical data was carried out using one-way ANOVAs. Non-parametric tests (ANOVA on ranks) were used where assumptions were not met. All data are presented as mean ±SEM. Results were considered to be statistically significant if $p<0.05$.

1.2 Results

1.2.1 Air puff stimulation of the whisker pad elicits nociceptive behaviors in mice with EAE.

Figure 1 shows the EAE disease course and the air puff response scores for EAE and control animals over a period of 35 days post induction (PI). At day 7 PI, when EAE mice did not show any overt signs of disease (Fig. 1A), EAE response scores were similar to controls (Fig. 1B) (EAE: 1.9±0.5 vs. CFA: 1.8±0.6, P=0.9). At day 14 PI however, EAE response scores were significantly greater than control animal scores (EAE: 5.3±0.5 vs. CFA: 1.9±0.6, P<0.001). The EAE response scores remained significantly greater than controls for up to 28 days post- induction (Day 21: EAE: 4.8±0.5 vs. CFA:

0.9±0.6, *P*<0.001; Day 28: EAE: 5.3±0.5 vs. CFA: 2.9±0.6, *P*=0.004). EAE response scores were greater than controls at day 35 PI, however this did not reach statistical significance (EAE: 4.2±0.5 vs. CFA: 2.9±0.6, *P*=0.1). We found that the increased sensitivity of EAE mice to air puff stimulation coincided with the time when the mice begin to show signs of motor deficits (Fig. 1A). Indeed, at disease onset (clinical grade 1) EAE response scores were significantly greater than control animal scores (Fig. 1C) (EAE: 3.6±0.6 vs. CFA: 1.9±0.4, *P*=0.034). Figure 1D and E show non-nociceptive (D) and nociceptive (E) behaviors evoked by air puff stimulation in a control and EAE animal, respectively, at day 14 PI. At baseline and in CFA controls, we found that the majority of responses consisted of a brisk withdrawal of the head from the stimulus probe (Fig. 1D). The withdrawal response was also observed in EAE mice. However, mice with EAE responded more frequently with a series of continuous unilateral, and sometimes bilateral, forepaw swipes down the snout (Fig. 1E). Taken together, these data demonstrate prominent and persistent facial hypersensitivity in EAE.

1.2.2 Satellite glial cell activation and immune cell infiltration in the trigeminal ganglia of mice with EAE.

We next set out to identify cellular mechanisms that may underlie the facial hypersensitivity observed in EAE mice. We began by looking for changes in the trigeminal ganglion (TG), where the majority of trigeminal primary afferent cell bodies reside[96]. A previous report demonstrated that satellite glial cells (SGCs) are activated in the dorsal root ganglia (DRG) of mice with EAE[95]. Consistent with this study, we found that the number of TG neurons surrounded by GFAP-positive SGCs increased significantly at disease onset relative to control (Kruskal-Wallis H test H_2=30.108, *P*<0.001, followed by *post hoc* analysis with Dunn's Method, Q=4.764, *P*<0.001) (Fig. 2A, D, J). This increase appeared to be transient however, as the number of neurons surrounded by GFAP-positive SGCs returned to control levels in the chronic stages of the disease (Kruskal-Wallis H test H_2=30.108, *P*<0.001, followed by *post hoc* analysis with Dunn's Method, Q=0.256, *P*=1.00) (Fig. 2A, G, J). T cell levels were also significantly increased in the TG at disease onset relative to control (Kruskal-Wallis H test H_2=39.580, *P*<0.001, followed by *post hoc* analysis with Dunn's Method, Q=6.283, *P*<0.001) (Fig. 2B, E, K). At the chronic stage of the disease, the number of CD4-positive cells in the TG was significantly diminished relative to onset (Kruskal-Wallis H test H_2=39.580, *P*<0.001, followed by *post hoc* analysis with Dunn's Method, Q=2.422, *P*=0.046) (Fig. 2E,

H, K). However, T cell levels in the chronic stage remained significantly greater than controls (Kruskal-Wallis H test H_2=39.580, P<0.001, followed by *post hoc* analysis with Dunn's Method, Q=3.157, P=0.005) (Fig. 2B, H, K). Similar to the pattern of SGC activation, we found a significant but transient increase in TG macrophage levels at disease onset ($F_{2,40}$=10.501, P<0.001) (Fig. 2C, F, I, L). Taken together, these data show that EAE is associated with dynamic changes in glial and immune cell reactivity in the TG.

1.2.3 Inflammation and demyelination at the central-peripheral myelin transition zone in EAE.

The central-peripheral myelin transition zone (TZ) refers to the part of a primary afferent root where CNS myelin interfaces with peripheral nervous system (PNS) myelin[31]. The trigeminal TZ occurs outside of the brainstem in both mice[97] and humans[98] and is easily visualized with GFAP staining (Fig. 5E). In mice with EAE, we found significant demyelination on the CNS side of the TZ at both the onset and chronic stages of the disease ($F_{2,57}$=12.132, P<0.001, followed by *post hoc* analysis with Tukey Test, onset vs. control: q=4.796, P=0.004; chronic vs. control: q=6.671, P<0.001) (Fig. 3A, E, I, L). The degree of demyelination was not significantly different between the onset and chronic time points ($F_{2,57}$=12.132, P<0.001, followed by *post hoc* analysis with Tukey Test, q=2.573, P=0.173). Regions of decreased myelin immunoreactivity (IR) were densely packed with DAPI-labeled nuclei (Fig. 3D, H, L) that likely represent T lymphocytes, macrophages, microglia and astrocytes. Indeed, relative to controls, we found significantly more CD4-positive cells at the TZ in EAE mice at both the onset and chronic time points (Kruskal-Wallis H test H_2=45.238, P<0.001, followed by *post hoc* analysis with Dunn's Method, onset vs. control: Q=6.687, P<0.001; chronic vs. control: Q=3.509, P=0.001) (Fig. 3B, F, J, M). Many of the CD4-positive cells at the TZ in EAE animals co-localized with regions of decreased myelin-IR (Fig. 3H, L, H', L'). Similar to that observed in the TG, the number of CD4-positive cells decreased in the chronic stages of the disease (Fig. 3F, J, M). However, this did not reach statistical significance (Kruskal-Wallis H test H_2=45.238, P<0.001, followed by *post hoc* analysis with Dunn's Method, Q=2.209, P=0.082). We also observed a significant increase in the number of Iba1-positive cells at the TZ of mice with EAE (Kruskal-Wallis H test H_2=27.713, P<0.001, followed by *post hoc* analysis with Dunn's Method, onset vs control: Q=5.131, P<0.001; chronic vs control: Q=3.164, P=0.005) (Fig. 4B, F, J, M). Again, the number of Iba1-positive cells was somewhat diminished in the chronic stages but was not significantly different compared to onset (Kruskal-Wallis H

test H_2=27.713, P<0.001, followed by *post hoc* analysis with Dunn's Method, Q=0.157, P=1.00). Confocal imaging revealed that Iba1-positive cells at the TZ of control animals were small with ramified processes (Fig. 4D', arrow). By contrast, Iba1-positive cells at the TZ of EAE animals were large and amoeboid-shaped (Fig. 4H', L', arrows). When assessing GFAP at the TZ, we observed a significant decrease in staining at disease onset relative to control (Kruskal-Wallis H test H_2=30.046, P<0.001, followed by *post hoc* analysis with Dunn's Method, Q=2.692, P=0.021) (Fig. 4A, E, L). Interestingly, in the chronic stages of the disease, GFAP-IR was restored and was significantly greater than control levels (Kruskal-Wallis H test H_2=30.046, P<0.001, followed by *post hoc* analysis with Dunn's Method, Q=3.074, P=0.006) (Fig. 4A, I, L). Confocal imaging revealed that GFAP-positive cells in control animals had small cell bodies and thin processes (Fig. 4D', arrowhead). By contrast, GFAP-positive cells at the onset and chronic stage had large cell bodies and thick processes (Fig. 4H', L', arrowheads). Additionally, at the chronic stage of the disease we observed that the processes of GFAP-positive cells often enveloped one or more Iba1-positive cells (Fig. 4L', asterisks). Collectively, these data show that EAE is associated with significant demyelination and inflammation at the level of the TREZ.

1.2.4 T cell infiltration, glial activation and demyelination in the trigeminal brainstem complex of mice with EAE.

The central processes of trigeminal afferents terminate primarily within the trigeminal brainstem complex[96]. This complex is a collection of nuclei that consists of the trigeminal principle sensory nucleus (Pr5; Fig. 5A) and the spinal trigeminal nucleus (Sp5)[96]. The spinal trigeminal nucleus can be further divided into the subnucleus oralis (Sp5O; Fig 5. B), subnucleus interpolaris (Sp5I; Fig. 5C) and subnucleus caudalis (Sp5C; Fig. 5D)[96]. At the level of the TREZ, the intrapontine aspect of the trigeminal sensory root (s5) lies adjacent to Pr5 (Fig. 5A) and transitions into the spinal trigeminal tract (sp5) as the primary afferents project caudally[99]. To investigate brainstem mechanisms that may contribute to facial hypersensitivity in EAE, we assessed T cell levels, glial reactivity and myelin integrity at the level of the Pr5, Sp5O, Sp5I and Sp5C.

Very few, if any, CD4-positive cells were found in any of the examined nuclei or tracts in CFA controls. By contrast, significant numbers of CD4-positive cells were found at all levels of the brainstem

complex in EAE mice at both the onset and chronic stages of the disease (Pr5: Kruskal-Wallis H test H_2=22.062, P<0.001, followed by *post hoc* analysis with Dunn's Method, onset vs. control: Q=4.623, P<0.001, chronic vs. control: Q=3.188, P=0.004; Sp5O: Kruskal-Wallis H test H_2=20.411, P<0.001, followed by *post hoc* analysis with Dunn's Method, onset vs. control: Q=3.948, P<0.001, chronic vs. control: Q=3.966, P<0.001; Sp5I: Kruskal-Wallis H test H_2=22.181, P<0.001, followed by *post hoc* analysis with Dunn's Method, onset vs. control: Q=2.908, P=0.011, chronic vs control: Q=3.188, P=0.004; Sp5C: $F_{2,37}$=5.592, P<0.001, followed by *post hoc* analysis with Tukey Test, onset vs. control: q=3.566, P=0.042, chronic vs control: q=4.583, P=0.007) (Fig. 6). The amount of T cells in each nucleus was not significantly different between the two time points (Pr5: Kruskal-Wallis H test H_2=22.062, P<0.001, followed by *post hoc* analysis with Dunn's Method, onset vs. chronic: Q=1.445, P=0.0446; Sp5O: Kruskal-Wallis H test H_2=20.411, P<0.001, followed by *post hoc* analysis with Dunn's Method, onset vs. chronic: Q=0.084, P=1.00; Sp5I: Kruskal-Wallis H test H_2=22.181, P<0.001, followed by *post hoc* analysis with Dunn's Method, onset vs. chronic: Q=1.918, P=0.165; Sp5C: $F_{2,37}$=5.592, P<0.001, followed by *post hoc* analysis with Tukey Test, onset vs. chronic: q=1.160, P=0.693).

We next investigated microglia/macrophage reactivity in the trigeminal brainstem complex with Iba1 (Fig. 7). Compared to CFA controls, the percentage area of each nucleus and adjacent tract occupied by Iba1-positive cells was significantly larger in mice with EAE at both the onset and chronic time points (Pr5: Kruskal-Wallis H test H_2=19.282, P<0.001, followed by *post hoc* analysis with Dunn's Method, onset vs. control: Q=4.051, P<0.001, chronic vs. control: Q=3.516, P=0.001; Sp5O: Kruskal-Wallis H test H_2=17.211, P<0.001, followed by *post hoc* analysis with Dunn's Method, onset vs. control: Q=3.935, P<0.001, chronic vs. control: Q=3.223, P=0.004; Sp5I: $F_{2,22}$=6.859, P=0.005, followed by *post hoc* analysis with Tukey Test, onset vs. control: q=3.728, P=0.039, chronic vs control: q=5.192, P=0.004; Sp5C: Kruskal-Wallis H test H_2=12.866, P=0.002, followed by *post hoc* analysis with Dunn's Method, onset vs. control: Q=3.520, P=0.001, chronic vs. control: Q=2.501, P=0.037). The percentage area of each nucleus and tract occupied by Iba1 staining was not significantly different between the two groups (Pr5: Kruskal-Wallis H test H_2=19.282, P<0.001, followed by *post hoc* analysis with Dunn's Method, onset vs. chronic: Q=0.313, P=1.00; Sp5O: Kruskal-Wallis H test H_2=17.211, P<0.001, followed by *post hoc* analysis with Dunn's Method, onset vs. chronic: Q=0.617, P=1.00; Sp5I: Sp5I: $F_{2,22}$=6.859, P=0.005,

followed by *post hoc* Tukey Test, onset vs. chronic: q=2.630, *P*=0.174; Sp5C: Kruskal-Wallis H test H_2=12.866, *P*=0.002, followed by *post hoc* analysis with Dunn's Method, onset vs. chronic: Q=1.022, *P*=0.921). In CFA controls, Iba1-positive cells had small cell bodies and were highly ramified. In contrast, many of the Iba1-positive cells in EAE animals had large cell bodies and retracted, thick processes (Fig. 7, insets).

We then assessed astroglial reactivity in the trigeminal brainstem complex (Fig. 8). Compared to CFA controls, the percentage area of each nucleus and tract occupied by GFAP-positive cells was significantly increased at the chronic, but not onset, time point (Pr5: Kruskal-Wallis H test H_2=13.461, *P*<0.001, followed by *post hoc* analysis with Dunn's Method, onset vs. control: Q=0.536, *P*=1.00, chronic vs. control: Q=3.347, *P*=0.002; Sp5O: $F_{2,38}$=6.548, *P*=0.004, followed by *post hoc* Tukey Test, onset vs. control: q=1.446, *P*=0.568, chronic vs. control: q=4.901, *P*=0.004; Sp5I: $F_{2,22}$=15.002, *P*<0.001, followed by *post hoc* analysis with Tukey Test, onset vs. control: Q=1.009, *P*=0.758, chronic vs control: q=5.454, *P*=0.002; Sp5C: Kruskal-Wallis H test H_2=21.603, *P*<0.001, followed by *post hoc* analysis with Dunn's Method, onset vs. control: Q=1.925, *P*=0.163, chronic vs. control: Q=2.533, *P*=0.034). In control and EAE onset animals, GFAP-positive cells had small cell bodies and thin processes (Fig. 8A, B, D, E, G, H, J, K, insets). By contrast, in the chronic stages of the disease many of the GFAP-positive cells had a hypertrophic morphology (Fig. 8C, F, I, L, inserts).

Finally, we looked for evidence of demyelination of s5 and sp5 (Fig. 9). Compared to CFA controls, the percentage area of s5 immunoreactive for myelin was not significantly decreased at the onset and chronic stages of the disease ($F_{2,31}$=1.649, *P*=0.209). We did however find evidence of demyelination in some animals (Fig. 9A, B, C). Myelin-IR at the level of Sp5O was also not significantly different at the onset and chronic stages of the disease relative to controls ($F_{2,38}$=2.787, *P*=0.074). However, we did observe demyelination in some animals (Fig. 9D, E, F). At the level of Sp5I, we found significant demyelination at the chronic, but not onset, time point (Kruskal-Wallis H test H_2=6.887, *P*<0.032, followed by *post hoc* analysis with Dunn's Method, onset vs. control: Q=2.245, *P*=0.074, chronic vs. control: Q=2.449, *P*=0.043). While not statistically significant, there was evidence of demyelination at Sp5I in some animals at disease onset (Fig 9G, H, I). Finally, at the level of Sp5C we found significant

demyelination at both the onset and chronic time points (Kruskal-Wallis H test H_2=9.942, P=0.007, followed by *post hoc* analysis with Dunn's Method, onset vs. control: Q=2.752, P=0.018, chronic vs. control: Q=2.794, P=0.016). Across all brainstem regions, the areas of decreased myelin-IR were densely packed with DAPI-labeled nuclei that likely represent macrophages, T-lymphocytes, microglia and astrocytes (Fig. 8B', D', F'). Taken together, these findings demonstrate that EAE is associated with inflammation, glial activation and demyelination throughout the trigeminal brainstem complex.

1.3 Discussion

We show here, for the first time, that mice with EAE exhibit prominent and persistent behaviors indicative of facial hypersensitivity. Previous studies have shown that EAE is associated with tactile and thermal hypersensitivity in the hind paws[78,92]. However, it becomes increasingly difficult to assess pain behaviors in the hind paws because of the progressive motor deficits characteristic of EAE[92]. We found that mice with EAE were able to respond to air puff stimulation for up to three weeks after the development of hind limb weakness. Thus, assessment of orofacial sensitivity represents a novel way to investigate sensory changes in the chronic stages of EAE.

To identify mechanisms that may contribute to facial hypersensitivity in EAE, we looked for cellular changes at several points along the trigeminal primary afferent pathway. Warwick et al. found increased SGC expression of GFAP in the DRG of mice with EAE[95]. Consistent with these findings, at disease onset we found a significant increase in the amount of TG neurons surrounded by GFAP-positive SGCs. This increase was transient however, as the amount of neurons surrounded by GFAP-positive SGCs returned to control levels in the chronic stages of the disease. Xu et al. also found a significant, but transient, increase in GFAP-positive SGCs in the TG after partial ligation of the infraorbital nerve in mice[100]. It is well-recognized that SGCs have the ability to modulate neuronal activity and contribute to facial hypersensitivity induced by peripheral trigeminal injury and inflammation[101,102]. However, it is not yet clear how a transient increase in SGC expression of GFAP relates to changes in facial sensitivity.

In addition to changes in SGC reactivity, we found a significant increase in the amount of T cells and macrophages present within the TG. T cells and macrophages invade sensory ganglia after a

peripheral nerve injury and release cytokines such as tumor necrosis factor (TNF)-α that can directly modulate neuronal excitability[44]. Previous studies have shown increased expression of TNF-α in the DRG of rats with EAE[103,104]. The source of TNF-α is postulated to be T lymphocytes and macrophages that migrate into the DRG[103]. Therefore, T cell- and macrophage-mediated production and release of proinflammatory cytokines in the TG may be one mechanism contributing to facial hypersensitivity in EAE.

At the level of the TREZ, we found that EAE is associated with significant demyelination on the CNS side of the central-peripheral myelin TZ. Accompanying the loss of myelin was a significant increase in the number CD4- and Iba1-positive cells at the TZ. Similar to that observed in the TG, there was a trend towards greater numbers of immune cells at disease onset compared to the chronic stage of the disease. This suggests that inflammation of the extra-pontine aspects of the trigeminal pathway may subside, at least partially, over time. The demyelination and immune cells observed at the TZ in EAE mice represent additional mechanisms that may contribute to facial hypersensitivity in EAE. Demyelinated trigeminal roots in cats and monkeys generate ectopic nerve impulses[86] that may increase the excitability of neurons in the TG and trigeminal brainstem complex[87]. In peripheral nerve injury and inflammation models, immune cells recruited to the injury site release pro-inflammatory cytokines that can sensitize axons and facilitate pain hypersensitivity[72]. Interestingly, we found a transient decrease in GFAP-IR at the TZ at disease onset. GFAP is an intermediate filament protein that is critical for astrocyte activation after nervous system injury and disease[105]. In the EAE model, preventing astrocyte activation has been shown to exacerbate disease progression and immune cell infiltration into the spinal cord[62]. The transient decrease in GFAP expression may therefore reflect a temporary breakdown of the astrocytic barrier that separates the central and peripheral nervous systems and normally functions to restrict leukocyte migration into the CNS[36]. We suspect that the eventual restoration and increased expression of GFAP may be related to the diminished inflammation at the TZ in the chronic stages of the disease.

In EAE mice we found significant T cell infiltration at all levels of the trigeminal brainstem complex. We also found evidence of microglial/macrophage activation and infiltration throughout the complex. Interestingly, we did not find evidence of astrocyte activation at the onset time point. We did however find evidence of astrocyte activation and proliferation in the chronic stages of the disease. This is

consistent with a previous study demonstrating that the astrocyte response in the trigeminal brainstem complex is delayed relative to the microglial response[106]. The delayed response suggests that brainstem astrocytes may play a role in the maintenance, rather than the development, of facial hypersensitivity in EAE. Of the various nuclei that comprise the trigeminal brainstem complex, Sp5C is well-recognized as a critical structure for orofacial pain processing[107]. Compared to Sp5C, relatively less is known about the contribution of Pr5, Sp5O and Sp5I to orofacial nociception. However, there are interconnections between Sp5C and the rostral nuclei that may modulate sensory transmission in the trigeminal brainstem complex[107]. Sp5C has a laminated structure and is morphologically and functionally organized like the spinal cord dorsal horn[96,107]. Peripheral nerve injury elicits an influx of T cells into the dorsal horn that can directly sensitize neurons[108]. Similar to T cells, glial cells can also directly modulate neuronal activity in the dorsal horn[44]. Consistent with our findings, inferior alveolar transection in rats increases the area of Sp5C occupied by Iba1- and GFAP-positive cells[70,72]. Moreover, inhibiting glial function results in a suppression of injury-induced pain behaviors and Sp5C hyperexcitability[70,72]. Therefore, the T cells and activated glia observed at Sp5C may contribute to facial hypersensitivity in EAE just as they do in neuropathic pain models induced by peripheral nerve injury[44]. A recent study has demonstrated that pain hypersensitivity induced by peripheral nerve injury is driven by different cell populations in male and female mice[109]. At present, it is not yet clear if a similar dimorphism applies to central neuropathic pain such as that encountered in EAE and MS. However, Rahn et al. have previously demonstrated that in EAE, female, but not male, mice show neuropathic pain behaviors in the hind paws[110]. Thus, there may be a sexual dimorphism, similar to that described by Sorge et al.[109], in the cell types that mediate pain hypersensitivity in EAE. For a future experiment, we are planning on assessing facial sensitivity in male mice with EAE to examine whether there are sex differences in trigeminal pathology and orofacial pain processing.

Finally, in EAE mice we found demyelination of the intrapontine aspect of the trigeminal sensory root as well as the spinal trigeminal tract. A particularly promising finding from of our study is that the pattern of trigeminal demyelination seen in EAE mice is similar to that described in MS. In a post-mortem study of an MS patient with trigeminal neuralgia (TN), Olafson et al. found plaques at the intrapontine aspect of the trigeminal sensory root and the descending trigeminal tract[32]. Similar observations have

been made in other post-mortem studies of patients with MS and TN (reviewed in Ref. 30). Consistent with these findings, MRI studies have detected abnormalities of the TREZ and/or trigeminal nuclei in 3-23% of MS patients[2,27,85]. Lesions at the TREZ and/or trigeminal brainstem complex have been associated with trigeminal sensory disturbances such as dysesthesia, hypoesthesia, ongoing pain and TN[2].

Our observation of TREZ demyelination in EAE mice may have implications for improving current understanding of the relationship between TREZ demyelination and TN. Briefly, TN is characterized by sharp, stabbing, electric shock-like facial pain that can be triggered by everyday behaviors such as talking and eating[111]. Approximately 2-6% of people with MS have TN[10,81]. Additionally, TN is estimated to be 20-times more common in people with MS compared to the general population[112]. While the exact etiology remains unclear, TN is believed to be caused by TREZ demyelination[88]. Electron microscopy studies have shown demyelination of the TREZ in MS patients with TN[83,84]. Interestingly, in some cases the demyelination extended to the central-peripheral myelin transition zone[84]. Additionally, numerous astrocyte processes were found in close proximity to the regions of demyelination[84]. It is worth noting that the demyelination and astrogliosis described in these studies seems similar to what we observed in EAE mice. Thus, EAE may be a useful model for identifying novel mechanisms, such as neuro-immune interactions, that contribute to the pathophysiology of TN.

In summary, our results demonstrate that mice with EAE show behaviors indicative of facial hypersensitivity. Accompanying these behaviors is immune cell infiltration, glial activation and demyelination at several points along the trigeminal primary afferent pathway. Given that the pattern of trigeminal pathology observed in EAE mice is similar to that described in MS, our data suggest that EAE may be a valuable tool for identifying novel mechanisms underlying MS-related trigeminal neuropathic pain.

1.4 Figures

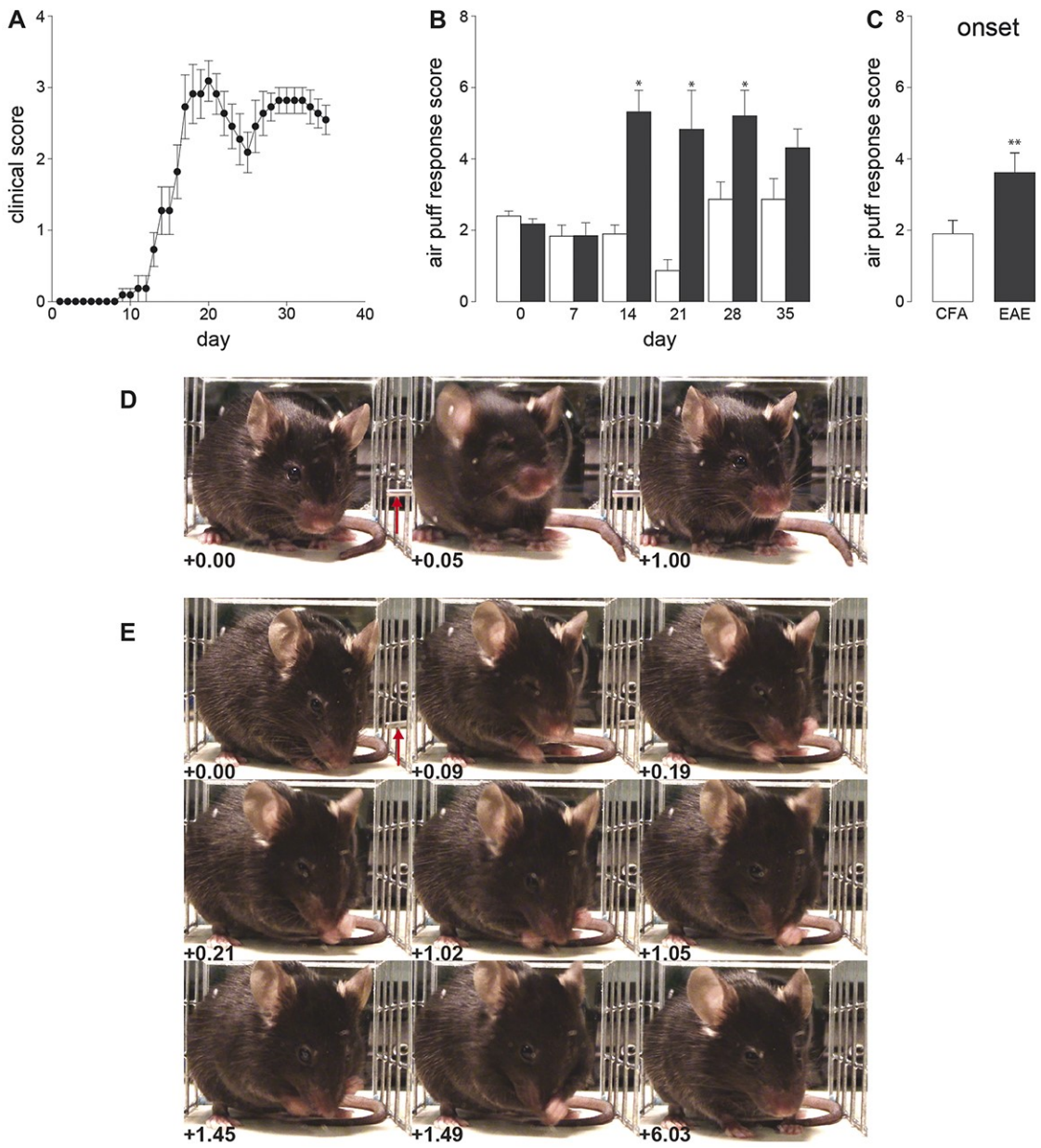

Figure 1.1 Mice with EAE show increased sensitivity to air puffs applied to the whisker pad. (A), Disease progression in EAE mice over a period of 35 days post-induction (PI). (B), EAE (n=11) and control animal (n=8) air puff response scores over the observation period. At day 7 PI, EAE response scores were similar to control animal scores. On days 14, 21 and 28 PI, EAE response scores were significantly greater than control animal scores. EAE response scores remained higher than controls on day 35 PI, however this did not reach statistical significance. (C), At disease onset (clinical grade 1), the response scores of EAE mice

were significantly greater than the scores for control animals tested on the same day. (D), Representative non-nociceptive response typically observed at baseline and in CFA controls. The response consists of a brisk withdrawal of the head away from the stimulus probe (arrow) followed by a return of the head to resting position. (E), Example of a nociceptive response evoked by air puff stimulation in an EAE animal at day 14 PI. Note the continuous unilateral forepaw swipes down the snout. The arrow in E indicates the position of the stimulus probe. The time, in seconds, after the stimulus has been applied is shown in the bottom-left corner of each frame. 0.00 indicates the time at which the air puff is being applied. Number of animals in each group are as follows: CFA: n=8, EAE: n=11. $^{*}P < 0.05$, two-way repeated measures ANOVA followed by *post hoc* Tukey Test, $^{\#}P < 0.05$, *t*-test. Data is mean ±SEM.

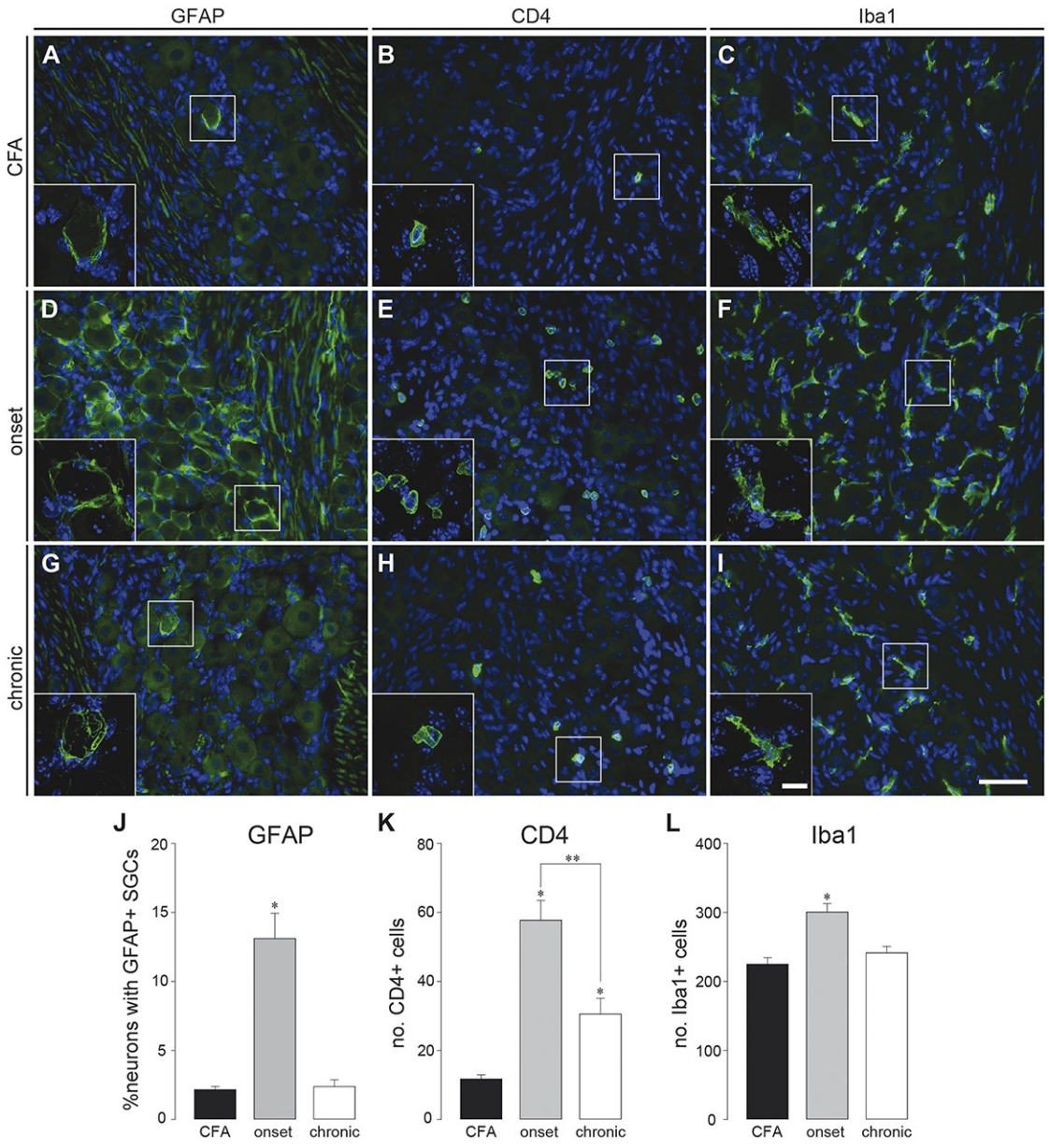

Figure 1.2 Satellite glial cell (SGC) activation and immune cell infiltration in the trigeminal ganglia (TG) of mice with EAE. Compared to controls (A), the number of TG neurons surrounded by GFAP-positive SGCs was significantly increased at the onset (D), but not chronic (day 35 post-EAE induction, G), stage of the disease (J). Significantly more CD4-positive T cells were found in the TG at disease onset (E) relative to control (B). The number of CD4-positive cells in the TG at the chronic stage of EAE (H) was significantly diminished compared to onset, but remained significantly greater than controls (K). Similar to GFAP-positive SGCs, the number of Iba1-positive macrophages in the TG was significantly increased at the onset (F), but

not chronic (I), time point relative to controls (C, L). Number of animals in each group are as follows: (J), CFA: n=22, onset: n=23, chronic: n=15; (K), CFA: n=22, onset: n=24, chronic: n=15; (L), CFA: n=14, onset: n=24, chronic: n=5. *P<0.05 relative to control, Kruskal-Wallis H test followed by *post hoc* analysis with Dunn's Method. **P=0.059, one-way ANOVA followed by *post hoc* Tukey Test. $^{\#}P$<0.05, Kruskal-Wallis H test followed by *post hoc* analysis with Dunn's Method. Scale bar in I = 50μm and applies to all images. Scale bar in the inset in I =10μm and applies to all other scale bars. Data is mean ±SEM.

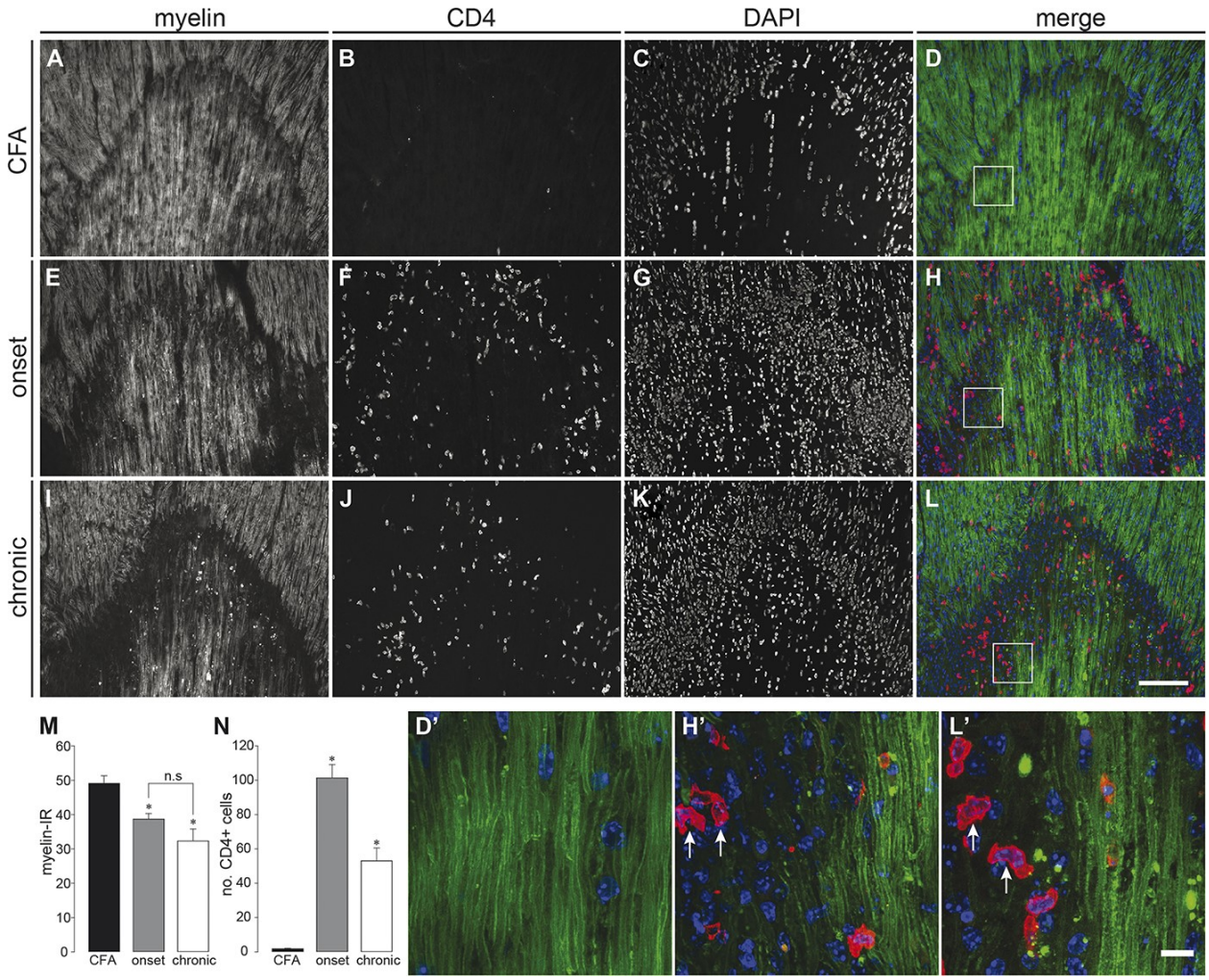

Figure 1.3 Demyelination and T cell infiltration at the central-peripheral myelin transition zone (TZ) in EAE mice. Myelin-immunoreactivity (IR) at the TZ was significantly decreased (M) in EAE animals (E, I) compared to CFA controls (A). The degree of demyelination was not significantly different between the onset and chronic (day 35 post-EAE induction) stage of the disease. (N), significantly more CD4-positive T cells were found at the TZ in EAE animals at both the onset (F) and chronic time points (J) relative to controls (B). There also appeared to be an increase in the number DAPI-labeled nuclei at the TZ of EAE animals compared to controls (C, G, K, not quantified). (D'), 126-times magnification confocal image of the area outlined in D. (H', L'), 126-times magnification confocal images of the areas outlined in H and L, respectively, showing regions of demyelination adjacent to myelinated axons. T cells in the regions of demyelination can be seen in each (arrows). Number of animals in each group are as follows: (L), CFA:

n=22, onset: n=24, chronic: n=14; (M), CFA: n=22, onset: n=23, chronic: n=13. *P<0.05 relative to control, one-way ANOVA followed by *post hoc* Tukey Test (M), Kruskal-Wallis H test followed by *post hoc* analysis with Dunn's Method (N). **P=0.082, Kruskal-Wallis H test followed by *post hoc* analysis with Dunn's Method. n.s = not significant. Scale bar in L = 100μm and applies to A-L. Scale bar in L' = 10μm and applies to D', H' and L'. Data is mean ±SEM.

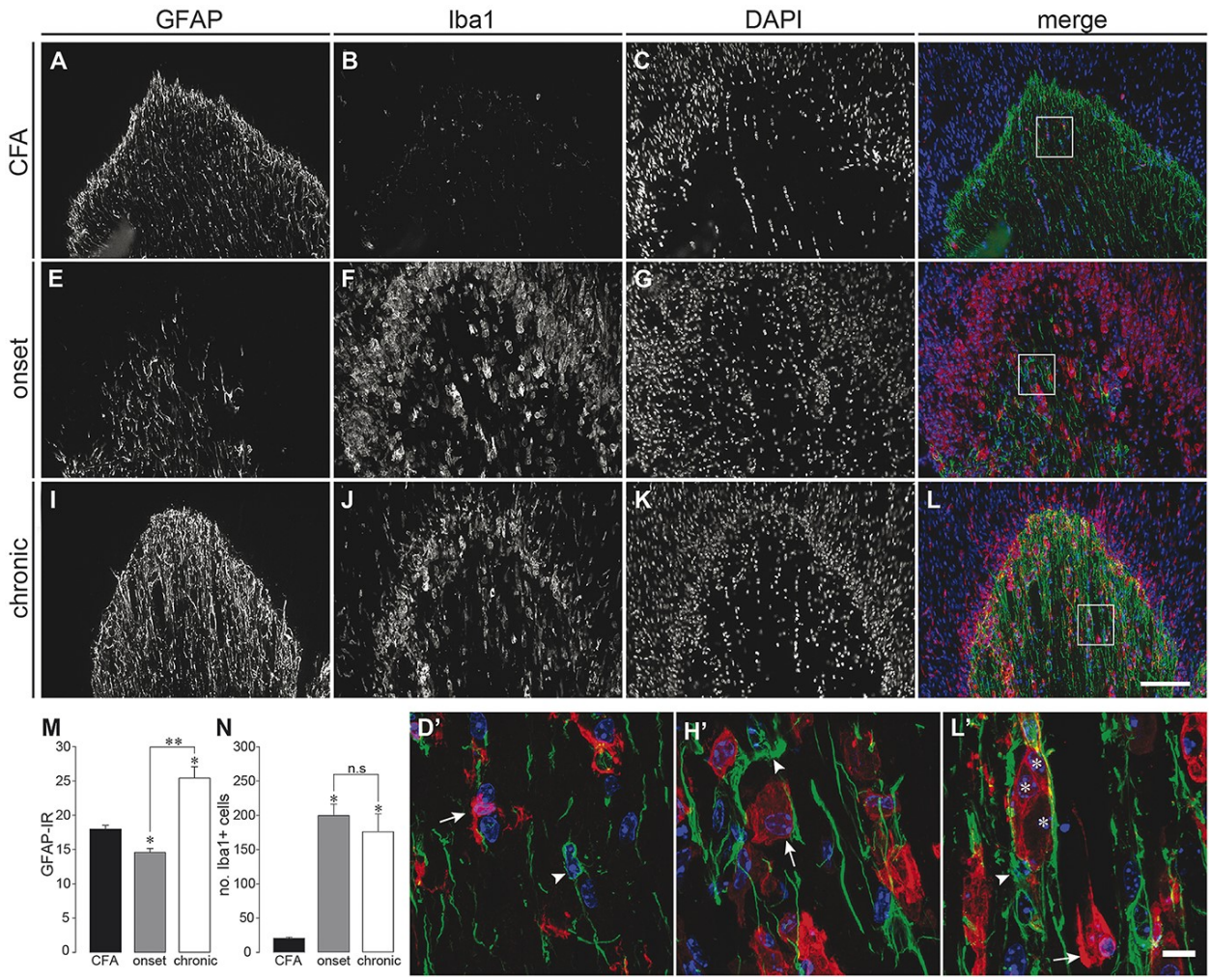

Figure 1.4 Astrocyte and microglia/macrophage activation at the central-peripheral myelin transition zone in mice with EAE. (M), compared to CFA controls (A), GFAP-immunoreactivity at the TZ was significantly decreased at disease onset (E). At the chronic time point, GFAP-IR was restored and significantly increased relative to controls (I). (N), the number of Iba1-positive cells was significantly increased at both the onset (F) and chronic (J) stage of the disease relative to controls. (D'), 126-times magnification confocal image of the region outlined in D. The arrow indicates a representative Iba-1 positive cell with a small soma and ramified processes. The arrowhead indicates a GFAP-positive cell with a thin cell body and processes. (H', L'), Confocal images of the regions outlined in H and L, respectively. Many of the GFAP positive cells at the TZ of EAE animals had thickened cell bodies and processes (arrowheads). Compared to the cells observed in CFA controls, Iba1-positive cells in EAE animals were large and amoeboid-shaped (arrows).

At the chronic stage of the disease, many of the Iba1-positive cells appeared to be enveloped by the processes of GFAP-positive cells (asterisks). Number of animals in each group are as follows: (L), CFA: n=22, onset: n=23, chronic: n=14; (M), CFA: n=14, onset: n=24, chronic: n=5. $^{*}P<0.05$ relative to control, Kruskal-Wallis H test followed by *post hoc* analysis with Dunn's Method. $^{**}P<0.001$, Kruskal-Wallis H test followed by *post hoc* analysis with Dunn's Method. n.s = not significant. Scale bar in L = 100μm and applies to A-L. Scale bar in L' = 10μm and applies to D', H' and L'. Data is mean ±SEM.

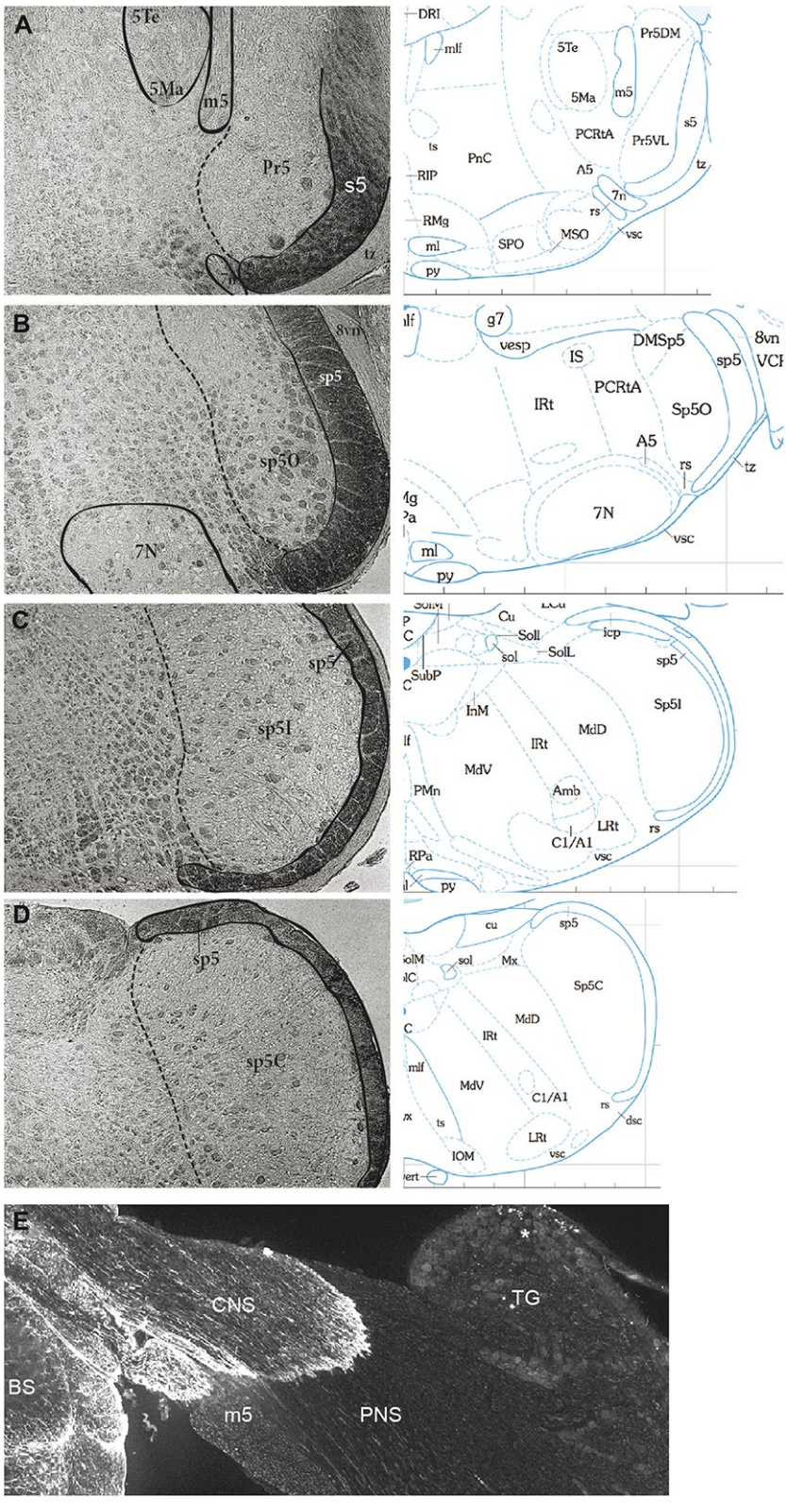
A
5Te
5Ma
m5
Pr5
s5
tz
DRI
mlf
5Te
Pr5DM
5Ma
m5
s5
PCRtA
Pr5VL
ts
PnC
A5
tz
RIP
7n
rs
RMg
MSO
vsc
ml
SPO
py
B
8vn
sp5
sp5O
7N
g7
vesp
IS
DMSp5
8vn
sp5
PCRtA
IRt
Sp5O
A5
rs
tz
7N
vsc
ml
py
C
sp5
sp5I
Cu
SolI
icp
sol
SolL
sp5
SubP
InM
Sp5I
MdD
IRt
MdV
PMn
Amb
LRt
rs
C1/A1
RPa
vsc
py
D
sp5
sp5C
cu
sp5
sol
Mx
Sp5C
MdD
IRt
MdV
C1/A1
rs
ts
dsc
LRt
vsc
IOM
E
CNS
TG
BS
m5
PNS

Figure 1.5 Anatomy of the trigeminal brainstem complex and central-peripheral myelin transition zone (TZ). (A), Phase contrast image of the principle sensory nucleus (Pr5) and the intrapontine portion of the trigeminal sensory root (s5). (B-D), Phase contrast images of the subnucleus oralis (Sp5O; B), interpolaris (Sp5I; C) and caudalis (Sp5C; D). Adjacent to the oral, interpolar and caudal nuclei is the spinal trigeminal tract (sp5). Pictured next to each image is the stereotactic atlas figure that was used to identify each nucleus (adapted from ref. 98). (E), horizontal section of the trigeminal nerve stained for GFAP demonstrating the relationship between the brainstem, TZ and trigeminal ganglion (TG). Note that the TZ occurs outside of the brainstem and the clear demarcation of the CNS-PNS border. Also evident are the cell bodies of neurons belonging to the mandibular (V3) distribution of the trigeminal nerve. Scale bar in E = 200μm and applies to A-E.

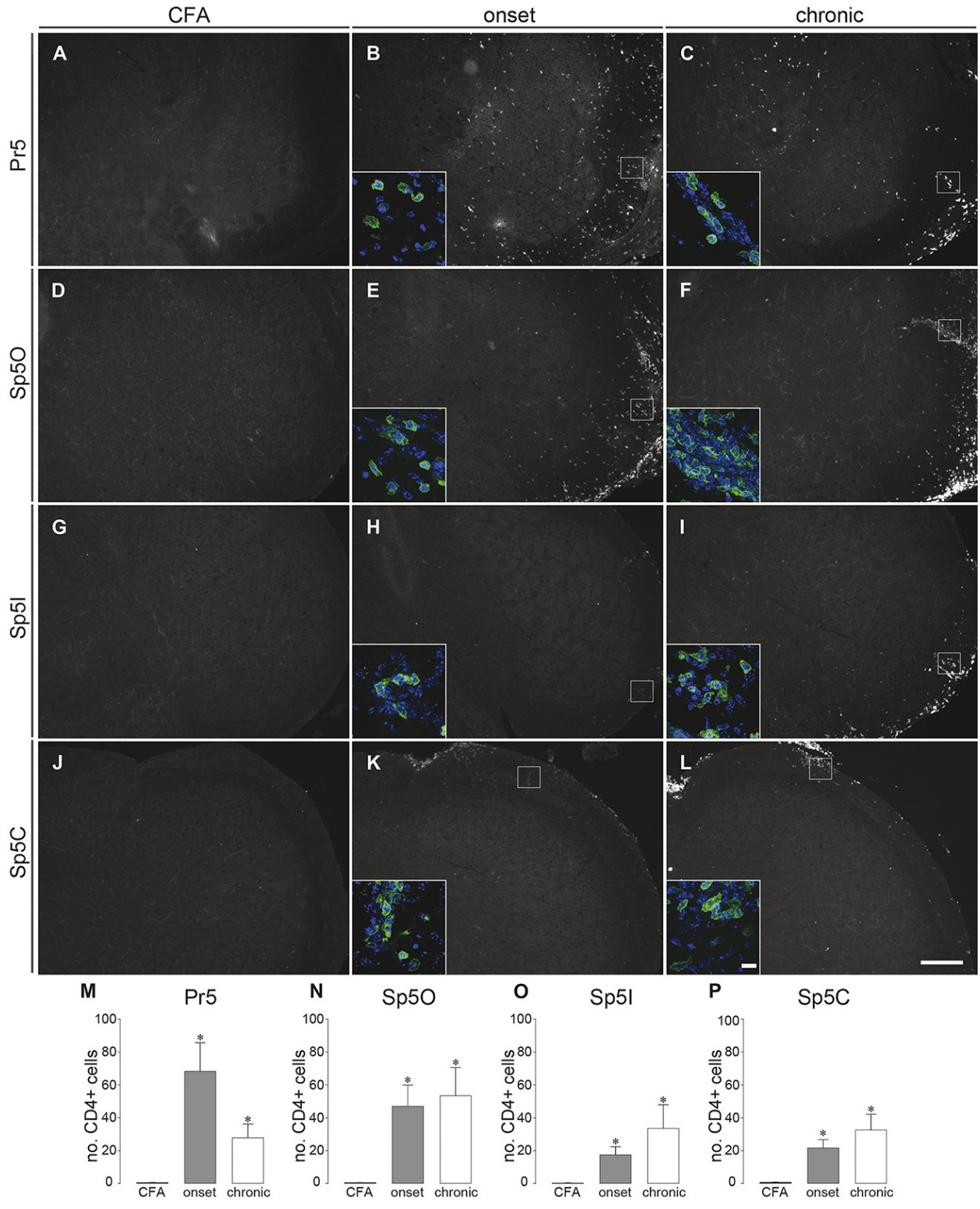
CFA
onset
chronic
A
B
C
Pr5
D
E
F
Sp5O
G
H
I
Sp5I
J
K
L
Sp5C
M
Pr5
N
Sp5O
O
Sp5I
P
Sp5C
no. CD4+ cells
0
20
40
60
80
100
CFA
onset
chronic

Figure 1.6 T cell infiltration in the trigeminal brainstem complex of mice with EAE. (A-L), Representative images showing CD4 immunoreactivity in the trigeminal brainstem complex of control animals (A, D, G, J) and animals with EAE sacrificed at the onset (B, E, H, K) or chronic (day 35 post induction; C, F, I, L) time point. (M-P), Compared to controls, significantly more T cells were found at each level of the trigeminal brainstem complex in EAE animals. For each level of the complex, T cell levels were not significantly different between the two time points. Insets are 157.5-times magnification images of the cell(s) outlined in each picture demonstrating that staining is associated with DAPI-labeled nuclei. The number of animals in each group are as follows: (M), CFA: n=11, onset: n=14, chronic: n=13; (N), CFA: n=12, onset: n=15, chronic: n=14; (O), CFA: n=12, onset: n=15, chronic: n=5; (P), CFA: n=11, onset: n=15, chronic: n=14. **P*<0.05 relative to control, Kruskal-Wallis H test followed by *post hoc* analysis with Dunn's Method (M, N, O), one-way ANOVA followed by *post hoc* Tukey Test (P). Scale bar in L = 200μm and applies to A-L. Scale bar in the inset in L = 10μm and applies to all insets. Data is mean ±SEM.

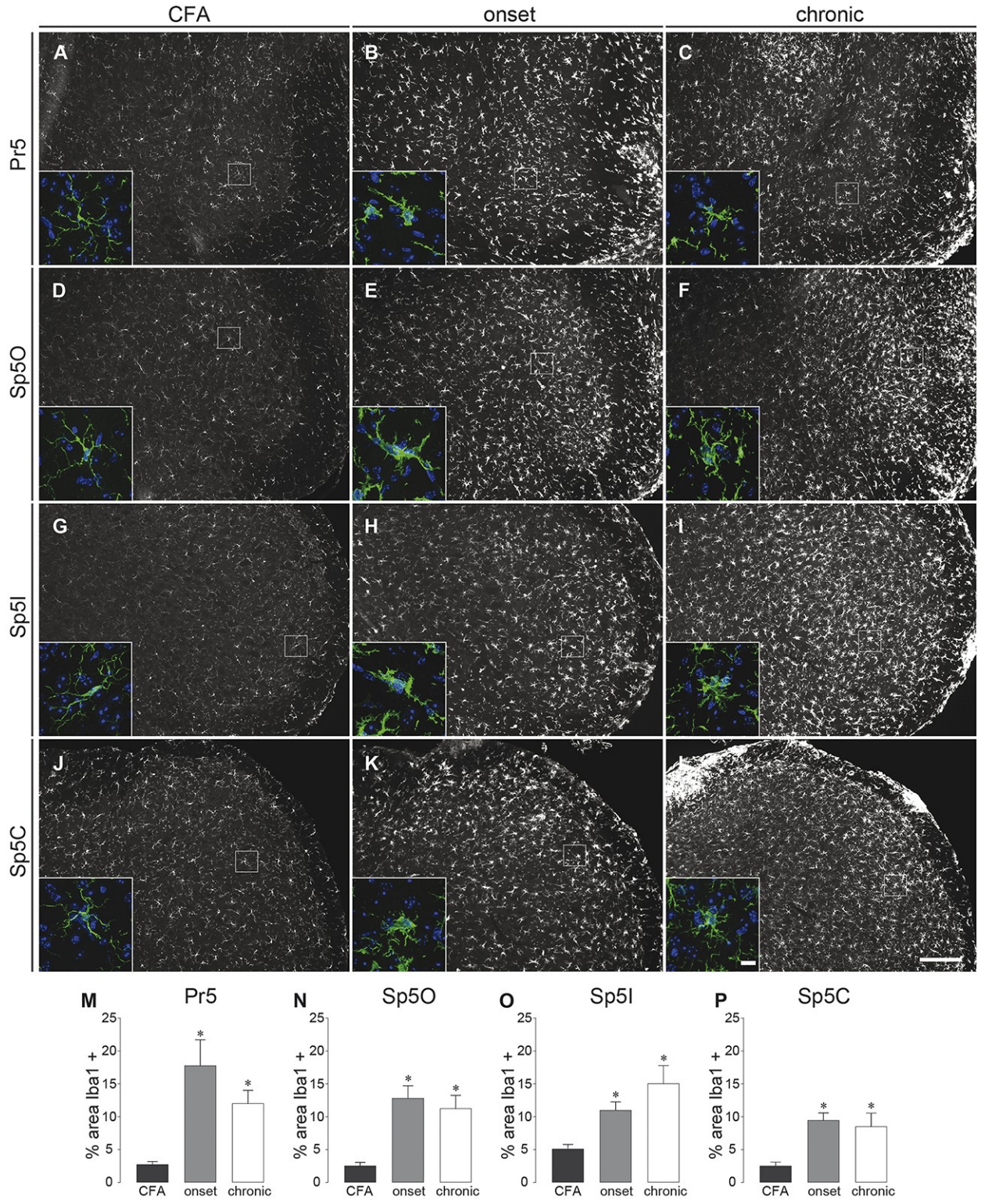
CFA
onset
chronic
Pr5
Sp5O
Sp5I
Sp5C
A
B
C
D
E
F
G
H
I
J
K
L
M
Pr5
N
Sp5O
O
Sp5I
P
Sp5C
% area Iba1 +
0
5
10
15
20
25
CFA
onset
chronic
*

Figure 1.7 Microglia/macrophage activation in the trigeminal brainstem complex of mice with EAE. (A-L), Representative images showing microglia/macrophage immunoreactivity (IR) in the trigeminal brainstem complex of control animals (A, D, G, J) and animals with EAE sacrificed at the onset (B, E, H, K) or chronic (day 35 post induction; C, F, I, L) time point. The percentage area of each nucleus and tract occupied by Iba1 staining was significantly greater in EAE animals compared to controls. No significant difference between the two groups was detected. Insets are 157.5-times magnification confocal images of the cell(s) outlined in each picture demonstrating that staining is associated with DAPI-labeled nuclei. Iba1-positive cells in CFA controls had thin, highly ramified processes. By contrast, Iba1-positive cells in EAE animals had short, thick processes. The number of animals in each group are as follows: (M), CFA: n=12, onset: n=14, chronic: n=11; (N), CFA: n=12, onset: n=15, chronic: n=13; (O), CFA: n=5, onset: n=15, chronic: n=5; (P), CFA: n=12, onset: n=15, chronic: n=14. *P<0.05 relative to control, Kruskal-Wallis H test followed by *post hoc* analysis with Dunn's Method (M, N, P), one-way ANOVA followed by *post hoc* Tukey Test (O). Scale bar in L= 200 µm and applies to A-L. Scale bar in the inset in L = 10µm and applies to all insets. Data is mean ±SEM.

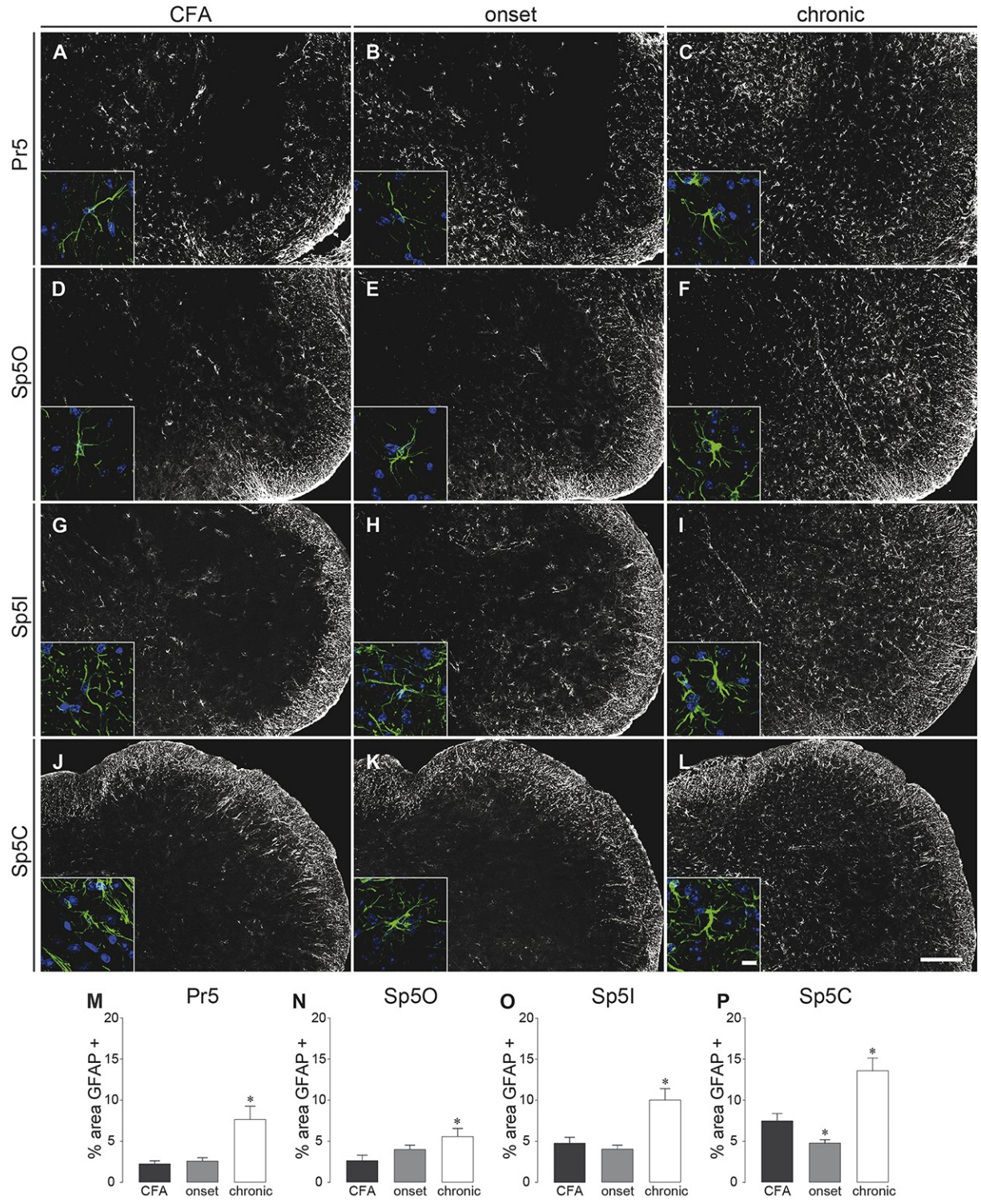
CFA
onset
chronic
Pr5
Sp5O
Sp5I
Sp5C
A
B
C
D
E
F
G
H
I
J
K
L
M
Pr5
N
Sp5O
O
Sp5I
P
Sp5C
% area GFAP +
0
5
10
15
20
CFA
onset
chronic
*

Figure 1.8 Astrocyte activation in the trigeminal brainstem complex of mice with EAE. (A-L), Representative images showing GFAP immunoreactivity (IR) in the trigeminal brainstem complex of control animals (A, D, G, J) and animals with EAE sacrificed at the onset (B, E, H, K) or chronic (day 35 post induction; C, F, I, L) time point. Compared to controls, the percentage area of each nucleus and tract occupied by GFAP staining was significantly increased in EAE animals at the chronic, but not onset, stage of EAE. For each level of the complex, GFAP immunoreactivity was not significantly different between controls and animals sacrificed at disease onset. Insets are 157.5-times magnification confocal images of representative cells from each picture demonstrating that staining is associated with DAPI-labeled nuclei. GFAP-positive cells in control animals and mice sacrificed at onset had thin cell bodies and processes. By contrast, GFAP-positive cells in mice sacrificed at the chronic time point were hypertrophic with thickened cell bodies and processes. The number of animals in each group are as follows: (M), CFA: n=12, onset: n=14, chronic: n=14; (N), CFA: n=12, onset: n=15, chronic: n=14; (O), CFA: n=5, onset: n=15, chronic: n=5; (P), CFA: n=12, onset: n=15, chronic: n=13. *P<0.05 relative to control, Kruskal-Wallis H test followed by *post hoc* analysis with Dunn's Method (M, P), one-way ANOVA followed by *post hoc* Tukey Test (N, O). Scale bar in L= 200μm and applies to A-L. Scale bar in the inset in L = 10μm and applies to all insets. Data is mean ±SEM.

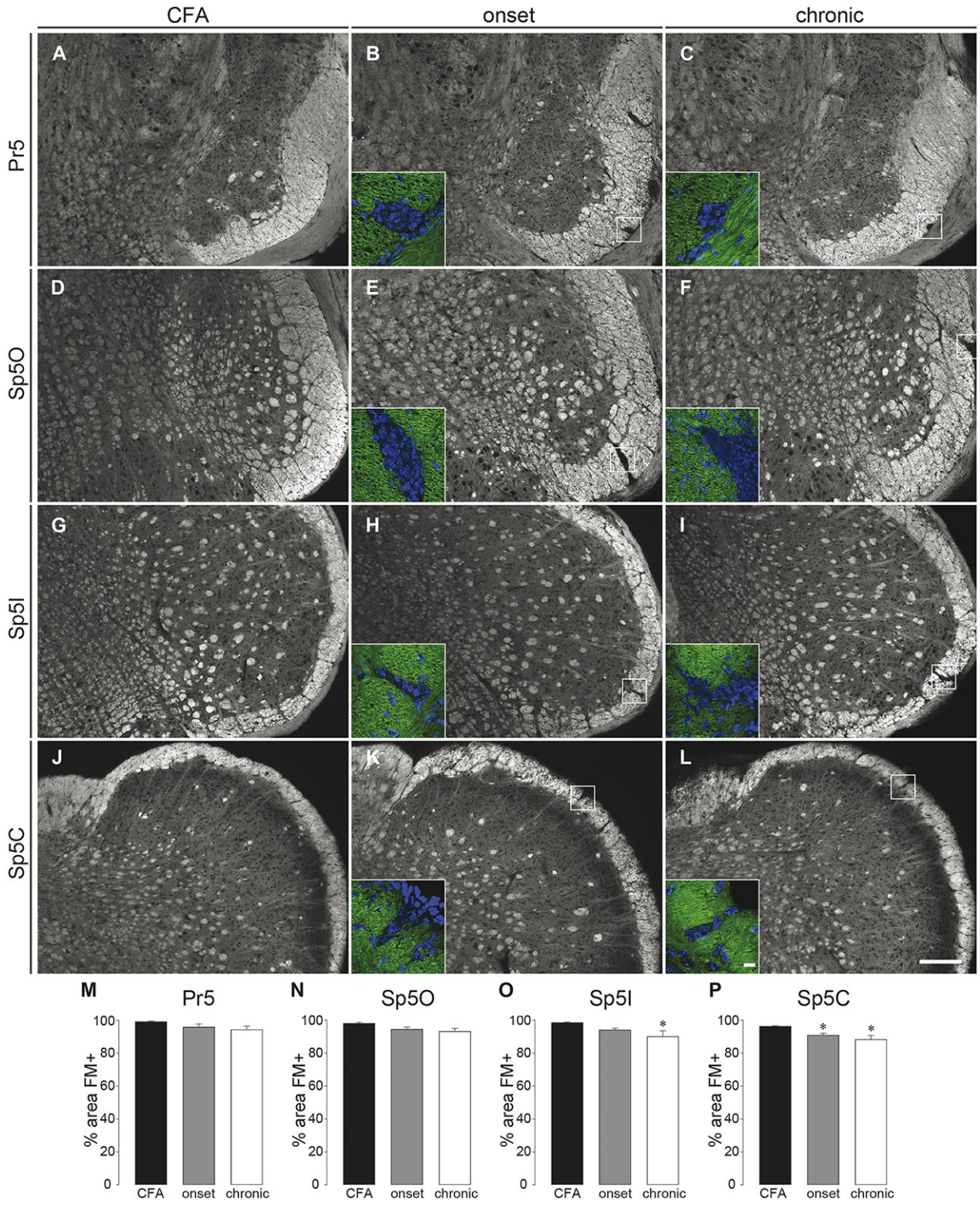
CFA
onset
chronic
Pr5
Sp5O
Sp5I
Sp5C
A
B
C
D
E
F
G
H
I
J
K
L
M
Pr5
N
Sp5O
O
Sp5I
P
Sp5C
% area FM+
100
80
60
40
20
0
CFA
onset
chronic
*

Figure 1.9 Demyelination of the intrapontine trigeminal sensory root and spinal trigeminal tract in mice with EAE. Representative images showing fluoromyelin immunoreactivity (IR) in the trigeminal brainstem complex of control animals (A, D, G, J) and animals with EAE sacrificed at the onset (B, E, H, K) or chronic (day 35 post induction; C, F, I, L) time point. The percentage area of s5 immunoreactive for myelin was not significantly different between the groups (M). Similarly, at the level of Sp5O, the percentage area of sp5 immunoreactive for myelin was not significantly decreased in EAE animals relative to controls (N). Significant demyelination of sp5 at the level of Sp5I was detected at the chronic, but not onset, time point (O). At the level of Sp5C, the percentage area of sp5 immunoreactive for myelin was significantly decreased at both the onset and chronic time points. Insets are 126-times magnification confocal images of the regions outlined in each picture demonstrating that regions of decreased myelin immunoreactivity are packed with DAPI-labeled nuclei. The number of animals in each group are as follows: (M), CFA: n=10, onset: n=15, chronic: n=9; (N): CFA: n=13, onset: n=15, chronic: n=13; (O), CFA: n=5, onset: n=15, chronic: n=5; (P), CFA: n=12, onset: n=15, chronic: n=14. *P<0.05 relative to control, Kruskal-Wallis H test followed by *post hoc* analysis with Dunn's Method (O, P), one-way ANOVA followed by *post hoc* Tukey Test (M, N). Scale bar in L= 200μm and applies to A-L. Scale bar in the inset in L = 10μm and applies to all insets. Data is mean ±SEM.

Chapter 2: Assessment of trigeminal primary afferent excitability in EAE

2.0 Introduction

CNS injury-induced changes to the structure and/or function of the PNS is a concept that is underappreciated in neuroscience. This notion is exemplified by the MS and EAE literature, which is dominated by studies that focus on the CNS. However, some of the symptoms associated with MS and EAE may be caused, at least in part, by pathological process that take place within PNS. For example, pain in MS and EAE may arise from cellular and molecular changes that occur within sensory ganglia[80,113–115]. In support of this idea, Yousuf et al. recently observed that immune cells infiltrate dorsal root ganglia in MS and EAE[114]. In mice with EAE, this immune infiltration was associated with increased expression of proinflammatory cytokines and neuronal hyperexcitability[113], changes that likely contribute to the pain behaviors observed in EAE. As discussed in the previous chapter, EAE is also associated with immune cell infiltration in the TG[80]. However, the impact of EAE on TG neuron function has yet to be examined. Thus, the goal for this chapter was to assess the excitability of TG neurons isolated from animals with EAE.

2.1 Methods

2.1.1 Animals

All animal procedures were carried out according to protocols approved by the University of Alberta Health Sciences Animal Care and Use Committee. A total of 12 C57Bl/6 female mice (Charles River, Montreal, QC, Canada) aged 8-10 weeks old were used for this study. Mice were housed in conventional caging (4-5 animals per cage), maintained on a 12-hour light-dark cycle, and were given access to food and water *ad libitum*.

2.1.2 EAE induction and assessment

EAE was induced by subcutaneous immunization with 50µg of myelin oligodendrocyte glycoprotein 35-55 (MOG35-55) emulsified in Complete Freund's Adjuvant (CFA; Sigma-Aldrich, Oakville, ON) at a

concentration of 1.5mg/ml. An intraperitoneal injection of 300ng Pertussis toxin (List Biological Laboratories, Cedarlane, Canada) was administered at the time of induction and 48h later. Control animals were treated with CFA (1.5mg/ml) and Pertussis toxin alone. Post induction, mice were monitored daily and assigned a clinical score according to the following grading scale: Grade 0, mouse appears normal with no overt signs of disease; Grade 1, flaccid or paralyzed tail; Grade 2, mild hind limb weakness with an intact righting reflex; Grade 3, severe hind limb weakness with an impaired righting reflex; Grade 4, unilateral or bilateral hind limb paralysis. Disease "onset" was designated as the day at which a mouse showed the first signs of motor impairment (clinical grade 1 in the majority of cases).

2.1.3 TG culture for Ca2+ imaging experiments

15mm coverslips were placed in a 12-well plate and were coated with poly-D lysine (25ug/ml) overnight at 4˚C. The following morning, the PDL was removed and the coverslips were washed five times with tissue culture water. The coverslips were then allowed to dry in a tissue culture hood. Just prior to dissection, the coverslips were coated with laminin diluted in modified Hank's Balanced Salt Solution (mHBSS) to a final concentration of 10ug/ml.

Mice in this experiment were euthanized at the disease onset timepoint (see above). Under terminal anesthesia (0.1mL of 340mg/mL euthansol), mice were intracardially perfused with ice-cold 0.9% saline. The TG were then dissected, collected in Hank's Balanced Salt Solution (HBSS) and transferred to a sterile conical tube. The DRGs were then washed three times with HBSS (1mL/wash). After the final wash, the HBSS was replaced with 3mL of HBSS containing 2mg/mL collagenase type IV (Worthington) and 0.1mg/mL DNase (Worthington). The DRG-containing conical was then placed in a water bath (heated to 37°C) with gentle shaking. After 45min in the enzyme solution, the tissue was gently triturated with a p1000 pipette 40 to 50 times and the conical was returned to the water bath for an additional 10-15 mins. The tissue was then triturated with a p1000 pipette (20-30 times) followed by a p200 pipette (20-30 times). Once the tissue was digested, the conical was centrifuged (5 mins at 500 r.c.f) and 2 mL of the enzyme solution was removed. The cell pellet was then resuspended in the remaining enzyme solution, which was subsequently passed through a 70uM filter and then placed onto 2mL of 150mg/mL bovine serum albumin (BSA). The conical was centrifuged again (5 mins at 900 r.c.f) and the supernatant was

aspirated. The cell pellet was then resuspended in 2mL of DMEM/F12 and centrifuged again (5 mins at 500 r.c.f). The DMEM/F12 was aspirated and the pellet was resuspended in DMEM/F12 containing 1% N2 and 1% penicillin/streptomycin (cell media). The cell suspension was then spread across 15mm glass coverslips which were then transferred to an incubator (37oC, 5% CO2). One hour after plating, wells with coverslips were flooded with 1mL of warm cell media.

2.1.3 Calcium Imaging

Calcium imaging was carried out 16-18h after the neurons were placed on the coverslips. Prior to imaging, each coverslip was incubated at 37^{o}C in HBSS containing Fluo-4 AM for 30 mins. After the incubation period, each coverslip was then transferred to a chamber that was continually perfused (4mL/min) with artificial cerebrospinal fluid (ACSF; in mM; 120 NaCl, 3 KCl, 1 $CaCl_2$, 2 $MgSO_4$, 20 glucose). After a 5-10 min acclimation period, a 5 minute recording was initiated which consisted of: 30s perfusion with ACSF, 30s perfusion with ACSF containing a specific agonist (see below), 4min perfusion with ACSF. A second recording was initiated 1-2 min after the first and consisted of: 30s perfusion with ACSF, 30s perfusion with ACSF containing 30mM KCl, 4min perfusion with ACSF. The recordings were carried out on an Olympus FV1000. Images were captured at 1 frame per second and all image acquisition settings were kept constant throughout the experiment. Analysis of Ca2+ dynamics was extracted using Olympus FV10-ASW software.

2.1.4 Statistical Analysis

Data were analyzed using Prism Software. Comparisons of cell sensitivity to various agonists, as well as the amplitude of evoked calcium transients, were made using t-tests. Unless otherwise stated, data is ±standard deviation (SD).

2.2 Results

2.2.1 Assessment of ATP-evoked calcium transients in TG neurons

In addition to being an energy source, ATP can directly activate neurons in sensory ganglia via cationic purinergic receptors[116]. ATP receptor activation has been implicated in trigeminal inflammatory and

neuropathic pain[116–118]. Additionally, ATP-induced calcium transients in TG neurons were observed to be increased in an animal model of migraine[117]. Therefore, I began my assessment of TG excitability in EAE by stimulating dissociated TG neurons with ATP. Ionotropic ATP receptors are preferentially expressed in small and medium sized neurons[119]. To ensure that similar populations of control and EAE neurons were assessed, the cell diameter of each stimulated neuron was measured and recorded. The average cell body diameter of analyzed neurons was not different between CFA controls and animals with EAE (Fig 2.1A). Additionally, sensitivity to ATP was unaltered by EAE, as the percentage of neurons responding to various concentrations of ATP (1uM, 10uM, and 100uM) was similar in CFA and EAE (Fig 2.1B). Finally, the amplitude of the responses evoked by 100uM ATP was not significantly different between CFA and EAE neurons (Fig 2.1C,D).

2.2.2 Assessment of GABA-evoked calcium transients in TG neurons

GABA is the principle inhibitory neurotransmitter of the CNS[120]. However, within the PNS GABA acts as an excitatory neurotransmitter and may potentiate primary afferent excitability[120]. Given the excitatory nature of GABA within sensory ganglia, I next assessed its effects on TG neurons. The average diameter of cells stimulated with GABA was not significantly different between CFA and EAE neurons (Fig 2.2A). Sensitivity to various concentrations of GABA (0.25, 2.5, and 25uM) was also not different between CFA and EAE neurons (Fig 2.2B). Finally, the amplitude of the GABA-evoked (25uM) calcium transients was not different between CFA and EAE neurons (Fig 2.2C,D).

2.2.3 Assessment of capsaicin-evoked calcium transients in TG neurons

Transient receptor potential (TRP) channels are preferentially expressed in small and medium sized nociceptive afferents and can be activated by a variety of exogenous compounds, including capsaicin. TRP channel activation has been associated with trigeminal hyperactivity[71]. Additionally, in obese mice that exhibit orofacial hypersensitivity, TG neurons were found to exhibit enhanced calcium transients when stimulated with capsaicin[121]. Given the pro-excitatory and nociceptive effects of TRP channel activation, I next assessed capsaicin-induced calcium transients in TG neurons. The average cell diameter of analyzed neurons was not different between the CFA and EAE groups (Fig 2.3A).

Additionally, sensitivity to capsaicin was unaffected by EAE (Fig 2.3B). Finally, the amplitude of the responses evoked by 1uM capsaicin was not different between CFA and EAE neurons (Fig 2.3C,D).

2.2.4 Assessment of KCl-evoked calcium transients in TG neurons

KCl is typically applied to neurons at the end of a stimulation protocol to ensure that the cells are viable[71,121]. However, calcium transients evoked by KCl can also give an indication about a neurons overall excitability[121]. Again, the average diameter of neurons analyzed was similar in CFA and EAE (Fig 2.4A). In contrast to previous agonist-induced calcium transients however, the amplitude of the responses evoked by KCl was significantly greater in EAE neurons compared to CFA neurons (Fig 2.4B,C).

2.3 Discussion

Overall, the results from this chapter indicate that the excitability of TG neurons is increased in EAE. This data is in line with recent work from the lab which demonstrated that DRG neurons become hyperexcitable in EAE[113]. The increased excitability of TG neurons in EAE may arise from signals that are extrinsic and/or intrinsic to neurons. For example, in headache and trigeminal neuropathic pain animal models, macrophages infiltrate the TG and resident satellite cells become reactive. Both cell types are involved in modulating facial sensation, as inhibiting their function (or reducing their numbers) results in an attenuation of facial pain behaviors[52,122]. The contribution of each cell to pathological facial pain is believed to be mediated, at least in part, by an increase in the expression and release of proinflammatory cytokines (e.g. TNF-α and IL-1β) which can sensitize TG neurons[44]. In the previous chapter I demonstrated that macrophages infiltrate the TG in EAE. Additionally, it was demonstrated that SGCs in the TG become reactive with EAE. Thus, macrophages and reactive SGCs are potential sources of neuron-extrinsic signals that may alter the excitability of TG neurons in EAE.

Neuronal excitability can also be increased by mechanisms that are intrinsic to neurons. In response to injury, neurons undergo cellular and molecular changes that function to promote survival, growth, and hyperexcitability[123]. This was first demonstrated in *Aplysia*[124], and it is believed that these changes are driven by a loss and/or gain of electrical and molecular signals that are retrogradely propagated from a site of injury towards neuronal soma[123–125]. As will be demonstrated in Chapter 3, TG neurons in EAE are

damaged and have impaired axonal transport (as indicated by an accumulation of amyloid precursor protein at the TREZ). Therefore, altered excitability of TG neurons in EAE may also be caused by a loss and/or gain of signals that are propagated from a site of injury to the TG. In support of this idea, focal demyelination of trigeminal roots in cats results in the generation of ectopic actions potentials that retrogradely propagate to the TG[86]. These action potentials are believed to induce TG hyperexcitability, which in turn results in altered facial sensitivity[89].

The finding that ATP-, GABA- and capsaicin-evoked calcium transients were unaltered by EAE is surprising, as all three molecules have been implicated in generating sensory disturbances. For example, ATP-evoked calcium transients are elevated in TG neurons obtained from an animal model of migraine[117]. Additionally, capsaicin-evoked calcium transients are increased in TG explants obtained from mice with CCI-ION[71]. In contrast to ATP and capsaicin, the effect of GABA on TG neurons is largely unexplored. Within the PNS, GABA is an excitatory neurotransmitter and may amplify action potentials[120]. Yousuf et al. observed that DRG expression of the sodium–potassium-chloride co-transporter NKCC1 is unaltered in EAE[126]. This could explain why GABA-evoked calcium transients were similar in CFA and EAE neurons, as GABA-mediated depolarization is dependent on NKCC1-mediated accumulation of intracellular chloride[127]. The lack of effect of these agonists could also stem from the CNS based nature of trigeminal pathology in EAE. In the studies examining ATP- and capsaicin-evoked calcium transients in the TG, the trigeminal nerve was manipulated genetically[117] or through the induction of a peripheral injury[71]. As mentioned in the introduction, peripheral injuries are associated with the induction of cellular and molecular changes that differ from CNS-induced injuries[73,74]. Therefore, enhanced ATP- and capsaicin-mediated currents may not be a feature shared across trigeminal pathologies. Additionally, it is not known if the expression of ATP and receptors and TRP channels are altered by EAE. Future studies could follow up on the data presented here to examine if expression of ATP receptors and/or TRP channels is altered by EAE. Alternatively, future studies could conduct high throughput analyses of other targets (e.g. sodium channels) that may contribute to the altered responses evoked by KCl in EAE neurons.

In Chapter 1, I demonstrated that mice with EAE become hypersensitive to puffs of air applied to the whisker pad. A puff of air against the face represents a dynamic (i.e. moving) stimulus that likely activates an array of primary afferent subtypes that differs from that activated by a punctate (e.g. von frey filament) or noxious stimulus[128,129]. Specifically, dynamic stimuli involve the activation of large diameter Aβ fibers[128] which were not analyzed in the data presented above due to technical complications (large diameter neurons are lost during the dissociation protocol). Thus, future studies could involve refinements to the culture protocol to ensure that large diameter neurons are retained during the dissociation protocol. Alternatively, TG explants obtained from animals with neuron-specific, genetically-encoded calcium indicators[71] could be employed to allow for a more comprehensive assessment of TG excitability.

Nevertheless, the finding that TG neurons become hyperexcitable in EAE provides a mechanism that could underlie the facial hypersensitivity described in Chapter 1. Future studies aimed at understanding the basis of this hyperexcitability could identify targets for novel therapeutics for managing MS-related trigeminal sensory disturbances.

2.4 Figures

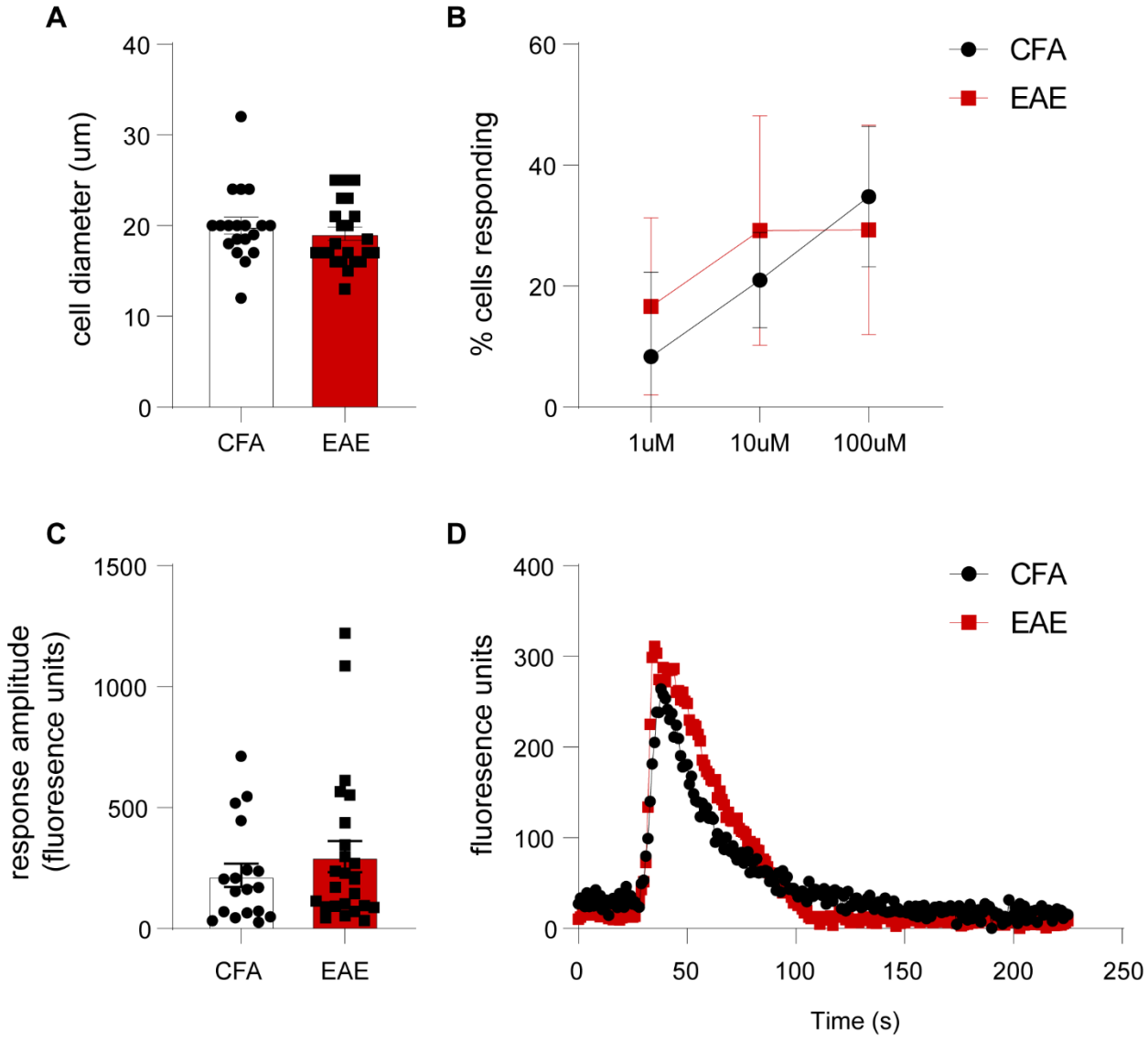

Figure 2.1 Assessment of ATP-evoked calcium transients in TG neurons isolated from CFA controls or animals with EAE. (A) Cell diameter of analyzed neurons was not significantly different between CFA and EAE. (B) The proportion of CFA and EAE neurons that responded to 1uM, 10uM, and 100uM ATP was not significantly different. (C) The amplitude of the responses evoked by 100uM ATP was not significantly different between CFA and EAE neurons. (D) Representative traces of calcium transients evoked by 100uM ATP in a CFA (black) and EAE (red) neuron.

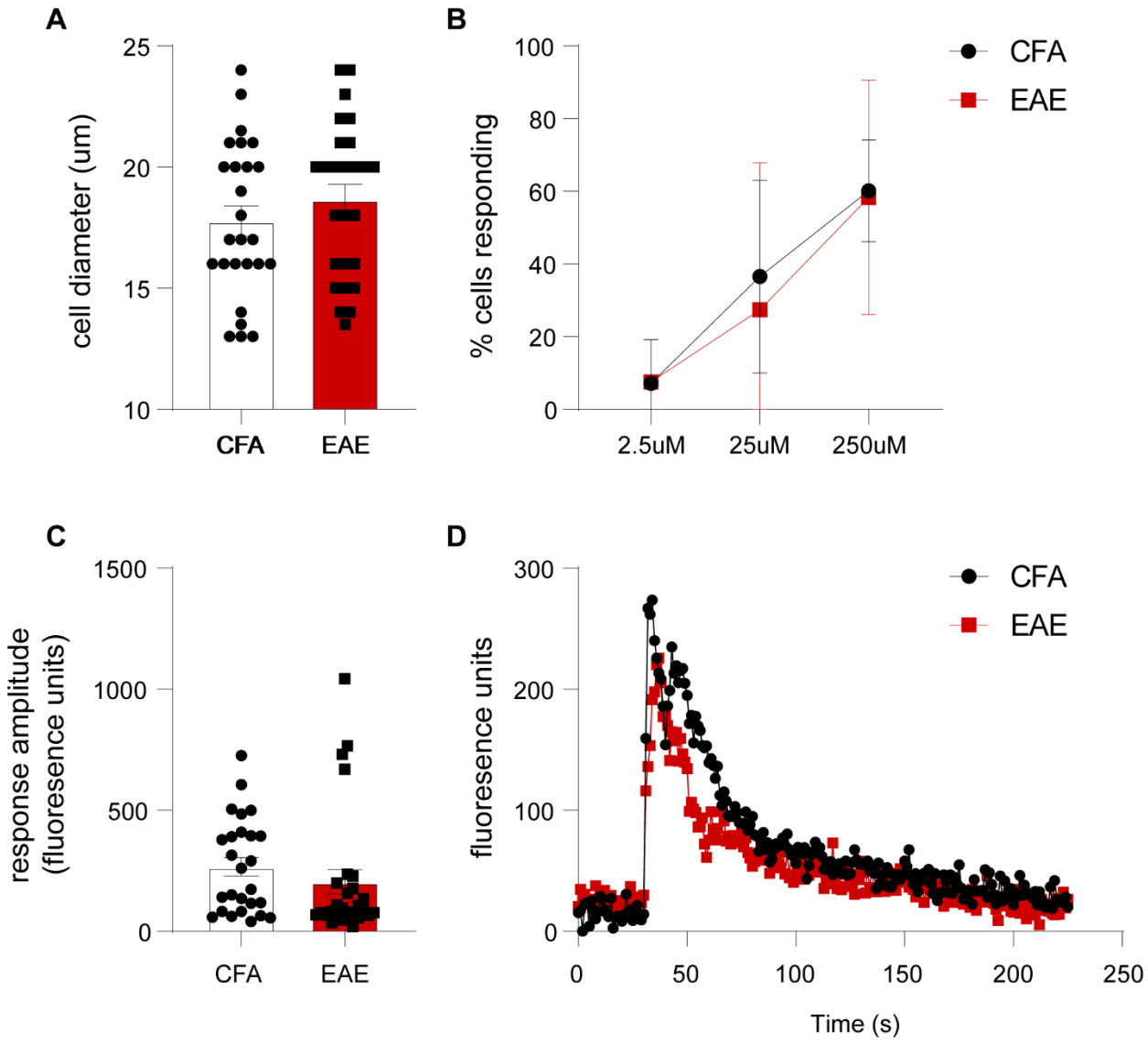

Figure 2.2 Assessment of GABA-evoked calcium transients in dissociated TG neurons obtained from CFA controls or animals with EAE. (A) The average cell diameter of analyzed neurons was not significantly different between CFA and EAE. (B) The percentage of cells that responded to 2.5uM, 25uM, and 250uM GABA was not significantly different between CFA and EAE neurons. (C) The amplitude of the calcium response evoked by 250uM GABA was not significantly different between CFA and EAE neurons. (D) Representative traces of calcium responses evoked by 250uM GABA in a CFA (black) and EAE (red) neuron.

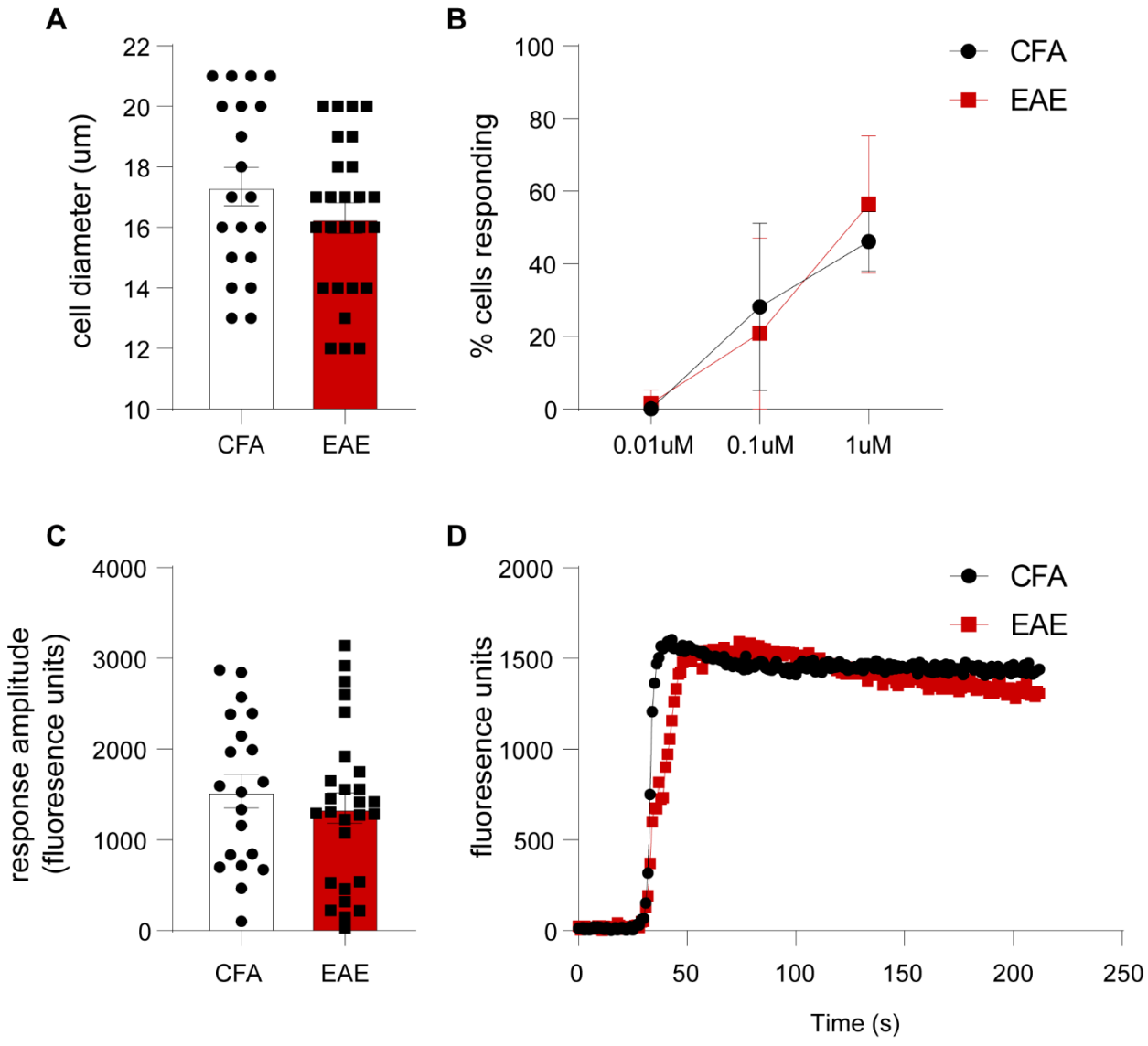

Figure 2.3 Assessment of calcium transients evoked by capsaicin in TG neurons obtained from CFA controls or animals with EAE. (A) The average diameter of analyzed cells was not significantly different between CFA and EAE neurons. (B) The proportion of cells that responded to 0.01uM, 0.1uM, and 1uM capsaicin was not significantly different between CFA and EAE cells. (C) The amplitude of the calcium transient evoked by 1uM capsaicin was not significantly different in CFA and EAE neurons. (D) Representative traces depicting a calcium transient evoked by 1uM capsaicin in a CFA (black) and EAE (red) neuron.

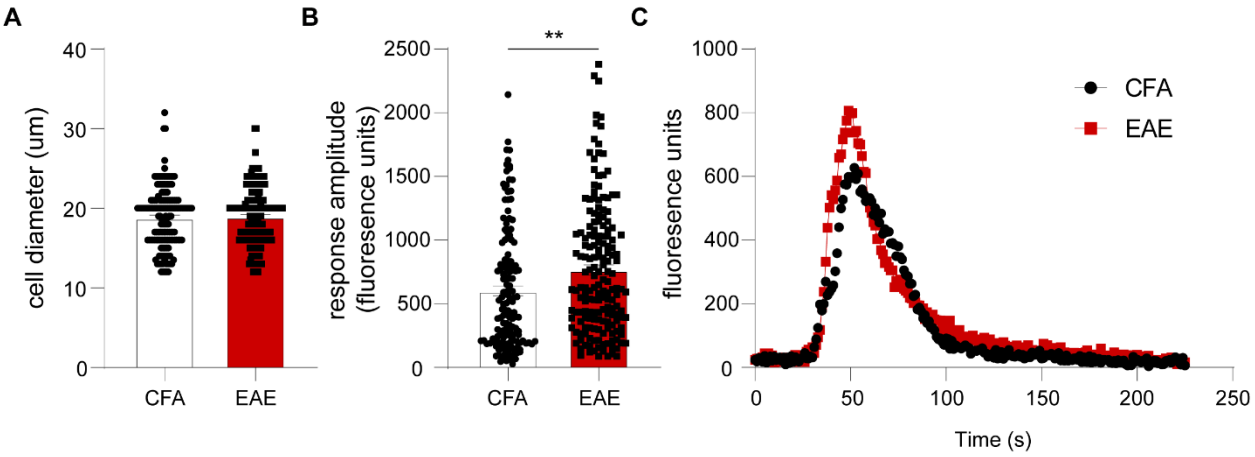

Figure 2.4 Assessment of calcium transients evoked by KCl in TG neurons obtained from CFA controls and animals with EAE. (A) Average diameter of analyzed cells was not significantly different between CFA and EAE. (B) The amplitude of KCl-evoked calcium transients was significantly greater in EAE neurons relative to CFA neurons. (C) Representative traces of calcium responses evoked by KCl in a CFA (black) and EAE (red) neuron. **p=0.0032, t-test.

Chapter 3: Astrocyte loss in experimental autoimmune encephalomyelitis is associated with exacerbated inflammation, demyelination and axonal injury

3.0 Introduction

Multiple Sclerosis (MS) is a demyelinating disease of the central nervous system (CNS)[1]. MS is associated with a diverse array of physical and psychological complications. However, the disease typically results in progressive and irreversible disability[1]. At the cellular level, irreversible disability in MS is believed to be the result of neuronal injury and degeneration[130,131]. Given the limited treatment options to halt disease progression[1], as well as the limited capacity of the CNS to regenerate[61], there is a need to better understand the mechanisms that underlie neurodegeneration in MS.

The pathological hallmark of MS is focal demyelination that is disseminated throughout the CNS[1,35]. A well-recognized feature of MS lesions is the presence of astrocytes that appear reactive (identified by their hypertrophic morphology and elevated expression of glial fibrillary acidic protein (GFAP))[35,65,132]. At present, it is not entirely clear how reactive astrocytes influence MS and EAE. On the one hand, conditional ablation of reactive astrocytes exacerbates EAE severity and CNS pathology, indicating that the cells may have a protective role[62]. On the other hand, reactive astrocytes may adopt a gene expression profile that has been associated with a neurotoxic phenotype[57,67], suggesting that the cells can also be detrimental. In addition to becoming reactive, astrocytes can be injured in MS and EAE. Electron microscopy studies of MS and EAE tissue have observed astrocytes with endfeet that appear swollen, which may indicate that the cells have been damaged[68,133]. A loss of staining for astrocyte markers (e.g. GFAP and aquaporin-4 (AQP4)) has also been observed in MS and EAE tissue[65,69,134].

At sensory root entry zones, the peripheral nervous system (PNS) interfaces with the CNS and the delineation between the two tissue types is achieved via the glia limitans that is formed by astrocytes[31]. During a previous study of trigeminal pathology in EAE, we found that GFAP immunoreactivity is reduced at the trigeminal root entry zone (TREZ)[80]. Despite the reduction in astrocyte markers that we and others[65,69] have observed, it is not yet clear how astrocyte injury and loss influences MS and EAE

pathophysiology. Thus, the goal of this study was to investigate histological changes associated with GFAP disruption in EAE. We also wanted to examine how astrocyte biology is altered by injury.

3.1 Methods

3.1.1 Experimental autoimmune encephalomyelitis

All animal procedures were carried out in accordance with protocols approved by the University of Alberta Health Sciences Animal Care and Use Committee. Six to eight-week-old female and male C57BL/6 mice (Charles River Canada) were habituated to their surroundings (vivarium and laboratory space) for approximately two weeks prior to the induction of EAE. For the induction of EAE, mice were given a subcutaneous injection of myelin oligodendrocyte glycoprotein (MOG, 35-55 fragment, 50ug) emulsified in Complete Freund's Adjuvant (CFA). Immediately after the injection of MOG (or CFA alone for control animals), mice were given an intraperitoneal injection of pertussis toxin (300ng). 48h after the initial pertussis injection, mice were given a second injection of pertussis (300ng). After a 72h quarantine period, mice were assessed daily and assigned a clinical score according to the following grading scheme: grade 0: no overt signs of disease, grade 1: weak and/or paralyzed tail, grade 2: mild hindlimb weakness, grade 3: severe hindlimb weakness, grade 4: hindlimb paralysis. In this experiment, mice with EAE were euthanized at either the onset (first sign of motor impairment) or peak disease timepoint.

3.1.2 Tissue collection and processing

Mice were euthanized with 0.1mL of 340mg/mL euthansol. Animals were subsequently perfused with 0.9% saline followed by 4% paraformaldehyde (PFA) if tissue was to be used for immunohistochemistry (IHC). Tissue used for protein analysis was collected in a microfuge tube which was subsequently frozen in liquid nitrogen then stored at -80°C until needed. Tissue destined for IHC was post-fixed overnight in 4% PFA and then transferred to a 30% sucrose solution the following morning. Sucrose solution was refreshed every two to three days until the tissue had become saturated. Once saturated, tissue was dried on a Kimwipe, blocked in an embedding medium, frozen on liquid nitrogen and then stored at -80°C. For cryosectioning, trigeminal nerves and spinal cords were cut at 10 and 20 microns, respectively, and collected on glass slides. Slides with tissue sections were stored at -20°C until needed.

3.1.3 Immunohistochemistry

Slides were thawed at room temperature while the following solutions were prepared: (1) blocking solution – 1X phosphate buffered saline (PBS; diluted from a 10X stock – recipe from thelabrat.com) containing 0.2% triton X-100, and 10% donkey serum (2) antibody buffer – 1X PBS containing 0.2% triton X-100, 2% donkey serum and 2% bovine serum albumin (BSA). Once solutions were prepared, slides were washed three times in 1X PBS (10 min per wash). The slides were then incubated with blocking solution for 1h at room temperature. The blocking solution was replaced with antibody buffer containing the primary antibodies of interest. Tissue sections were incubated with primary antibodies overnight at room temperature in a humidified chamber. The following morning, slides were washed twice in 1X PBS containing 0.2% Tween-20 (PBStw) and once in 1X PBS (10 min per wash). Slides were then incubated in antibody buffer containing the relevant secondary antibodies (Jackson Immunoresearch) at 1:500 dilution for 30 min at room temperature. After incubation with the secondary, slides were washed twice with PBStw and once with 1X PBS. Slides were then coverslipped with vectashield mounting medium and imaged.

For fluoromyelin staining with GFAP, tissue sections were thawed at room temperature for approximately 10mins. Slides were then washed three times in 1X PBS (10 mins per wash). The slides were then incubated in a coplin jar containing 1X PBS with fluoromyelin diluted 1:500. The slides were left in the fluoromyelin solution for 30min while placed on a rocker and were protected from light. Following the incubation with fluoromyelin, slides were washed three times in 1X PBS and then coverslipped and imaged. After each section had been imaged, coverslips were removed and slides went through the IHC protocol described above to visualize GFAP.

3.1.4 Image acquisition

All images used for analysis and in figures were obtained on a Zeiss Observer Z1 inverted fluorescence microscope.

3.1.5 Quantification of immunohistochemistry

For quantification of GFAP disruption at the TREZ, we captured two images of each TREZ analyzed. One image was obtained with a phase contrast filter to visualize the PNS-CNS interface (see Figure 3.1A, D, G). The other image was obtained using fluorescence to visualize GFAP at the TREZ. On the phase contrast image, we traced a line (using Fiji) where we believed that PNS interfaced with the CNS. The length of the line was then measured and taken to represent the total length of the interface. We then stacked the phase contrast and fluorescent images of each TREZ (see Figure 3.1C, F, I). The length of GFAP was then traced and recorded as described above. To determine the %length of interfaced lined with GFAP, we divided the length of the line traced on the phase/fluorescent image by the length of line traced on the phase contrast image. Admittedly, our estimation of the PNS-CNS interface with the phase contrast image alone did not always match the actual shape of the interface seen with GFAP. This resulted in our measured values deviating from the 100% that one would expect.

For quantification of CD4, Iba1, and amyloid precursor protein, we used 10X phase contrast images of the trigeminal root and traced around the CNS portion of the TREZ. This region of interest (ROI) was then saved (using the ROI manager in FIJI) and superimposed on the corresponding fluorescent image for each marker. We then determined the %area of the superimposed ROI occupied by staining by thresholding each image to a level that we believe accurately detected the fluorescent signal. Importantly, for each stain the thresholding values that were selected were applied to all images regardless of an animal's treatment group.

For quantification of fluoromyelin we again used superimposed ROIs to determine the %area of TREZ that was labeled for fluoromyelin. The %area demyelinated was then determined according to the formula: 100-%area TREZ fluoromyelin positive.

3.1.6 Western Blot Analysis of GFAP Fragmentation

Spinal cords were homogenized in 200uL of radioimmunoprecipitation (RIPA) buffer containing protease inhibitor. The homogenate was then spun at 16,000g for 10min at 4°C. After removal of the supernatant, the RIPA-insoluble pellet was then resuspended in 200uL of a urea-based buffer containing 7M urea,

50mM Tris-HCl, pH=7.5, 10mM NaCl, 1mM EDTA and 1X protease inhibitor. The homogenate was then spun again at 16,000g for 10min at 4°C. After the second centrifugation, the supernatant was collected, and an aliquot was taken to determine protein concentration via a BCA assay. After protein concentration was calculated, the protein was diluted to 1mg/mL and stored in aliquots at -80°C until needed. Protein samples were electrophoresed on a 10% SDS gel. Protein was then transferred onto a PVDF membrane (Transblot Turbo). The membrane was blocked in PBStw containing 5% BSA (1 hour at room temperature) and then incubated overnight with GFAP antibody (diluted 1:1000 in PBStw containing 1% BSA) at 4°C. The following morning, membranes were washed three times with PBStw (10 min each) then incubated with goat anti-rat HRP (diluted 1:25,000 in PBStw containing 1% BSA) for 1h at room temperature. Membranes were then washed as above and the HRP was detected using ECL Prime Western Blotting Detection Kit. Membranes were visualized on a Biorad. For determination of total protein, membranes were washed once in 1X PBS (5min) and then incubated for 5 min in a Coomassie blue staining solution (50% methanol, 7% acetic acid, 0.1% (weight/volume) Coomassie blue). The volume of a band on the original blot using Image Lab software. The volume of the same band was then measured on the blot after it was stained for Coomassie blue. Expression of GFAP fragments was quantified by diving the volume of the GFAP band by the volume of the corresponding Coomassie blue band.

3.1.7 Cell culture

Immunopanning of astrocytes and neurons was carried out according to a previously described protocol[64] with modifications to the panning sequence. Two to three CD1 mouse pups (aged two to three days old) were rapidly decapitated and the brains were removed and collected in Dulbecco's Phosphate Buffered Saline (D-PBS). After removal of the midbrain and meninges, cortices were transferred to a sterile 10cm petri dish and subsequently minced. A pre-equilibrated enzyme solution containing 7.5units/mL of papain (Worthington) was then added to the dish which was subsequently moved to a dry bath incubator that was continually perfused with 95% oxygen/5% carbon dioxide (CO_2) and set to 35°C. After approximately 40 min in the enzyme solution, the tissue chunks were transferred to a 50mL conical and washed with a pre-equilibrated trypsin inhibitor solution. After centrifugation and removal of the trypsin inhibitor, cells

were resuspended in a BSA-containing buffer and passed sequentially through a 40- and 20-micron cell strainer. The cells were then placed in a 10% CO2 incubator for 30min to allow antigens to return to the cell surface. After the recovery period, the cell suspension was passed sequentially over antibody-coated petri dishes to eliminated unwanted cells from the suspension. After incubating on the final dish (HEPAcam for astrocytes and CD90 for neurons), dishes were washed with D-PBS then incubated with a trypsin solution for 3min at 37°/10% CO2 to weaken cells adhesion to the dish. After incubation with the trypsin, adherent cells were dislodged from the dish by repeated pipetting with a solution containing 30% fetal bovine serum. Once the cells were dislodged, they were collected in a 50mL conical and centrifuged. Following the centrifugation, the supernatant was discarded, and the cell pellet was resuspended in either astrocyte or neuron media. The cells were then counted using a hemocytometer and plated. Neurons were plated in 24 well glass bottom dishes (50,000 cells per well in a 100uL pre-plate) while astrocytes were plated in 24 well plastic dishes (20,000 cells per well added 500uL of pre-equilibrated astrocyte media). Neuron cultures were concluded within 24h of plating. Astrocyte cultures were maintained for seven to ten days prior to starting experiments, with 50% media changes being conducted every two to three days.

3.1.8 Immunocytochemistry

Cells were fixed by adding a volume of warm 8% PFA equivalent to that in which the cells resided. Following the addition of PFA, cells were left to sit at room temperature for 10 min. The PFA was subsequently removed and cells were washed three times with D-PBS. Cells were then incubated in D-PBS containing 0.2% Triton X-100 and 10% donkey serum (blocking solution) for 30min at room temperature. The blocking solution was then removed and replaced with D-PBS containing 0.2% triton X-100, 2% donkey serum, 2% BSA (antibody buffer) and the primary antibody. Cells were left overnight at 4°C to incubate with the primary antibody. The following morning, cells were washed three times with D-PBS then incubated with the appropriate secondary antibody (Jackson Immunoresearch) diluted in antibody buffer. Also included with the secondary was DAPI (diluted 1:3000). Following incubation with the secondary, cells were washed three times with D-PBS then visualized.

3.1.9 Assessment of neurite outgrowth

The cell culture plates on which neurons were grown were imaged on an ImageXpress system. A grid of 16 pictures, centered on each well, was acquired for each well. Images were then exported and analyzed using the neurite outgrowth module provided with MetaXpress software.

3.1.10 Statistical Analysis

Data were analyzed using Prism Software. Comparisons between intact and disrupted tissue sections were made using t-tests. For neurite outgrowth experiments, data was analyzed using a one-way ANOVA with correction for multiple comparisons. Unless otherwise stated, data is ±SD.

3.2 Results

3.2.1 Characterization of TREZ GFAP disruption in mice with EAE

At the TREZ, the demarcation between the CNS and PNS is easily visualized with GFAP immunofluorescence (Figure 3.1). Consistent with our previous study, we found that there can be an overt loss of TREZ GFAP in mice with EAE (Figure 3.1G-I). However, this loss of GFAP was not a ubiquitous phenomenon amongst the tissue sections analyzed. Specifically, in female mice we found that a disruption of GFAP staining occurred in only 27 of 102 (26%) sections analyzed. Similarly, in male mice, GFAP disruption was detected in 17 of 60 (28%) sections analyzed. In addition to differences in TREZ GFAP between animals, we found that there could be considerable heterogeneity in tissue sections obtained from a single animal (Supplemental Figures 3.1 and 3.2). Given this heterogeneity, we qualitatively classified EAE tissue sections as “intact” or “disrupted” based on the absence or presence of overt GFAP staining loss, respectively. In intact tissue sections, the percent length of interface that was lined with GFAP was 103.5±3.1% in female animals and 102.6±3.1% in males. In disrupted sections, the percent length of interface that was lined with GFAP was significantly reduced to 25.4±35.8% in female animals (Figure 3.1J) and 48.5±23.0% in males (Figure 3.1K; t=test, female: $t(101)=18.8$, $p<0.0001$; male: $t(59)=15.2$, $p<0.0001$). While it was not a specific aim of this study to directly compare males and females, we did find that the loss of TREZ GFAP was significantly greater in females relative to males (t-test; $t(44)=2.4$, $p=0.01$). To investigate if the reduction in GFAP staining was due to a loss of astrocytes or

the GFAP protein itself, we stained trigeminal sections for aquaporin-4 (AQP4), a well-established marker of astrocyte endfeet[135]. In disrupted sections, we found that AQP4 staining appeared to be reduced to the same extent as GFAP (Figure 3.2), suggesting that astrocytes are lost at the TREZ in disrupted tissue sections.

3.2.2 GFAP loss at the TREZ is associated with exacerbated inflammation, demyelination and axonal injury

Given the stark contrast in GFAP staining between intact and disrupted sections, we next wanted to examine histological changes associated with the loss of GFAP. We previously demonstrated that in EAE there is an influx of CD4-positive T cells into the TREZ[80]. Since astrocytes play a critical role in limiting T cell migration into the CNS[36,62,136], we first wanted to assess the relationship between T cell levels and TREZ GFAP. A significantly greater proportion of the TREZ was occupied by CD4 immunoreactivity in disrupted tissue sections relative to intact sections (Figure 3.3). The increase in CD4 was observed in both female and male animals (t-test, female: $t(106)=7.1$, $p<0.0001$; male: $t(62)=3.2$, $p=0.0017$) but was not significantly different between the sexes (t-test, $t(39)=1$, $p=0.31$). We next compared microglia/macrophage levels between intact and disrupted sections (Figure 3.4). In disrupted sections from both female and male mice, a significantly greater percentage area of TREZ was immunoreactive for Iba1 (Figure 3.4C, F; t-test, female: $t(99)=7.4$, $p<0.0001$; male: $t(66)=3.1$, $p=0.0021$). Additionally, we found that there was a difference between the sexes, with female disrupted sections having significantly greater expression of Iba1 at the TREZ relative to male disrupted sections (t-test, $t(45)=3.1$, $p=0.0033$). To assess potential consequences of astrocyte loss and exacerbated TREZ inflammation, we next examined markers of myelin and axonal injury. In both female and male mice, a significantly greater proportion of the TREZ was demyelinated in disrupted sections relative to intact sections (Figure 3.5; t-test, female: $t(57)=4.6$, $p<0.0001$; male: $t(27),=3.3$, $p=0.0026$). The extent of demyelination was not significantly different between the sexes however (t-test, $t(26)=0.85$, $p=0.4$). Axonal injury was next assessed by staining trigeminal sections for amyloid precursor protein (APP), the expression of which has previously been shown to increase in damaged axons in both MS[137] and EAE[138]. Relative to intact tissue sections, a significantly greater proportion of the TREZ was APP-positive in disrupted sections (Figure

3.6). The increased APP immunoreactivity in disrupted sections was observed in both females (t-test, $t(115)=7.7$, $p<0.0001$) and males (t-test, $t(68)=4.5$, $p<0.0001$), but was not different between the sexes (t-test, $t(48)=1.8$, $p=0.0686$). Taken together, these data suggest that astrocyte injury/loss at the TREZ is associated with exacerbated inflammation, demyelination, and axonal injury.

3.2.3 GFAP loss and fragmentation in the spinal cords of mice with EAE

We next wanted to see if GFAP disruption was restricted to the TREZ. In spinal cord sections obtained from mice with EAE, we detected lesions (evident with phase microscopy; Figure 3.7A, B) in which GFAP staining appeared to be lost (Figure 3.7A', B'). The areas with apparent GFAP loss contained APP-immunoreactive puncta (Figure 3.7A'', B''), which may represent axonal end bulbs[139,140]. To quantify the extent of GFAP disruption in the spinal cord, we next assessed fragmentation of the GFAP protein with western blot analysis. As shown in figure 7, expression of a 26kDa GFAP fragment was significantly increased in animals with EAE compared to CFA controls. While GFAP fragmentation was detected in both females and males, expression of the fragment was not significantly different between the sexes. Collectively, these data demonstrate that GFAP disruption in EAE is not a phenomenon unique to the TREZ.

3.2.4 Disruption of astrocytes impairs their ability to facilitate neuronal growth

To follow up on our IHC data suggesting that neuronal health is compromised when astrocytes are disrupted, we examined the effect that injured astrocytes have on neurite outgrowth in vitro. To model the astrocyte disruption we observed in vivo, we exposed immunopanned murine astrocytes to staurosporine, a well-recognized inducer of apoptosis. Astrocyte conditioned media (ACM) was then collected and used to grow immunopanned murine cortical neurons. Neurons grown in media collected from unstimulated astrocyte cultures (i.e. ACM) grew significantly longer neurites than neurons grown in unconditioned astrocyte media (i.e astrocyte base media; Figure 3.8A, B, D; one-way ANOVA $F(2,9)=57.19$, $p<0.0001$ with post-hoc Tukey's multiple comparison test $q(9)=4.9$, $p=0.01$). By contrast, neurons grown in media collected from injured astrocyte cultures (staurosporine ACM) extended significantly shorter neurites compared to neurons grown in astrocyte base media (Figure 8C, D; one-way ANOVA $F(2,9)=57.19$,

p<0.0001 with post-hoc Tukey's multiple comparison test q(9)=9.9, p=0.0002). The blunting of neurite growth with staurosporine ACM suggests that injured astrocytes lose their ability to support neuronal growth.

3.2.5 Axonal injury at the TREZ is associated with facial hypersensitivity

To investigate if axonal injury at the TREZ is associated with altered facial sensitivity, trigeminal nerves were obtained from CFA controls, EAE mice that did not exhibit a change in sensitivity to air puffs (EAE-), and EAE mice that showed a change in sensitivity to air puffs (EAE+). Collected nerves were subsequently sectioned and stained for APP. Compared to non-hypersensitive animals, mice with EAE that became hypersensitive to the air puffs had significantly more APP staining at the TREZ (Figure 3.9; one-way ANOVA F(2,7)=94.55, p<0.0001 with post-hocTukey's multiple comparison test q(7)=16.00, p<0.0001).

3.3 Discussion

Building on our observations from a previous study[80], the data presented here demonstrates that a loss of astrocytes in EAE is associated with exacerbated inflammation, demyelination, and axonal injury. In concordance with our findings, astrocyte loss and injury has been reported by others in both MS and EAE. For example, Brosnan and Raine have described MS lesions in which astrocytes appear to have retracted their endfeet away from the basal lamina of blood vessels. Within these lesions, astrocyte endfeet also appear glassy, swollen, and degenerative, suggesting that the cells had sustained damage[68]. Additionally, Prineas and Lee observed active MS lesions devoid of GFAP and AQP4 immunoreactivity[134]. A loss of GFAP-positive astrocytes has also been observed in MS-related cortical gray matter lesions[69]. Similar to MS, astrocytes with swollen endfeet have been observed in the spinal cords of rats with EAE[133]. Additionally, a recent study demonstrated that astrocyte cell bodies and processes are displaced away from cortical blood vessels[141]. Finally, astrocytes in the retina of mice with EAE also appear to sustain damage, as indicated by a loss of AQP4 staining[65]. The GFAP disruption that we and others have observed contrasts the vast body of literature demonstrating that GFAP expression is elevated in MS and EAE[65,132]. Indeed, even previous reports from our lab have demonstrated that GFAP

expression increases in the spinal cords of mice with EAE[78,142]. One explanation for this discrepancy could be that there are regional differences in how astrocytes respond to EAE-related inflammation. Our lab recently demonstrated that in mice with EAE, GFAP expression increases in the dorsal horn of the spinal cord[142]. However, subsequent examination of the same tissue set revealed that astrocyte disruption was present in spinal cord white matter, two examples of which are depicted in Figure 7. We believe that astrocyte disruption could also be missed if an insufficient amount of serial tissue sections are analyzed. At the trigeminal root, we observed that astrocyte disruption was not always uniform throughout a nerve (Supplemental Figure 3.1) and in some cases GFAP disruption could only be detected in one of the two or three sections analyzed. This also appears to be the case in the spinal cord based on a preliminary assessment of the previously mentioned tissue set[142]. Another explanation for the discrepancy in GFAP expression could be that astrocyte injury only occurs in a subset of lesions. Indeed, Sharma et al. observed that glia limitans disruption could only be detected in a minority of MS lesions[143]. Additionally, Parrat and Prineas detected astrocyte injury in only four of nine MS samples examined[144]. That astrocyte injury may only occur in a subgroup of lesions suggests that there is a feature of these lesions which may incite astrocyte disruption and/or loss.

Brosnan and Raine suggested that astrocyte injury in MS may be the result of toxic mediators released from infiltrating immune cells[68]. However, data from in vitro studies does not lend evidence to this idea. Sun and Wekerle demonstrated that a co-culture of myelin-reactive T cells and astrocytes, in the presence of a myelin antigen, results in astrocyte cell death[145]. Domingues et al. also observed that co-culturing MOG-activated T cells with astrocytes results in astrocyte death. However, the astrocyte cytotoxicity appears to be mediated by a cell-to-cell contact mechanism, as conditioned media from the T cell cultures failed to induce astrocyte death[146]. In addition to being cytotoxic to astrocytes, non-specifically activated-T cells have been shown to be able to induce GFAP fragmentation in co-cultured astrocytes[147]. This fragmentation is blocked however if the T cells are prevented from physically interacting with astrocytes[147]. Collectively, these data suggest that direct contact between astrocytes and encephalitogenic T cells could trigger astrocyte injury in MS and EAE.

To investigate histological changes associated with astrocyte disruption at the TREZ, we examined markers of T-cells, microglia/macrophages, myelin and axonal injury. Consistent with our previous report[80], we found that T-cells invade the TREZ in EAE. We also observed that T cell levels were significantly increased in absence of an astrocyte glia limitans. In the study conducted by Domingues et al., the authors found that T cells polarized toward a Th1, but not Th17, phenotype were capable of inducing astrocyte death[146]. This suggests that astrocyte injury in EAE could be dictated by the relative amount of T cell subtypes that are present at a lesion. We also found increased Iba1 staining in disrupted tissue sections. An interesting feature of the Iba1 staining was that it appeared to fill in areas of the TREZ that were devoid of GFAP. Indeed, in disrupted sections the overall shape of the CNS-PNS interface could be appreciated with Iba1 staining even in the absence of a clear GFAP border (see Figure 4B, E). Eilam et al. observed that while astrocytes appear to retract from cortical blood vessels in mice with EAE, Iba1-positive cells (presumably microglia) appear to increase their interaction with the vessels[141]. Additionally, Joost et al. have demonstrated that in mice with EAE, microglia increase their endfeet contact with blood vessels[148]. Collectively, these data suggest that microglia and/or macrophages may reinforce injured glia limitans in EAE. In addition to changes in inflammation, we also observed exacerbated demyelination in disrupted tissue sections. Interestingly, APP-immunoreactivity, a well-recognized marker of axonal injury[138], was only ever detected in disrupted tissue sections. Additionally, the APP staining appeared to be localized specifically to areas devoid of GFAP. That inflammation is present in both intact and disrupted sections, yet axonal injury is only detected in the later, suggests that astrocytes at the TREZ may be protecting axons from the ongoing inflammation. Our findings are in line with a previous study that examined EAE after reactive astrocytes were conditionally ablated. In that study, deletion of reactive astrocytes resulted in enhanced CNS immune infiltration, demyelination, and axonal injury[62]. Taken together, our immunohistochemical data suggest that astrocytes are protective but can become injured during inflammatory demyelination, ultimately resulting in axonal injury.

One question that we wanted to address was whether astrocyte disruption in EAE was unique to the TREZ. We found immunohistochemical evidence that GFAP loss can also be detected in the EAE spinal cord. Similar to what we observed at the TREZ, APP-immunoreactive puncta were present in regions with disrupted GFAP staining. Additionally, we observed that GFAP fragmentation is significantly increased in

the spinal cords of mice with EAE. Interestingly, fragmentation of GFAP has also been observed in tissue samples obtained from MS patients. In our tissue samples, we found that the GFAP fragment was approximately 26kDa. Chen et al. have demonstrated that caspase 6 can cleave GFAP in vitro to generate a 26kDa fragment[149]. At present we do now know if caspase 6 is responsible for generating the fragment we observed in EAE spinal cord homogenates. Additionally, the implication of GFAP fragmentation for MS and EAE is not known. However, given that GFAP fragmentation increases under conditions in which astrocytes are injured, we, and others[147], believe that this may be a suitable marker to monitor astrocyte disruption in MS and EAE.

We wanted to examine how neuronal health is impacted by astrocyte injury. It is well-recognized that neuron survival and growth are significantly increased when the cells are grown in co-culture with astrocytes or in ACM[150]. Given the pronounced trophic effect that astrocytes have on neuronal growth in vitro, we assessed neurite outgrowth in ACM obtained from healthy and injured astrocyte cultures. To model astrocyte injury in vitro, we exposed astrocytes to staurosporine, an inducer of apoptosis that is commonly used to study astrocyte cell death[151]. We found that neurons grew significantly shorter processes when incubated in media obtained from staurosporine-exposed astrocyte cultures. This data, in conjunction with our IHC results, suggest that injured astrocytes lose their capacity to support and protect neurons.

Finally, we examined how the presence of TREZ APP may relate to the facial hypersensitivity introduced in Chapter 1. Relative to mice with EAE that did not exhibit a change in facial sensitivity, animals that were hypersensitive to the air puffs had significantly more APP staining at the TREZ. Collectively this data indicates that injury of trigeminal root axons is associated with altered facial sensitivity in EAE.

In conclusion, we have provided evidence that astrocyte injury is associated with exacerbated pathology in EAE. The data presented here could improve our understanding of the mechanisms underlying axonal injury and degeneration in MS. Our data suggest that targeting injured astrocytes could limit inflammation, demyelination and axonal injury. This in turn could lessen the progressive and irreversible disability that is often associated with MS.

3.4 Figures

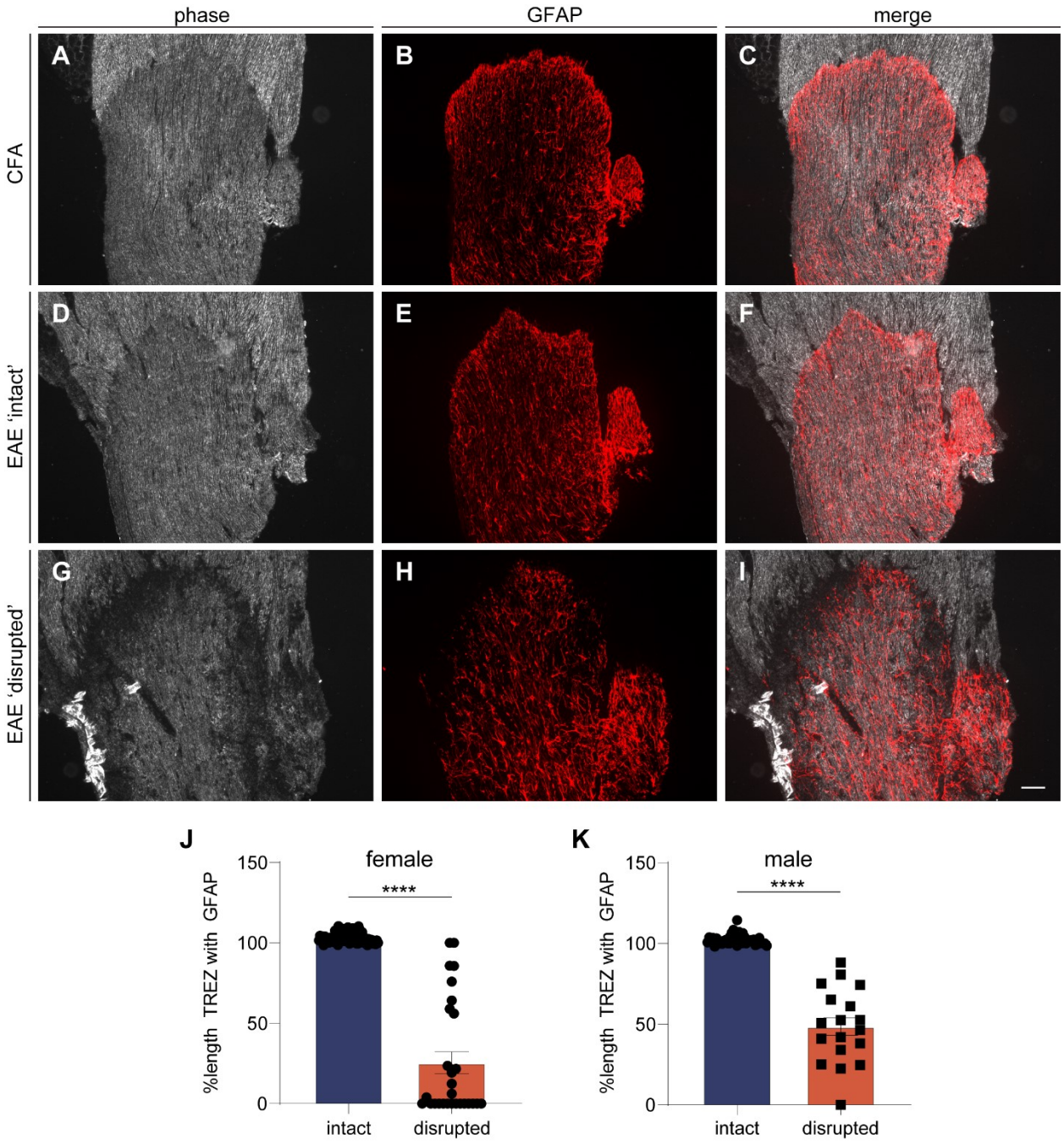

Figure 3.1 Classification of glia limitans disruption at the trigeminal root entry zone in EAE. (**A, D, G**) On a phase contrast image of the TREZ, there is an arch-like shape which indicates where the PNS interfaces with the CNS. In tissue sections from control animals (**B**), as well as some animals with EAE (**E**), GFAP immunofluorescence is well-defined and extends up to the arch-shaped PNS-CNS interface (**C, F**). In some

animals with EAE, GFAP staining is less well-defined (**H**) and no longer extends to the PNS-CNS interface (**I**). In both female (**J**) and male (**K**) mice with EAE, the %length of interface that is lined with GFAP is significantly reduced in disrupted sections relative to intact sections. ****p<0.0001, t-test. Scale bar in I=100μm and applies to all images in the figure. Data is ±SEM.

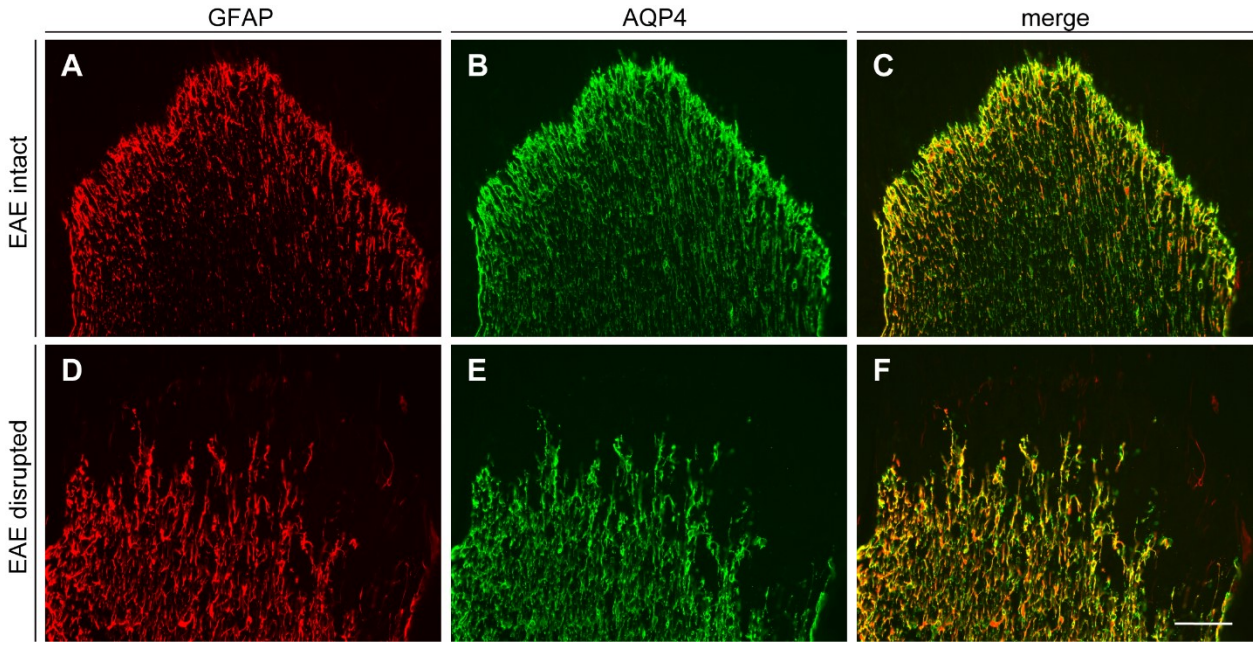

Figure 3.2 Loss of aquaporin-4 staining at the TREZ in EAE. GFAP (**A)** and aquaporin-4 (AQP4; **B**) immunofluoresence in intact sections is well-defined and has an arch-like shape. By contrast, the sharp, border-like staining of both GFAP and AQP4 are lost in disrupted sections (**D**, **E**). Scale bar in F=20μm and applies to all images in the figure.

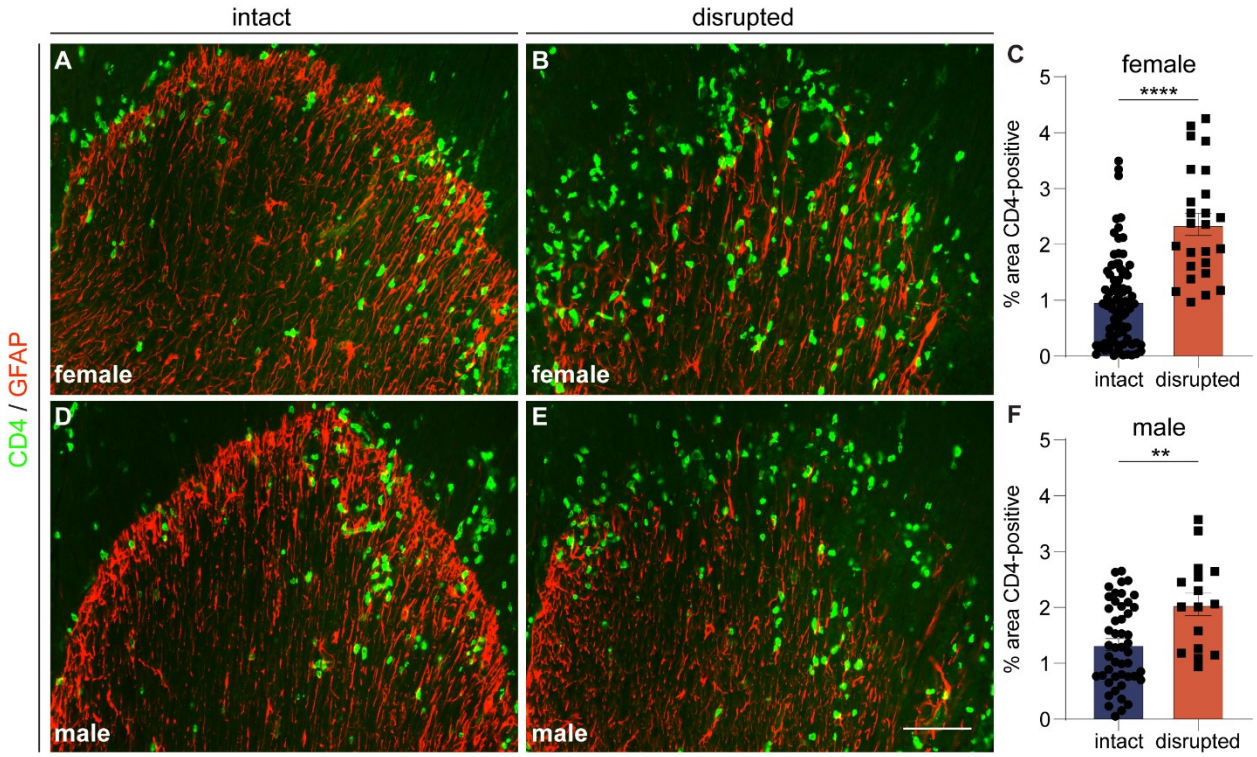

Figure 3.3 Assessment of T cell infiltration in intact and disrupted tissue sections. In disrupted tissue sections, obtained from both female (**B**) and male (**E**) mice, a significantly greater proportion of the TREZ is occupied by CD4-immunoreactivity compared to intact sections (**A, C, D, F**). ****p<0.0001, t-test. **p=0.0017, t-test. Scale bar in E=20μm and applies to all images in the figure. Data is ±SEM.

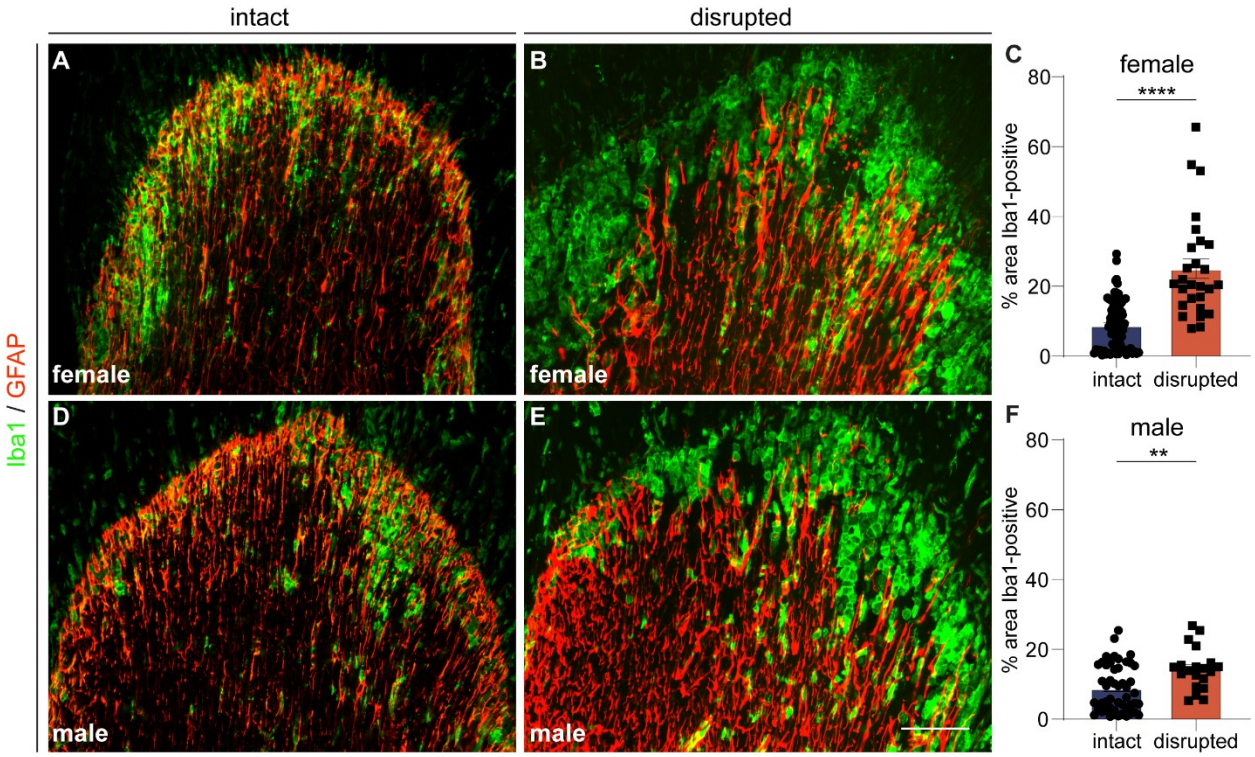

Figure 3.4 Assessment of microglia and macrophage reactivity in intact and disrupted tissue sections. In both female (**A, B**) and male (**D, E**) mice, a significantly greater proportion of the TREZ is occupied by Iba1 immunoreactivity in disrupted tissue sections relative to intact sections (**C, F**). ****p<0.0001, t-test. **p=0.0021, t-test. Scale bar in E=20μm and applies to all images in the figure. Data is ±SEM.

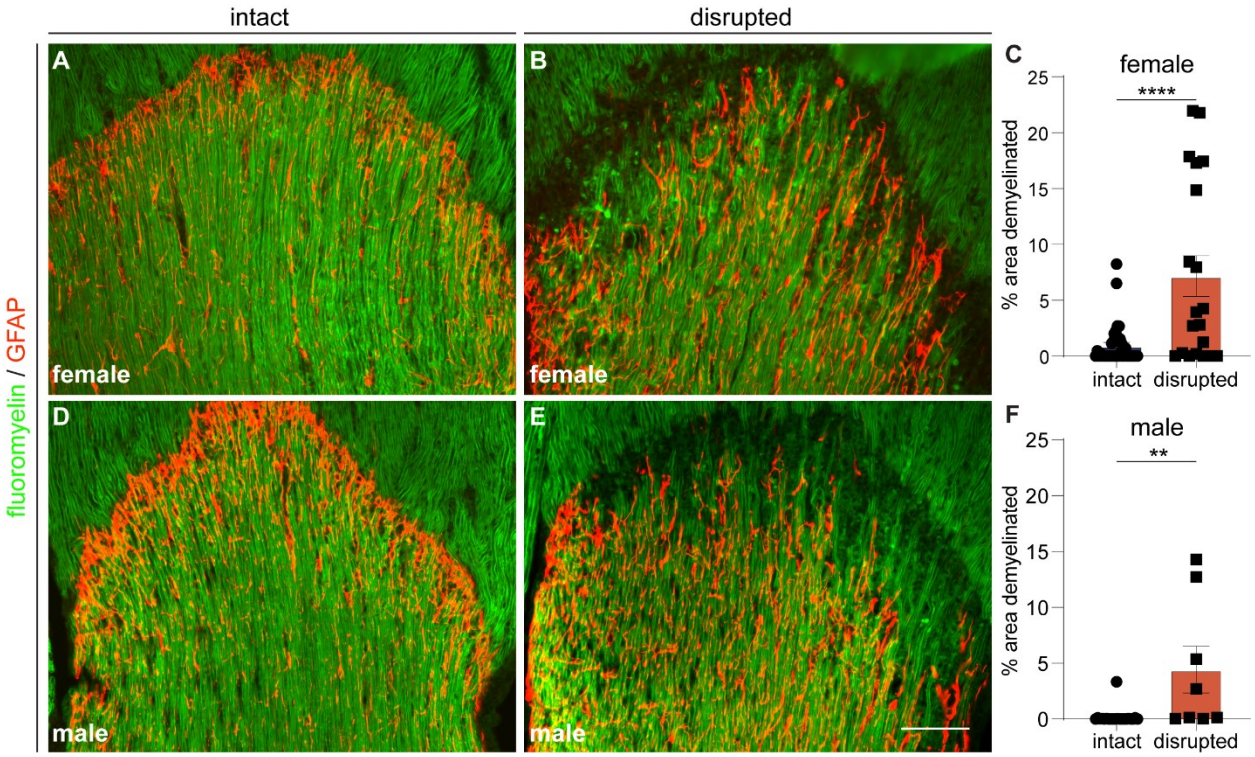

Figure 3.5 Assessment of demyelination in intact and disrupted tissue sections. Compared to intact sections (**A, D**), a significantly greater proportion of the TREZ is demyelinated in disrupted sections (**B, C, E, F**). ****p<0.0001, t-test. **p=0.0026, t-test. Scale bar in E=20μm and applies to all images in the figure. Data is ±SEM.

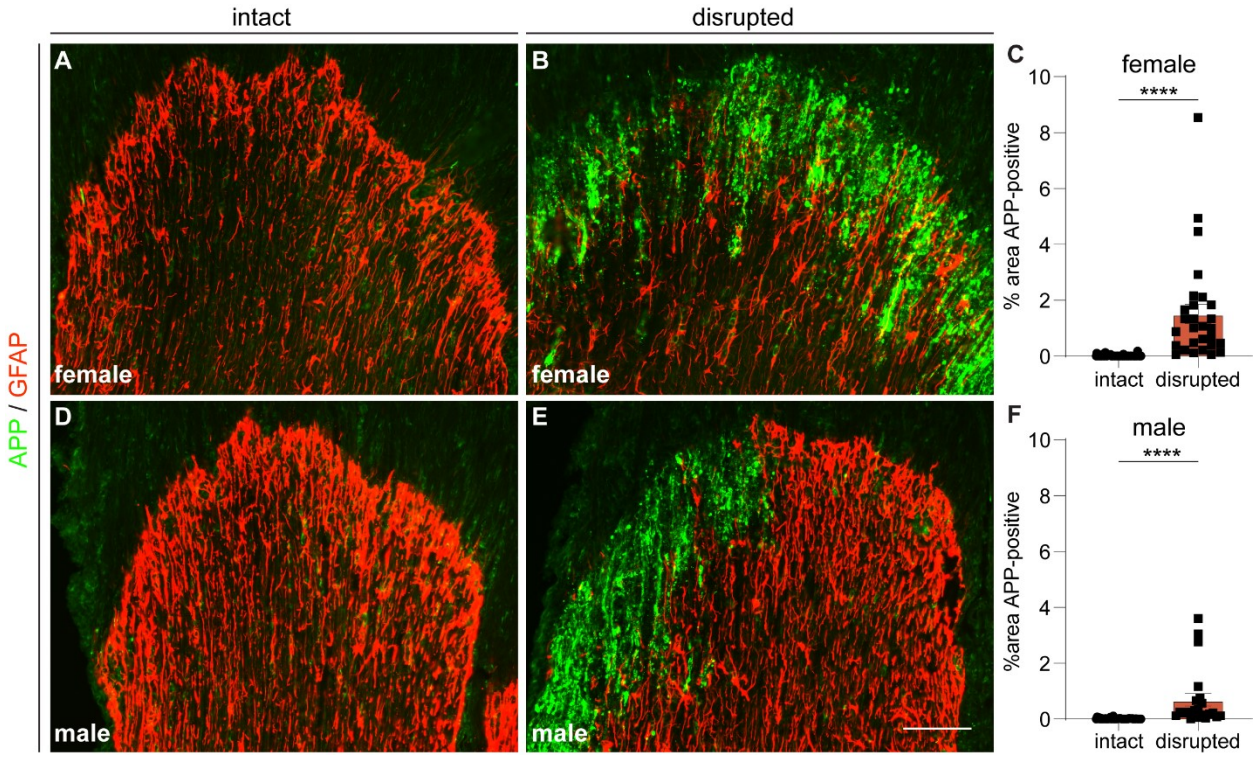

Figure 3.6 Assessment of axonal injury in intact and disrupted tissue sections. In tissue sections obtained from both female (**A, B**) and male mice (**D, E**), a significantly greater proportion of the TREZ is occupied by APP-immunofluoresence in disrupted sections relative to intact sections (**C, F**). ****p<0.0001, t-test. Scale bar in E=20μm and applies to all images in the figure. Data is ±SEM.

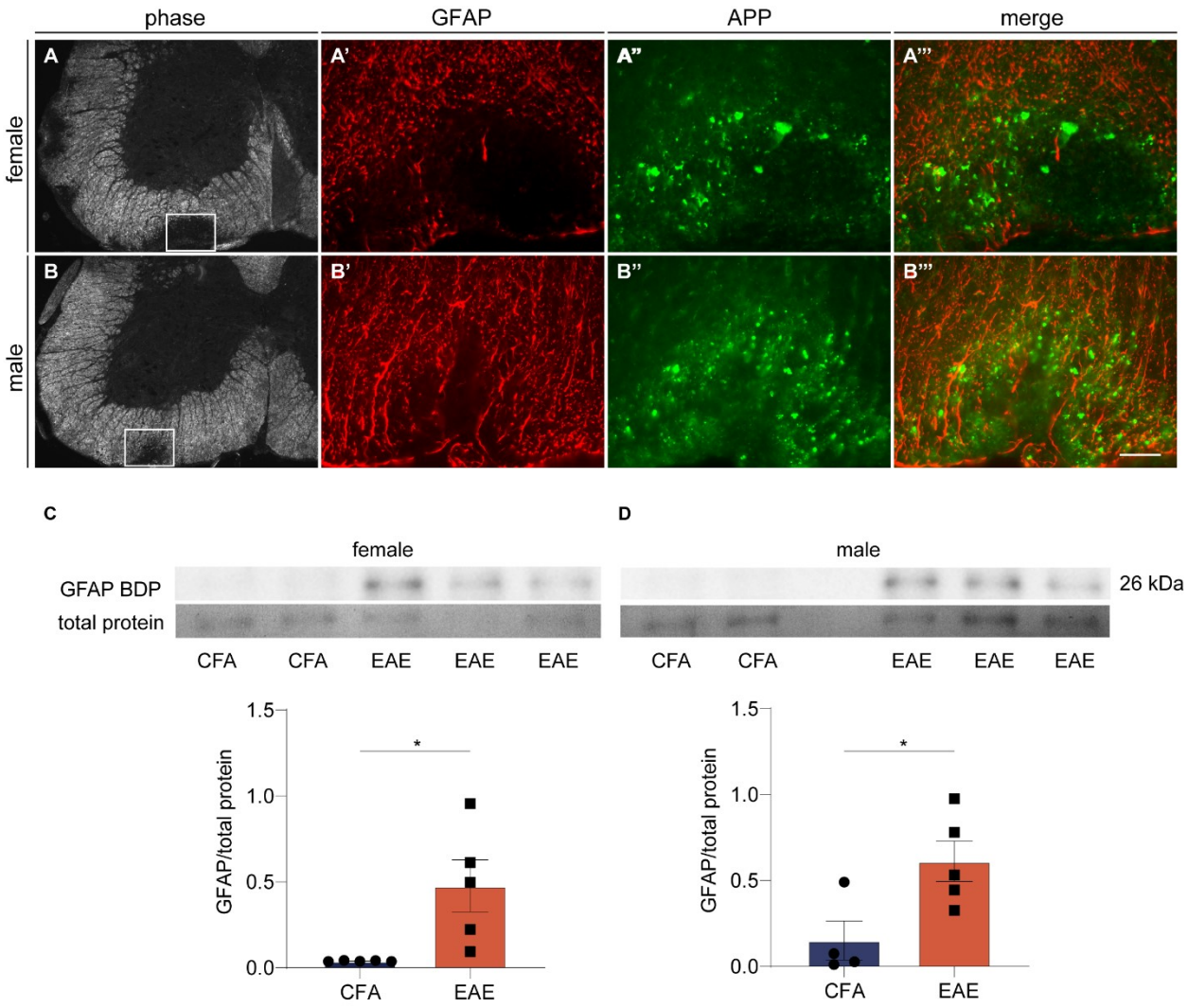

Figure 3.7 Assessment of astrocyte disruption in the EAE spinal cord. Phase contrast images of EAE spinal cord sections show lesions in the white mater, two examples of which are outlined in **A** and **B**. Higher magnification of the regions outlined in **A** and **B** demonstrate that there is a blatant loss of GFAP (**A', B'**) as well as the appearance of APP-positive puncta (**A'', B''**). Merging of the GFAP and APP images demonstrates that APP immunofluorescence co-localizes with regions in which GFAP staining is lost (**A''', B'''**). In spinal cord homogenates obtained from female (**C**) and male (**D**) mice with EAE, a 26kDa fragment of the GFAP protein can be detected with gel electrophoresis. Quantification of the GFAP fragment shows that expression is significantly increased in both female and male mice with EAE relative to CFA controls. *p=0.02, t-test. Scale bar in B'''=50μm and applies to A', B', A'', B'', and A'''. Data is ±SEM.

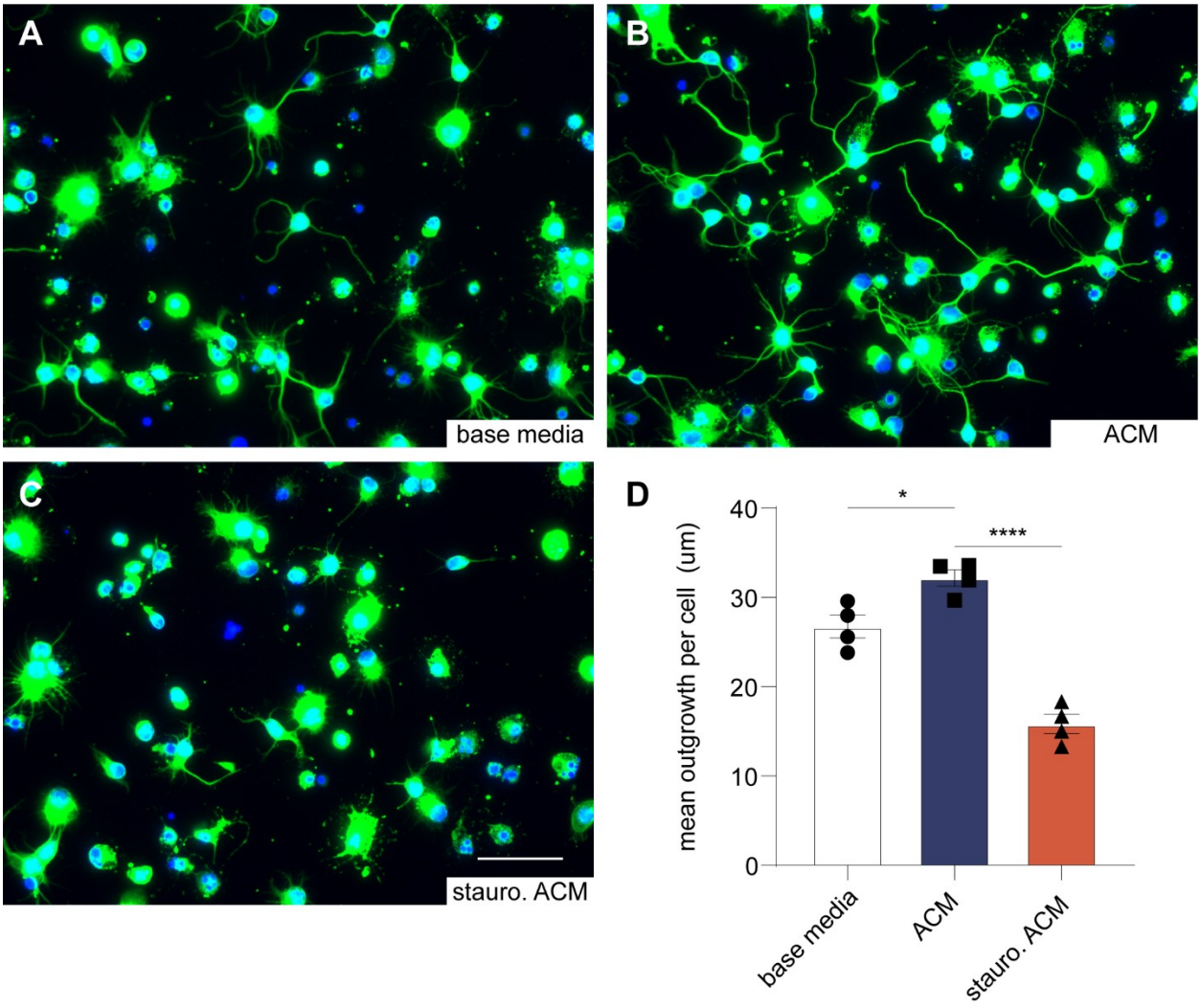

Figure 3.8 Examination of the effects of injured astrocytes on neurite outgrowth. Relative to neurons grown in base astrocyte media (**A**), neurons grown in astrocyte conditioned media grew significantly longer neurites (**B**). By contrast, neurons grown in ACM collected from injured astrocyte cultures grew significantly shorter neurites compared to control conditions (**C, D**). *p=0.0169, one-way ANOVA with post-hoc Tukey's multiple comparison test. ****p<0.0001, one-way ANOVA with post-hoc Tukey's multiple comparison test. Scale bar in C=50μm and applies to all images in the figure. Data is ±SEM.

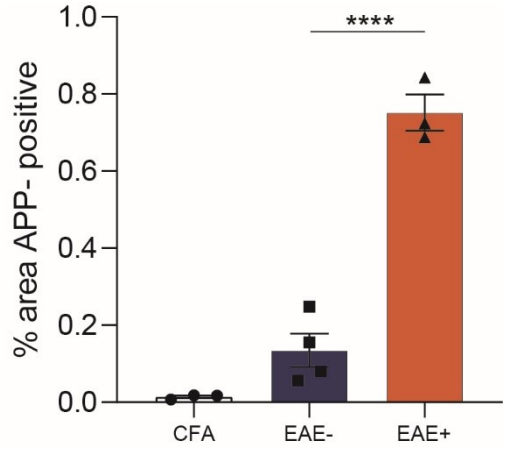

Figure 3.9 Examination of the relationship between TREZ APP and facial hypersensitivity in EAE. Relative to animals that did not become hypersensitive to air puffs (EAE-), animals that exhibited a change in facial sensitivity (EAE+) had significantly more APP immunoreactivity at the TREZ. ****p<0.0001, one-way ANOVA with post-hoc Tukey's multiple comparison test. Data is ±SEM.

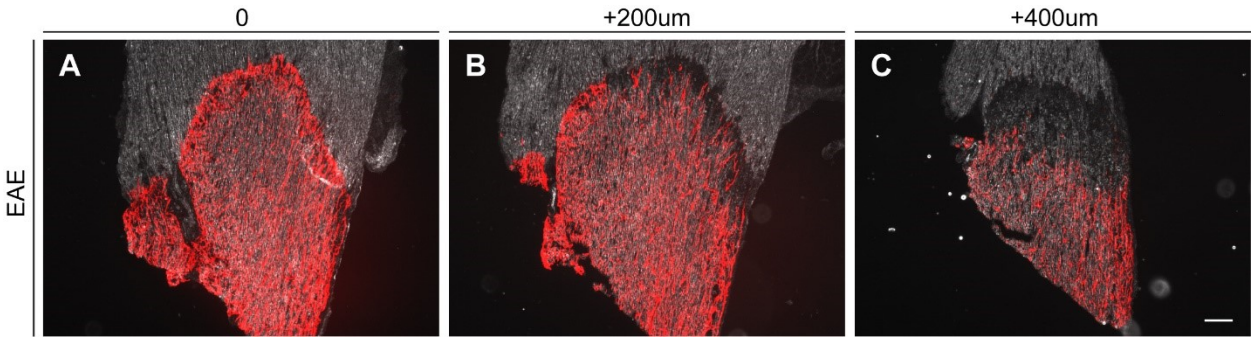

Supplemental Figure 3.1 Demonstration of astrocyte disruption heterogeneity within a nerve. Multiple sections from a single trigeminal nerve show that GFAP disruption is not always uniform throughout the nerve. (**A**) In the first section, GFAP staining appears intact. (**B**) In a tissue section obtained 200 microns from (**A**), some GFAP disruption can be seen. (**C**) 400 microns from (**A**), there is substantial loss of GFAP at the CNS-PNS interface. Scale bar in C=100μm and applies to all images in the figure.

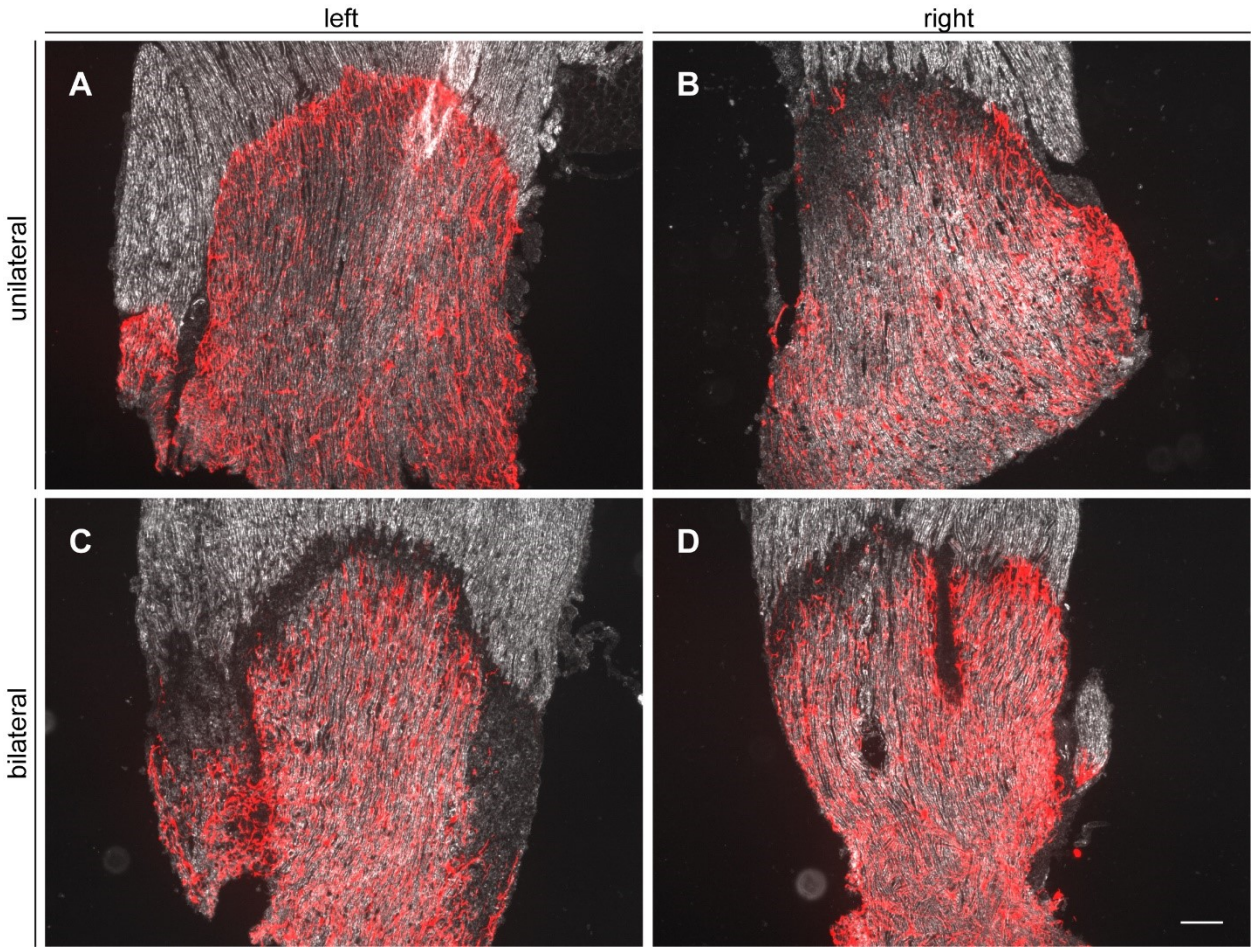

Supplemental Figure 3.2 Demonstration of astrocyte disruption heterogeneity between nerves from a single animal. Comparing the left and right trigeminal nerves reveals that GFAP disruption can be unilateral (**A, B**) or bilateral (**C, D**). Scale bar in D=100μm and applies to all images in the figure.

Conclusions

It is well-recognized that MS is associated with trigeminal lesions[2,6,32,152] and dysfunction[2,4]. Additionally, altered sensation along the distribution of the trigeminal nerve is a frequently encountered symptom of MS[2,4,25,81]. However, the relationship between trigeminal lesions, dysfunction, and altered facial sensation are poorly understood. This can be attributed, at least in part, to the lack of animal models that feature trigeminal lesions and sensory symptoms akin to that observed in MS. The work presented in this thesis suggests that the animal model EAE could be an invaluable tool for studying trigeminal involvement in MS.

In Chapter 1, I found that mice with EAE become hypersensitive to puffs of air applied to the face. This change in facial sensitivity was then shown to be associated with inflammation, glial activation, and demyelination at several points along the trigeminal primary afferent pathway. The data presented in Chapter 1 was the first report to demonstrate that EAE is associated with trigeminal pathology and altered sensation in the orofacial region. This work also established EAE as a unique animal model of trigeminal dysfunction because of its CNS-based pathology (which contrasts the peripheral-based pathology of most other models)[90]. Trigeminal symptoms in MS are diverse and can range from a loss of sensation to excruciating facial pain[2]. It would be interesting to examine if mice with EAE also show behaviors indicative of hypoesthesia and/or paresthesia/dysesthesia. During my initial assessment of facial sensitivity, air puffs were applied at 10 psi which, admittedly, is likely a supra-threshold stimulus that would evoke a response even in hypoesthetic animals. Thus, hyposthesia could potentially be assessed using a variety of air pressures that range from sub- (e.g. 1 psi) to supra-threshold values. To assess paresthesia and dysesthesia, it would have been interesting to assess the frequency in which animals engage in spontaneous behaviors such as face-directed grooming and body tensing/freezing[153] prio to- and following a facial stimulation protocol. Presumably, animals experiencing orofacial paresthesia/dysesthesia would engage in these behaviors more frequently before and/or after facial stimulation. Additionally, different stimulus modalities (e.g. touch via von frey hairs and temperature via acetone) could be introduced to the testing paradigm to make for a more comprehensive assessment of facial sensitivity in EAE. Given that EAE exhibits trigeminal pathology reminiscent of that observed in MS,

I believe this is a significantly better model for studying trigeminal dysfunction in MS compared to the peripheral nerve injury models. One downside to the EAE model however is that pathology was observed throughout the entirety of the trigeminal primary afferent pathway. Thus, it is not yet clear if a lesion to a specific part of the pathway is sufficient and/or necessary to elicit changes in facial sensitivity. This is an important distinction to make because it is not known if and/or how the spatial location of a trigeminal lesion impacts orofacial sensation in MS[152]. Thus, it would have been interesting to conduct a follow-up study that involved inducing targeted demyelination at the various parts of the trigeminal afferent pathway that are affected in EAE. This could have been achieved by stereotaxic injection of lysolecitihin into the TREZ or various parts of the trigeminal brainstem complex. An interesting aspect of lysolecithin-induced demyelination is that it is transient and affected axons can undergo spontaneous remyelination, even within the growth-inhibitory CNS[154]. Therefore, lysolecithin-induced injures would give an investigator the ability to assess facial sensitivity in animals with targeted trigeminal lesions at specific times when lesions are known to be in a demyelinating, remyelinating, or chronic phase. Importantly, this experiment could also provide insight into the role that demyelination plays in MS-related trigeminal symptoms. Nevertheless, the data presented in Chapter 1 establishes that EAE is associated with altered facial sensation and MS-like trigeminal pathology.

In Chapter 2, I demonstrated that the excitability of TG neurons is increased in EAE. This finding is interesting, as it could explain why mice with EAE are hypersensitive to facial stimulation. The data obtained in Chapter 1 could serve as a basis for future experiments investigating the mechanisms underlying this change in TG excitability. Specifically, in Chapter 1 I demonstrated that T cells infiltrate the TG in EAE and SGCs within the TG become reactive. T cells and SGCs release a variety of molecules (e.g. cytokines) which could directly impact neuronal excitability[44,101]. Thus, one experiment could involve assessing calcium transients in TG neurons that were grown in media collected from myelin-reactivated T cell cultures. Alternatively, TG neurons could be grown in direct co-culture with myelin-reactive T cells prior to the assessment of excitability. In line with this idea, previous work from the lab has demonstrated that media obtained from myelin-reactivated splenocytes increases the excitability of DRG neurons[155]. The data presented in Chapter 2 could also be followed up by studies that assess EAE-induced changes in the expression and/or function of various ion channels within the TG. Injury and disease-induced

changes in ion channel expression and/or function are a likely basis for a variety of orofacial sensory disturbances, especially painful conditions such as TN[89,156]. Therefore a future experiment could assess EAE-induced changes in TG sodium (e.g. Nav1.7[156]), potassium (e.g. Kir1.4[122]) and calcium (e.g. Cav3.2[157]) channel expression to identify specific ion channels that may contribute to facial sensory disturbances in EAE. This could then be followed up by electrophysiological experiments to assess the activity of these channels in dissociated TG neurons obtained from animals with EAE. An experiment such as that outlined above could lead to the identification of targets for novel therapeutics for managing trigeminal symptoms in MS.

Finally, in Chapter 3 I demonstrated that there can be an overt loss of astrocytes in EAE. Astrocyte disruption and loss in nervous system injury and disease is a concept that is rarely touched upon in neuroscience. This is clearly evident within the MS literature, which is dominated by studies that focus on the contributions of reactive astrocytes to disease pathophysiology[65]. I believe it would have been interesting to investigate what the cause of astrocyte loss in EAE is. Myelin-reactive T cells are potential instigators of astrocyte disruption in EAE and MS[145–147]. However, this has yet to be definitively proven. Thus, I believe it would be interesting to build upon the data presented in Chapter 3 by exposing immunopan-purified astrocytes to myelin-reactive T cells obtained from animals with EAE. The media from these co-cultures could also be collected and used to grow immunopan-purified neurons to examine the effects on neuron survival and neurite growth. Direct co-culture experiments could also have been carried out in which myelin-reactive T cells were added to astrocyte-neuron co-cultures or neuron cultures alone. In an experiment such as this, I would expect that the astrocytes would, at least initially, protect neurons from the toxic effects of the T cells[62,136]. However, following disruption of the astrocytes, I would expect to see detrimental effects on the neurons (e.g. reduced neurite growth and survival). An analysis of disrupted astrocyte gene expression would also make for a fascinating experiment. In recent years, there has been a surge of interest in identifying novel astrocyte phenotypes based on their gene expression profiles[57,63,66]. At the forefront of this trend was work from Ben Barres' lab demonstrating that similar populations of astrocytes adopt distinct, but overlapping, gene expression profiles depending on the context in which the astrocytes were stimulated. This data was recently built upon to show that a particular population of astrocytes (termed "A1" astrocytes) adopt neurotoxic properties that may

contribute to a variety of neurodegenerative diseases, including MS[57,63]. It is important to note here that the emphasis of these studies is on reactive astrocytes. Thus, I think it would be extremely interesting to compare the gene expression profile of a disrupted astrocyte relative to a reactive astrocyte. This idea could be explored by isolating astrocytes in disrupted and intact tissue sections via laser capture microdissection. Gene expression of the captured cells could then be compared to reactive and resting astrocytes to infer the function of disrupted astrocytes and how these cells may contribute to lesion dynamics. Finally, it would be interesting to investigate the impact that TREZ injury has on trigeminal excitability. This could be explored by assessing calcium transients in TG explants[71] or brainstem slices[71,158] obtained from mice with EAE. In either case, following the assessment of excitability, the tissue could then be fixed and stained to examine astrocyte disruption and axonal injury at the trigeminal root. An experiment such as that outlined above could provide critical information that sheds light on the relationship between trigeminal lesions and dysfunction in MS.

In conclusion, the data presented in this thesis demonstrates that EAE could be an excellent tool for studying facial sensory disturbances in MS. Specifically, the behavioral, electrophysiological, and histological data presented in this work could serve as a basis for future studies that aim to better understand the mechanisms underlying trigeminal sensory disturbances in MS.

Bibliography

1. Filippi, M. *et al.* Multiple sclerosis. *Nat. Rev. Dis. Prim.* **4**, (2018).

2. Cruccu, G. *et al.* Trigeminal neuralgia and pain related to multiple sclerosis. *Pain* **143**, 186–191 (2009).

3. Godazandeh, K., Martinez Sosa, S., Wu, J. & Zakrzewska, J. M. Trigeminal neuralgia: Comparison of characteristics and impact in patients with or without multiple sclerosis. *Mult. Scler. Relat. Disord.* **34**, 41–46 (2019).

4. Bergamaschi, R. *et al.* Usefulness of trigeminal somatosensory evoked potentials to detect subclinical trigeminal impairment in multiple sclerosis patients. *Acta Neurol. Scand.* **89**, 412–414 (1994).

5. Gebhardt, M., Kropp, P., Jürgens, T. P., Hoffmann, F. & Zettl, U. K. Headache in the first manifestation of Multiple Sclerosis – Prospective, multicenter study. *Brain Behav.* **7**, (2017).

6. Burkholder, D. B., Koehler, P. J. & Boes, C. J. Trigeminal Neuralgia and Multiple Sclerosis: A Historical Perspective. *Canadian Journal of Neurological Sciences* **44**, 589–593 (2017).

7. Zakrzewska, J. M. & Padfield, D. *The Patient's Journey Through Trigeminal Neuralgia*. (2014).

8. Laakso, S. M. *et al.* Trigeminal neuralgia in multiple sclerosis: Prevalence and association with demyelination. *Acta Neurol. Scand.* **142**, 139–144 (2020).

9. Di Stefano, G., Maarbjerg, S. & Truini, A. Trigeminal neuralgia secondary to multiple sclerosis: From the clinical picture to the treatment options. *Journal of Headache and Pain* **20**, (2019).

10. Putzki, N. *et al.* Prevalence of migraine, tension-type headache and trigeminal neuralgia in multiple sclerosis. *Eur. J. Neurol.* **16**, 262–267 (2009).

11. Cruccu, G. *et al.* Trigeminal neuralgia: New classification and diagnostic grading for practice and research. *Neurology* **87**, 220–228 (2016).

12. Ariai, M. S., Mallory, G. W. & Pollock, B. E. Outcomes after microvascular decompression for patients with trigeminal neuralgia and suspected multiple sclerosis. *World Neurosurgery* **81**, 599–603 (2014).

13. Broggi, G. *et al.* Operative Findings and Outcomes of Microvascular Decompression for Trigeminal Neuralgia in 35 Patients Affected by Multiple Sclerosis. *Neurosurgery* **55**, 830–839 (2004).

14. Wang, X. *et al.* The long-term clinical outcomes of microvascular decompression for treatment of trigeminal neuralgia compressed by the vertebra-basilar artery: A case series

review. *BMC Neurol.* **19**, 217 (2019).

15. Mohammad-Mohammadi, A., Recinos, P. F., Lee, J. H., Elson, P. & Barnett, G. H. Surgical outcomes of trigeminal neuralgia in patients with multiple sclerosis. *Neurosurgery* **73**, 941–950 (2013).

16. Krishnan, S., Bigder, M. & Kaufmann, A. M. Long-term follow-up of multimodality treatment for multiple sclerosis-related trigeminal neuralgia. *Acta Neurochir. (Wien).* **160**, 135–144 (2018).

17. Tuleasca, C. *et al.* Multiple sclerosis-related trigeminal neuralgia: A prospective series of 43 patients treated with gamma knife surgery with more than one year of follow-up. *Stereotact. Funct. Neurosurg.* **92**, 203–210 (2014).

18. Kowalec, K. *et al.* Comorbidity increases the risk of relapse in multiple sclerosis. *Neurology* **89**, 2455–2461 (2017).

19. Kister, I. *et al.* Migraine is comorbid with multiple sclerosis and associated with a more symptomatic MS course. *J. Headache Pain* **11**, 417–425 (2010).

20. Beckmann, Y. & Türe, S. Headache characteristics in multiple sclerosis. *Mult. Scler. Relat. Disord.* **27**, 112–116 (2019).

21. Edvinsson, J. C. A. *et al.* The fifth cranial nerve in headaches. *Journal of Headache and Pain* **21**, (2020).

22. Elliott, D. G. Migraine in Multiple Sclerosis. *International Review of Neurobiology* **79**, 281–302 (2007).

23. Gabelić, T., Skorić, M. K., Adamec, I., Mayer, D. & Habek, M. Tongue somatosensory-evoked potentials: Evaluation of the afferent trigeminal pathway in patients with early multiple sclerosis. *Clin. EEG Neurosci.* **44**, 286–290 (2013).

24. Bennett, A. J., Wastell, D. G., Barker, G. R., Blackburn, C. W. & Rood, J. P. Trigeminal somatosensory evoked potentials. A review of the literature as applicable to oral dysaesthesias. *Int. J. Oral Maxillofac. Surg.* **16**, 408–415 (1987).

25. Zhang, G. Q. & Meng, Y. Oral and craniofacial manifestations of multiple sclerosis: Implications for the oral health care provider. *Eur. Rev. Med. Pharmacol. Sci.* **19**, 4610–4620 (2015).

26. da Silva, C. J. *et al.* Trigeminal involvement in multiple sclerosis: Magnetic resonance imaging findings with clinical correlation in a series of patients. *Multiple Sclerosis* **11**, 282–285 (2005).

27. Mills, R. J., Young, C. A. & Smith, E. T. Central trigeminal involvement in multiple sclerosis using high-resolution MRI at 3 T. doi:10.1259/bjr/65228893

28. Swinnen, C., Lunskens, S., Deryck, O., Casselman, J. & Vanopdenbosch, L. MRI characteristics of trigeminal nerve involvement in patients with multiple sclerosis. *Mult.*

Scler. Relat. Disord. **2**, 200–203 (2013).

29. Villanueva, L. & Noseda, R. Trigeminal Mechanisms of Nociception. in *Wall and Melzack's Textbook of Pain* 793–802 (2013).

30. Chichorro, J. G., Porreca, F. & Sessle, B. Mechanisms of craniofacial pain. *Cephalalgia* **37**, 613–626 (2017).

31. JP, F. The transitional zone and CNS regeneration. *J. Anat.* **196 (Pt 1)**, (2000).

32. Olafson, R. A., Rushton, J. G. & Sayre, G. P. Trigeminal neuralgia in a patient with multiple sclerosis. An autopsy report. *J. Neurosurg.* **24**, 755–759 (1966).

33. Chen, D. Q. *et al.* Diffusivity signatures characterize trigeminal neuralgia associated with multiple sclerosis. *Mult. Scler.* **22**, 51–63 (2016).

34. Desouza, D. D., Hodaie, M. & Davis, K. D. Abnormal trigeminal nerve microstructure and brain white matter in idiopathic trigeminal neuralgia. *Pain* **155**, 37–44 (2014).

35. Kuhlmann, T. *et al.* An updated histological classification system for multiple sclerosis lesions. *Acta Neuropathol.* **133**, 13–24 (2017).

36. Sofroniew, M. V. Astrocyte barriers to neurotoxic inflammation. *Nature Reviews Neuroscience* **16**, 249–263 (2015).

37. Herz, J., Filiano, A. J., Smith, A., Yogev, N. & Kipnis, J. Myeloid Cells in the Central Nervous System. *Immunity* **46**, 943–956 (2017).

38. Absinta, M., Sati, P. & Reich, D. S. Advanced MRI and staging of multiple sclerosis lesions. *Nature Reviews Neurology* **12**, 358–368 (2016).

39. Alberts, B. *et al.* Lymphocytes and the Cellular Basis of Adaptive Immunity. (2002).

40. Kumar, B. V., Connors, T. J. & Farber, D. L. Human T Cell Development, Localization, and Function throughout Life. *Immunity* **48**, 202–213 (2018).

41. Alberts, B. *et al.* Innate Immunity. (2002).

42. Baecher-Allan, C., Kaskow, B. J. & Weiner, H. L. Multiple Sclerosis: Mechanisms and Immunotherapy. *Neuron* **97**, 742–768 (2018).

43. Panitch, H. S., Haley, A. S., Hirsch, R. L. & Johnson, K. P. EXACERBATIONS OF MULTIPLE SCLEROSIS IN PATIENTS TREATED WITH GAMMA INTERFERON. *Lancet* **329**, 893–895 (1987).

44. Ren, K. & Dubner, R. Interactions between the immune and nervous systems in pain. *Nature Medicine* **16**, 1267–1276 (2010).

45. Cao, L. & DeLeo, J. A. CNS-infiltrating CD4+ T lymphocytes contribute to murine spinal nerve transection-induced neuropathic pain. *Eur. J. Immunol.* **38**, 448–458 (2008).

46. Mishra, M. K. & Wee Yong, V. Myeloid cells — targets of medication in multiple sclerosis. (2016). doi:10.1038/nrneurol.2016.110

47. Bogie, J. F. J., Stinissen, P. & Hendriks, J. J. A. Macrophage subsets and microglia in multiple sclerosis. *Acta Neuropathologica* **128**, 191–213 (2014).

48. Kouwenhoven, M., Teleshova, N., Özenci, V., Press, R. & Link, H. Monocytes in multiple sclerosis: Phenotype and cytokine profile. *J. Neuroimmunol.* **112**, 197–205 (2001).

49. Metz, L. M. *et al.* Trial of Minocycline in a Clinically Isolated Syndrome of Multiple Sclerosis. *N. Engl. J. Med.* **376**, 2122–2133 (2017).

50. Miron, V. E. *et al.* M2 microglia and macrophages drive oligodendrocyte differentiation during CNS remyelination. *Nat. Neurosci.* **16**, 1211–1218 (2013).

51. Masuda, T. *et al.* Spatial and temporal heterogeneity of mouse and human microglia at single-cell resolution. *Nature* **566**, 388–392 (2019).

52. Batbold, D. *et al.* Macrophages in trigeminal ganglion contribute to ectopic mechanical hypersensitivity following inferior alveolar nerve injury in rats. *J. Neuroinflammation* **14**, (2017).

53. Beggs, S., Trang, T. & Salter, M. W. P2X4R + microglia drive neuropathic pain. *Nature Neuroscience* **15**, 1068–1073 (2012).

54. Verkhratsky, A. & Nedergaard, M. Physiology of astroglia. *Physiol. Rev.* **98**, 239–389 (2018).

55. Liddelow, S. A. & Sofroniew, M. V. Astrocytes usurp neurons as a disease focus. *Nat. Neurosci.* **22**, 512–513 (2019).

56. Sofroniew, M. V. & Vinters, H. V. Astrocytes: Biology and pathology. *Acta Neuropathologica* **119**, 7–35 (2010).

57. Liddelow, S. A. *et al.* Neurotoxic reactive astrocytes are induced by activated microglia. *Nature* **541**, 481–487 (2017).

58. Sofroniew, M. V. Astrogliosis. *Cold Spring Harb. Perspect. Biol.* **7**, (2015).

59. Escartin, C., Guillemaud, O. & Carrillo-de Sauvage, M. A. Questions and (some) answers on reactive astrocytes. *GLIA* **67**, 2221–2247 (2019).

60. McPhail, L. T., Plunet, W. T., Das, P. & Ramer, M. S. The astrocytic barrier to axonal regeneration at the dorsal root entry zone is induced by rhizotomy. *Eur. J. Neurosci.* **21**, 267–270 (2005).

61. Smith, G. M., Falone, A. E. & Frank, E. Sensory axon regeneration: Rebuilding functional connections in the spinal cord. *Trends in Neurosciences* **35**, 156–163 (2012).

62. Voskuhl, R. R. *et al.* Reactive astrocytes form scar-like perivascular barriers to leukocytes during adaptive immune inflammation of the CNS. *J. Neurosci.* **29**, 11511–11522 (2009).

63. Zamanian, J. L. *et al.* Genomic analysis of reactive astrogliosis. *J. Neurosci.* **32**, 6391–6410 (2012).

64. Foo, L. C. *et al.* Development of a method for the purification and culture of rodent astrocytes. *Neuron* **71**, 799–811 (2011).

65. Brambilla, R. The contribution of astrocytes to the neuroinflammatory response in multiple sclerosis and experimental autoimmune encephalomyelitis. *Acta Neuropathologica* **137**, 757–783 (2019).

66. Wheeler, M. A. *et al.* MAFG-driven astrocytes promote CNS inflammation. *Nature* **578**, 593–599 (2020).

67. Jin, J. *et al.* Glial pathology and retinal neurotoxicity in the anterior visual pathway in experimental autoimmune encephalomyelitis. *Acta Neuropathol. Commun.* **7**, 125 (2019).

68. Brosnan, C. F. & Raine, C. S. The astrocyte in multiple sclerosis revisited. *Glia* **61**, 453–465 (2013).

69. Magliozzi, R. *et al.* A Gradient of neuronal loss and meningeal inflammation in multiple sclerosis. *Ann. Neurol.* **68**, 477–493 (2010).

70. Okada-Ogawa, A. *et al.* Astroglia in medullary dorsal horn (trigeminal spinal subnucleus caudalis) are involved in trigeminal neuropathic pain mechanisms. *J. Neurosci.* **29**, 11161–11171 (2009).

71. Kim, Y. S. *et al.* Central terminal sensitization of TRPV1 by descending serotonergic facilitation modulates chronic pain. *Neuron* **81**, 873–887 (2014).

72. Shibuta, K. *et al.* Organization of hyperactive microglial cells in trigeminal spinal subnucleus caudalis and upper cervical spinal cord associated with orofacial neuropathic pain. *Brain Res.* **1451**, 74–86 (2012).

73. Colburn, R. W., Rickman, A. J. & Deleo, J. A. The effect of site and type of nerve injury on spinal glial activation and neuropathic pain behavior. *Exp. Neurol.* **157**, 289–304 (1999).

74. Seijffers, R., Mills, C. D. & Woolf, C. J. ATF3 increases the intrinsic growth state of DRG neurons to enhance peripheral nerve regeneration. *J. Neurosci.* **27**, 7911–7920 (2007).

75. Bjelobaba, I., Begovic-Kupresanin, V., Pekovic, S. & Lavrnja, I. Animal models of multiple sclerosis: Focus on experimental autoimmune encephalomyelitis. *J. Neurosci. Res.* **96**, 1021–1042 (2018).

76. Grace, P. M. *et al.* Behavioral assessment of neuropathic pain, fatigue, and anxiety in experimental autoimmune encephalomyelitis (EAE) and attenuation by interleukin-10 gene therapy. *Brain. Behav. Immun.* **59**, 49–54 (2017).

77. Aicher, S. A., Silverman, M. B., Winkler, C. W. & Bebo, B. F. Hyperalgesia in an animal

model of multiple sclerosis. *Pain* **110**, 560–570 (2004).

78. Olechowski, C. J., Truong, J. J. & Kerr, B. J. Neuropathic pain behaviours in a chronic-relapsing model of experimental autoimmune encephalomyelitis (EAE). *Pain* **141**, 156–164 (2009).

79. Wuerfel, J. *et al.* Mouse model mimics multiple sclerosis in the clinico-radiological paradox. *Eur. J. Neurosci.* **26**, 190–198 (2007).

80. Thorburn, K. C., Paylor, J. W., Webber, C. A., Winship, I. R. & Kerr, B. J. Facial hypersensitivity and trigeminal pathology in mice with experimental autoimmune encephalomyelitis. *Pain* **157**, 627–642 (2016).

81. Hooge, J. P. & Redekop, W. K. Trigeminal neuralgia in multiple sclerosis. *Neurology* **45**, 1294–1296 (1995).

82. Soustiel, J. F. *et al.* Brain-stem trigeminal and auditory evoked potentials in multiple sclerosis: Physiological insights. *Electroencephalogr. Clin. Neurophysiol. - Evoked Potentials* **100**, 152–157 (1996).

83. Lazar, M. L. & Kirkpatrick, J. B. Trigeminal neuralgia and multiple sclerosis: Demonstration of the plaque in an operative case. *Neurosurgery* **5**, 711–717 (1979).

84. Love, S., Gradidge, T. & Coakham, H. B. Trigeminal neuralgia due to multiple sclerosis: Ultrastructural findings in trigeminal rhizotomy specimens. *Neuropathol. Appl. Neurobiol.* **27**, 238–244 (2001).

85. Nakashima, I. *et al.* Linear pontine trigeminal root lesions in multiple sclerosis: Clinical and magnetic resonance imaging studies in 5 cases. *Arch. Neurol.* **58**, 101–104 (2001).

86. Burchiel, K. J. Abnormal impulse generation in focally demyelinated trigeminal roots. *J. Neurosurg.* **53**, 674–683 (1980).

87. Fromm, G. Pathophysiology of trigeminal neuralgia. in *Trigeminal neuralgia: current concepts regarding pathogenesis and treatment* (eds. Fromm, G. & Sessle, B. J.) 119–22 (Butterworth-Heinemann, 1991).

88. Love, S. & Coakham, H. B. Trigeminal neuralgia: Pathology and pathogenesis. *Brain* **124**, 2347–2360 (2001).

89. Devor, M., Amir, R. & Rappaport, Z. H. Pathophysiology of trigeminal neuralgia: The ignition hypothesis. *Clin. J. Pain* **18**, 4–13 (2002).

90. Dubner, R., Iwata, K. & Wei, F. Neuropathic orofacial pain mechanisms: insights from animal models. in *Orofacial Pain: Recent Advances in Assessment, Management, and Understanding of Mechanisms* (ed. Sessle, B. J.) 333-5,340–2 (IASP Press, 2014).

91. Constantinescu, C. S., Farooqi, N., O'Brien, K. & Gran, B. Experimental autoimmune encephalomyelitis (EAE) as a model for multiple sclerosis (MS). *British Journal of Pharmacology* **164**, 1079–1106 (2011).

92. Khan, N. & Smith, M. T. Multiple sclerosis-induced neuropathic pain: Pharmacological management and pathophysiological insights from rodent EAE models. *Inflammopharmacology* **22**, 1–22 (2014).

93. Olechowski, C. J. *et al.* A diminished response to formalin stimulation reveals a role for the glutamate transporters in the altered pain sensitivity of mice with experimental autoimmune encephalomyelitis (EAE). *Pain* **149**, 565–572 (2010).

94. Krzyzanowska, A. *et al.* Assessing nociceptive sensitivity in mouse models of inflammatory and neuropathic trigeminal pain. *J. Neurosci. Methods* **201**, 46–54 (2011).

95. Warwick, R. A., Ledgerwood, C. J., Brenner, T. & Hanani, M. Satellite glial cells in dorsal root ganglia are activated in experimental autoimmune encephalomyelitis. *Neurosci. Lett.* **569**, 59–62 (2014).

96. Johnson, L., Westrum, L. & Henry, M. Anatomic organization of the trigeminal system and the effects of deafferentation. in *Trigeminal neuralgia: current concepts regarding pathogenesis and treatment* (eds. Fromm, G. & Sessle, B. J.) 30, 39–41 (Butterworth-Heinemann, 1991).

97. Aita, M., Byers, M. R., Chavkin, C. & Xu, M. Trigeminal injury causes kappa opioid-dependent allodynic, glial and immune cell responses in mice. *Mol. Pain* **6**, (2010).

98. Peker, S., Kurtkaya, Ö., Üzün, I. & Pamir, M. N. Microanatomy of the central myelin-peripheral myelin transition zone of the trigeminal nerve. *Neurosurgery* **59**, 354–358 (2006).

99. C, W. The somatosensory system. in *The mouse nervous system* (eds. Watson, C., Paxinos, G. & Puelles, M.) 566–7 (Academic Press, 2012).

100. Xu, M., Aita, M. & Chavkin, C. Partial Infraorbital Nerve Ligation as a Model of Trigeminal Nerve Injury in the Mouse: Behavioral, Neural, and Glial Reactions. *J. Pain* **9**, 1036–1048 (2008).

101. Takeda, M. *et al.* Enhanced excitability of nociceptive trigeminal ganglion neurons by satellite glial cytokine following peripheral inflammation. *Pain* **129**, 155–166 (2007).

102. Katagiri, A. *et al.* Satellite glial cell P2Y 12receptor in the trigeminal ganglion is involved in lingual neuropathic pain mechanisms in rats. *Mol. Pain* **8**, (2012).

103. Begum, F., Zhu, W., Cortes, C., MacNeil, B. & Namaka, M. Elevation of tumor necrosis factor alpha in dorsal root ganglia and spinal cord is associated with neuroimmune modulation of pain in an animal model of multiple sclerosis. *J. Neuroimmune Pharmacol.* **8**, 677–690 (2013).

104. Melanson, M. *et al.* Experimental autoimmune encephalomyelitis-induced upregulation of tumor necrosis factor-alpha in the dorsal root ganglia. *Mult. Scler.* **15**, 1135–1145 (2009).

105. Yang, Z. & Wang, K. K. W. Glial fibrillary acidic protein: From intermediate filament assembly and gliosis to neurobiomarker. *Trends in Neurosciences* **38**, 364–374 (2015).

106. Lee, S. H., Zhao, Y. Q., Ribeiro-da-Silva, A. & Zhang, J. Distinctive response of CNS glial cells in oro-facial pain associated with injury, infection and inflammation. *Mol. Pain* **6**, (2010).

107. Sessle, B. J. Physiology of the trigeminal system. in *Trigeminal neuralgia: current concepts regarding pathogenesis and treatment* (eds. Fromm, G. & Sessle, B. J.) 78–83 (Butterworth-Heinemann).

108. Costigan, M. *et al.* T-cell infiltration and signaling in the adult dorsal spinal cord is a major contributor to neuropathic pain-like hypersensitivity. *J. Neurosci.* **29**, 14415–14422 (2009).

109. Sorge, R. E. *et al.* Different immune cells mediate mechanical pain hypersensitivity in male and female mice. *Nat. Neurosci.* **18**, 1081–1083 (2015).

110. Rahn, E. J., Iannitti, T., Donahue, R. R. & Taylor, B. K. Sex differences in a mouse model of multiple sclerosis: Neuropathic pain behavior in females but not males and protection from neurological deficits during proestrus. *Biol. Sex Differ.* **5**, (2014).

111. Zakrzewska, J. M. & Linskey, M. E. Trigeminal neuralgia. *BMJ* **350**, (2015).

112. Katusic, S., Willaims, D. B., Beard, C. M., Bergstralh, E. J. & Kurland, L. T. Epidemiology and clinical features of idiopathic trigeminal neuralgia and glossopharyngeal neuralgia: Similarities and differences, rochester, minnesota, 1945-19841. *Neuroepidemiology* **10**, 276–281 (1991).

113. Yousuf, M. S. *et al.* Sensory neurons of the dorsal root ganglia become hyperexcitable in a t-cell-mediated MOG-EAE model of multiple sclerosis. *eNeuro* **6**, (2019).

114. Yousuf, M. S. *et al.* Endoplasmic reticulum stress in the dorsal root ganglia regulates large-conductance potassium channels and contributes to pain in a model of multiple sclerosis. *FASEB J.* (2020). doi:10.1096/fj.202001163R

115. Duffy, S. S. *et al.* Peripheral and central neuroinflammatory changes and pain behaviors in an animal model of multiple sclerosis. *Front. Immunol.* **7**, (2016).

116. Messlinger, K., Balcziak, L. K. & Russo, A. F. Cross-talk signaling in the trigeminal ganglion: role of neuropeptides and other mediators. *Journal of Neural Transmission* **127**, 431–444 (2020).

117. Nair, A. *et al.* Familial hemiplegic migraine Ca(v)2.1 channel mutation R192Q enhances ATP-gated P2X3 receptor activity of mouse sensory ganglion neurons mediating trigeminal pain. *Mol. Pain* **6**, 48 (2010).

118. Shinoda, M. *et al.* P2X3 Receptor Mediates Heat Hyperalgesia in a Rat Model of Trigeminal Neuropathic Pain. *J. Pain* **8**, 588–597 (2007).

119. Xu, G. Y. & Huang, L. Y. M. Peripheral inflammation sensitizes P2X receptor-mediated responses in rat dorsal root ganglion neurons. *J. Neurosci.* **22**, 93–102 (2002).

120. Price, T. J., Cervero, F., Gold, M. S., Hammond, D. L. & Prescott, S. A. Chloride regulation in the pain pathway. *Brain Research Reviews* **60**, 149–170 (2009).

121. Rossi, H. L. *et al.* Abnormal trigeminal sensory processing in obese mice. *Pain* **157**, 235–246 (2016).

122. Ohara, P. T. *et al.* Gliopathic pain: When satellite glial cells go bad. *Neuroscientist* **15**, 450–463 (2009).

123. Liu, K., Tedeschi, A., Park, K. K. & He, Z. Neuronal intrinsic mechanisms of axon regeneration. *Annu. Rev. Neurosci.* **34**, 131–152 (2011).

124. Ambron, R. T., Zhang, X. P., Gunstream, J. D., Povelones, M. & Walters, E. T. Intrinsic injury signals enhance growth, survival, and excitability of Aplysia neurons. *J. Neurosci.* **16**, 7469–7477 (1996).

125. Rishal, I. & Fainzilber, M. Retrograde signaling in axonal regeneration. *Experimental Neurology* **223**, 5–10 (2010).

126. Yousuf, M. S., Zubkow, K., Tenorio, G. & Kerr, B. The chloride co-transporters, NKCC1 and KCC2, in experimental autoimmune encephalomyelitis (EAE). *Neuroscience* **344**, 178–186 (2017).

127. Sung, K. W., Kirby, M., McDonald, M. P., Lovinger, D. M. & Delpire, E. Abnormal GABA(A) receptor-mediated currents in dorsal root ganglion neurons isolated from Na-K-2Cl cotransporter null mice. *J. Neurosci.* **20**, 7531–7538 (2000).

128. Field, M. J., Bramwell, S., Hughes, J. & Singh, L. Detection of static and dynamic components of mechanical allodynia in rat models of neuropathic pain: Are they signalled by distinct primary sensory neurones? *Pain* **83**, 303–311 (1999).

129. Hansson, P. Difficulties in stratifying neuropathic pain by mechanisms. in *European Journal of Pain* **7**, 353–357 (W.B. Saunders Ltd, 2003).

130. Lassmann, H., Brück, W. & Lucchinetti, C. Heterogeneity of multiple sclerosis pathogenesis: Implications for diagnosis and therapy. *Trends in Molecular Medicine* **7**, 115–121 (2001).

131. Lee, J. Y., Taghian, K. & Petratos, S. Axonal degeneration in multiple sclerosis: Can we predict and prevent permanent disability? *Acta Neuropathologica Communications* **2**, 97 (2014).

132. Ludwin, S. K., Rao, V. T. S., Moore, C. S. & Antel, J. P. Astrocytes in multiple sclerosis. *Multiple Sclerosis* **22**, 1114–1124 (2016).

133. D'Amelio, F. E., Smith, M. E. & Eng, L. F. Sequence of tissue responses in the early stages of experimental allergic encephalomyelitis (EAE): Immunohistochemical, light microscopic, and ultrastructural observations in the spinal cord. *Glia* **3**, 229–240 (1990).

134. Prineas, J. W. & Lee, S. Multiple sclerosis: Destruction and regeneration of astrocytes in

acute lesions. *J. Neuropathol. Exp. Neurol.* **78**, 140–156 (2019).

135. Nagelhus, E. A. & Ottersen, O. P. Physiological roles of Aquaporin-4 in brain. *Physiol. Rev.* **93**, 1543–1562 (2013).

136. Horng, S. *et al.* Astrocytic tight junctions control inflammatory CNS lesion pathogenesis. *J. Clin. Invest.* **127**, 3136–3151 (2017).

137. Haines, J. D., Inglese, M. & Casaccia, P. Axonal damage in multiple sclerosis. *Mt. Sinai J. Med.* **78**, 231–243 (2011).

138. Höflich, K. M. *et al.* Acute axonal damage in three different murine models of multiple sclerosis: A comparative approach. *Brain Res.* **1650**, 125–133 (2016).

139. Bitsch, A., Schuchardt, J., Bunkowski, S., Kuhlmann, T. & Brück, W. Acute axonal injury in multiple sclerosis. Correlation with demyelination and inflammation. *Brain* **123**, 1174–1183 (2000).

140. Trapp, B. D. *et al.* Axonal transection in the lesions of multiple sclerosis. *N. Engl. J. Med.* **338**, 278–285 (1998).

141. Eilam, R. *et al.* Astrocyte disruption of neurovascular communication is linked to cortical damage in an animal model of multiple sclerosis. *Glia* **66**, 1098–1117 (2018).

142. Catuneanu, A., Paylor, J. W., Winship, I., Colbourne, F. & Kerr, B. J. Sex differences in central nervous system plasticity and pain in experimental autoimmune encephalomyelitis. *Pain* **160**, 1037–1049 (2019).

143. Sharma, R. *et al.* Inflammation induced by innate immunity in the central nervous system leads to primary astrocyte dysfunction followed by demyelination. *Acta Neuropathol.* **120**, 223–236 (2010).

144. De Parratt, J. & Prineas, J. W. Neuromyelitis optica: A demyelinating disease characterized by acute destruction and regeneration of perivascular astrocytes. *Mult. Scler.* **16**, 1156–1172 (2010).

145. Sun, D. & Wekerle, H. Ia-restricted encephalitogenic T lymphocytes mediating EAE lyse autoantigen-presenting astrocytes. *Nature* **320**, 70–72 (1986).

146. Domingues, H. S., Mues, M., Lassmann, H., Wekerle, H. & Krishnamoorthy, G. Functional and pathogenic differences of Th1 and Th17 cells in experimental autoimmune encephalomyelitis. *PLoS One* **5**, (2010).

147. Stopnicki, B. *et al.* Helper CD4 T cells expressing granzyme B cause glial fibrillary acidic protein fragmentation in astrocytes in an MHCII-independent manner. *Glia* **67**, 582–593 (2019).

148. Joost, E. *et al.* Microglia contribute to the glia limitans around arteries, capillaries and veins under physiological conditions, in a model of neuroinflammation and in human brain tissue. *Brain Struct. Funct.* **224**, 1301–1314 (2019).

149. Chen, M. H., Hagemann, T. L., Quinlan, R. A., Messing, A. & Perng, M. Der. Caspase cleavage of GFAP produces an assembly-compromised proteolytic fragment that promotes filament aggregation. *ASN Neuro* **5**, 293–308 (2013).

150. Yoshida, M., Saito, H. & Katsuki, H. Neurotrophic effects of conditioned media of astrocytes isolated from different brain regions on hippocampal and cortical neurons. *Experientia* **51**, 133–136 (1995).

151. D'Alimonte, I. *et al.* Staurosporine-induced apoptosis in astrocytes is prevented by A1 adenosine receptor activation. *Neurosci. Lett.* **418**, 66–71 (2007).

152. Skorić, M. K., Adamec, I., Madarić, V. N. & Habek, M. Evaluation of Brainstem Involvement in Multiple Sclerosis. *Can. J. Neurol. Sci.* **41**, 346–349 (2014).

153. Vos, B. P., Strassman, A. M. & Maciewicz, R. J. Behavioral evidence of trigeminal neuropathic pain following chronic constriction injury to the rat's infraorbital nerve. *J. Neurosci.* **14**, 2708–2723 (1994).

154. Keough, M. B., Jensen, S. K. & Wee Yong, V. Experimental demyelination and remyelination of murine spinal cord by focal injection of lysolecithin. *J. Vis. Exp.* **2015**, (2015).

155. Mifflin, K. A. *et al.* Voluntary wheel running reveals sex-specific nociceptive factors in murine experimental autoimmune encephalomyelitis. *Pain* **160**, 870–881 (2019).

156. Zakrzewska, J. M. *et al.* Safety and efficacy of a Nav1.7 selective sodium channel blocker in patients with trigeminal neuralgia: a double-blind, placebo-controlled, randomised withdrawal phase 2a trial. *Lancet Neurol.* **16**, 291–300 (2017).

157. Gambeta, E., Chichorro, J. G. & W. Zamponi, G. Trigeminal neuralgia: An overview from pathophysiology to pharmacological treatments. *Molecular Pain* **16**, 174480692090189 (2020).

158. Hirahara, M., Fujiwara, N. & Seo, K. Novel trigeminal slice preparation method for studying mechanisms of nociception transmission. *J. Neurosci. Methods* **286**, 6–15 (2017).